

## Chapter 1

### Strongly interacting two-dimensional Fermi gases

Jesper Levinsen\*

*Aarhus Institute of Advanced Studies, Aarhus University,  
DK-8000 Aarhus C, Denmark*

Meera M. Parish†

*London Centre for Nanotechnology, University College London,  
Gordon Street, London, WC1H 0AH, United Kingdom*

We review the current understanding of the uniform two-dimensional (2D) Fermi gas with short-range interactions. We first outline the basics of two-body scattering in 2D, including a discussion of how such a 2D system may be realized in practice using an anisotropic confining potential. We then discuss the thermodynamic and dynamical properties of 2D Fermi gases, which cold-atom experiments have only just begun to explore. Of particular interest are the different pairing regimes as the interparticle attraction is varied; the superfluid transition and associated finite-temperature phenomenology; few-body properties and their impact on the many-body system; the “Fermi polaron” problem; and the symmetries underlying the collective modes. Where possible, we include the contributions from 2D experiment. An underlying theme throughout is the effect of the quasi-2D geometry, which we view as an added richness to the problem rather than an unwanted complication.

#### 1. Introduction

Following the successful realisation of strongly interacting atomic Fermi gases in three dimensions (3D), attention has now turned to Fermi systems that have, in principle, even stronger correlations, such as low-dimensional gases and fermions with long-range dipolar interactions. Model two-dimensional (2D) systems are of particular interest, since they may

---

\*jfle@aiaas.au.dk

†meera.parish@ucl.ac.uk

provide insight into technologically important, but complex, solid-state systems such as the high-temperature superconductors,<sup>1</sup> semiconductor interfaces,<sup>2</sup> and layered organic superconductors.<sup>3</sup> Moreover, 2D gases pose fundamental questions in their own right, being in the so-called marginal dimension where particle scattering can be strongly energy dependent, and quantum fluctuations are large enough to destroy long-range order at any finite temperature.<sup>4,5</sup>

In this review, we focus on the uniform 2D Fermi gas with short-range interactions, since this has already been successfully realised experimentally.<sup>6–17</sup> Here, two species of alkali atom are confined to one or more layers using a 1D optical lattice or a highly anisotropic trap. The interspecies interactions may then be tuned using a Feshbach resonance, making cold atomic gases ideal for studying the behavior of fermions in low dimensions. While the cold-atom system is clearly much simpler than solid-state systems, where the long-range Coulomb interactions are difficult to treat and there are often complex crystal structures, the usual toy models for such systems neglect the long-range interactions and consider simple contact interactions like the ones described here in this review. In particular, the attractive 2D Fermi gas provides a basic model for understanding pairing and superconductivity in 2D.<sup>18–20</sup> Here, by varying the attraction, one can investigate the crossover from BCS-type pairing to the Bose regime of tightly bound dimers. In the interests of space, we do not consider further extensions such as dipolar interactions, spin-orbit coupling, or any lattice within the plane. Indeed, we note that a degenerate 2D dipolar Fermi gas has yet to be achieved experimentally, while the pursuit of the 2D Hubbard model is still ongoing.

The investigation of strongly interacting 2D Fermi gases, as described in the following, may be encompassed within several broad themes. Firstly, there is the interplay between Bose and Fermi behavior as the attraction is varied. This is particularly apparent at finite temperature where the normal state evolves from a Fermi to a Bose liquid, and one has the possibility of the so-called pseudogap regime. Potentially even richer behavior may be derived from Fermi-Fermi mixtures with unequal masses and/or imbalanced “spin” populations. While attempts to confine mass-imbalanced mixtures to 2D are still underway, experiments with equal masses have already realized the regime of extreme spin imbalance,<sup>14</sup> corresponding to a single impurity problem. Here, it has emerged that even the strongly interacting impurity can be well described by wave functions that only contain two- and three-body correlations. A related theme is the importance of few-

body phenomena in the many-body system. As well as being relevant to high temperatures, where the thermodynamic properties are well described by the behavior of few-body clusters (i.e., the virial expansion), few-body properties are also required to properly describe the Bose regime of the pairing crossover. Turning to themes unique to the 2D system, we have the existence of classical scale invariance and its impact on the collective modes in a harmonic trap. Finally, there is the question of how 2D experiments really are, since in practice there is always a finite transverse “size” of the quasi-2D geometry. To be in the 2D limit, we require the length scales associated with the gas (e.g., the dimer size) to be much larger than the confinement length. Ultimately, it would be interesting to understand how the gas evolves from 2D to 3D.

The review is organized as follows: Section 2 surveys the basic properties of two-body scattering in a two-dimensional geometry — since the literature offers multiple different definitions in the 2D scattering problem, this may be thought of as a reference section for the remainder of the review. We also present here an alternative formulation of the scattering problem in a quasi-2D geometry, and discuss the issue of confinement induced resonances. Section 3 focuses on recent advances in the understanding of few-body physics. We discuss elastic scattering properties, as well as the bound trimer and tetramer states that are predicted to occur in the heteronuclear Fermi gas, for a sufficiently large mass imbalance. Turning to the many-body physics in a 2D Fermi gas, Sec. 4 reviews the properties of the BCS-BEC crossover, including the mean-field approach and the equation of state at zero temperature. Section 5 considers the behavior of the gas at finite temperature, which includes an outline of the high-temperature virial expansion, a sketch of the phase diagram for superfluidity, and a discussion of the existence of the pseudogap. Section 6 discusses the recent experimental and theoretical advances in the 2D Fermi polaron problem, with both metastable states and the nature of the ground state being considered. In Sec. 7, dynamical quantities such as collective modes and spin diffusion are reviewed, as well as the breakdown of classical scale invariance in the interacting quantum system — the so-called quantum anomaly. Finally, Sec. 8 provides an outlook into future investigations of strongly interacting 2D Fermi gases.

## 2. Basics of the two-dimensional system

### 2.1. General properties of scattering in two dimensions

We now summarize several properties of two-body scattering in two dimensions that are relevant to the results presented in this review. In the following discussion, we mostly follow Refs. 21,22. The starting point is the 2D Schrödinger equation for two particles interacting via a short-range local potential  $V(\mathbf{r})$  at energy  $E$  in the center-of-mass frame:

$$-\frac{\hbar^2 \nabla^2}{2m_r} \psi(\mathbf{r}) + V(\mathbf{r})\psi(\mathbf{r}) = E\psi(\mathbf{r}). \quad (1)$$

Here, the reduced mass is defined in terms of the masses of particle 1 and 2 as  $m_r = m_1 m_2 / (m_1 + m_2)$ ,  $\mathbf{r} = (m_1 \mathbf{r}_1 - m_2 \mathbf{r}_2) / m_r$  is the relative coordinate, and  $\nabla$  is the 2D gradient. We further assume that the potential only depends on  $r \equiv |\mathbf{r}|$ ; then the Schrödinger equation is separable, the wavefunction may be written as  $\psi(\mathbf{r}) = R(r)T(\theta)$ , and the equation for the radial part takes the form

$$-\frac{\hbar^2}{2m_r} \frac{1}{r} \frac{d}{dr} \left( r \frac{dR}{dr} \right) + \frac{\hbar^2 \ell^2}{2m_r r^2} R + V(r)R = ER. \quad (2)$$

The quantum number  $\ell$  is determined from the azimuthal equation  $d^2 T / d\theta^2 = -\ell^2 T$  and corresponds to the angular momentum in the plane. In order for the wavefunction to be single valued we must have  $T_\ell(\theta) \propto e^{i\ell\theta}$  with  $\ell$  integer. Thus we have one  $s$ -wave component ( $\ell = 0$ ) but two of all higher partial wave components ( $p$ ,  $d$ , etc. corresponding to  $\ell = \pm 1, \pm 2$ , etc.). This may be thought of as clockwise and anti-clockwise rotation and should be compared with the degeneracy factor  $2\ell + 1$  in 3D.<sup>21</sup>

In the asymptotic limit, we write the wavefunction as a sum of an incident plane wave along the  $\hat{\mathbf{x}}$  direction and an outgoing circular wave

$$\psi(\mathbf{r}) \xrightarrow{r \rightarrow \infty} e^{ikx} - \sqrt{\frac{i}{8\pi kr}} f(\mathbf{k}) e^{ikr}, \quad (3)$$

with the incident relative wavenumber  $k$  defined by  $E = \hbar^2 k^2 / 2m_r$ . The vector  $\mathbf{k} \equiv k\hat{\mathbf{r}}$  is defined in the direction of the scattered wave at an angle  $\theta$  with respect to the incident wave. The dimensionless scattering amplitude  $f(\mathbf{k})$  may then be expanded in the partial waves as

$$f(\mathbf{k}) = \sum_{\ell=0}^{\infty} (2 - \delta_{\ell 0}) \cos(\ell\theta) f_\ell(k), \quad (4)$$

where the Kronecker delta takes account of the degeneracy within the partial wave.

The scattering amplitude gives access to the differential elastic cross section  $\frac{d\sigma}{d\theta} = \frac{|f(\mathbf{k})|^2}{8\pi k}$ , and to both the total and elastic cross sections:

$$\sigma_\ell^{\text{tot}}(E) = -\frac{1}{k} \text{Im}[f_\ell(k)](2 - \delta_{\ell 0}), \quad (5)$$

$$\sigma_\ell^{\text{el}}(E) = \frac{|f_\ell(k)|^2}{4k}(2 - \delta_{\ell 0}), \quad (6)$$

where the first equation corresponds to the well-known optical theorem. For both cross sections we use the partial wave expansion  $\sigma(E) = \sum_{\ell=0}^{\infty} \sigma_\ell(E)$ , noting that the partial waves decouple in the cross section. The inelastic cross section simply follows as  $\sigma^{\text{inel}}(E) = \sigma^{\text{tot}}(E) - \sigma^{\text{el}}(E)$ . Note that in 2D the cross section has dimensions of length.

The scattering amplitude may be related to the phase shift experienced by the scatterers at distances outside the range of the potential:

$$f_\ell(k) = \frac{-4}{\cot \delta_\ell(k) - i}. \quad (7)$$

The phase shifts are real for elastic scattering and have the low energy behavior (see, e.g., Ref. 19)

$$\cot \delta_s(k) = -\frac{2}{\pi} \ln(1/ka) + \mathcal{O}(k^2), \quad (8)$$

$$k^2 \cot \delta_p(k) = -s^{-1} + \mathcal{O}(k^2 \ln k), \quad (9)$$

where we denote the phase shifts  $\delta_s \equiv \delta_0$ ,  $\delta_p \equiv \delta_1$ , etc. Here,  $a > 0$  is a 2D scattering length, while  $s$  is a 2D scattering surface (of unit length squared). Interestingly, we see that  $\cot \delta_s$  diverges logarithmically at low energies, and thus the definition of the scattering length is ambiguous (indeed several conventions are used in the literature). The logarithmic divergence means that the scattering amplitude goes to zero at zero collision energy; this is manifestly different from the 3D behavior, where the scattering amplitude at zero energy equals minus the scattering length. While the  $p$ -wave amplitude also goes to zero in this limit, we see that it does so much faster than  $f_s$ . Indeed, while the  $s$ -wave cross section is seen to diverge at zero energy, the  $p$ -wave cross section  $\sigma_p \rightarrow 0$  in this limit. The low-energy behavior has important consequences in both few- and many-body physics of the 2D gas with short-range interactions.

## 2.2. Scattering with a short-range potential

We now specialize to the typical interactions occurring in the two-component Fermi gas in 2D. We use a spin notation for the two components,  $\sigma = \uparrow, \downarrow$ ; the spin indices may denote different hyperfine states of the same atom or, in the case of a heteronuclear mixture, single hyperfine states of two different atomic species. The atomic interaction is characterized by a van der Waals range  $R_e$  much shorter than both the average interparticle spacing and the thermal wavelength. Thus we may consider the interaction to be effectively a contact,  $s$ -wave interaction, and model the two-body problem with the following Hamiltonian

$$\mathcal{H} = \sum_{\mathbf{k}} \frac{\hbar^2 k^2}{2m_r} |\mathbf{k}\rangle\langle\mathbf{k}| + \frac{1}{A} \sum_{\mathbf{k}, \mathbf{k}'} g(\mathbf{k}, \mathbf{k}') |\mathbf{k}\rangle\langle\mathbf{k}'|. \quad (10)$$

Here,  $A$  is the system area and in the following we set  $A = \hbar = 1$ . The attractive contact interaction  $g(\mathbf{k}, \mathbf{k}') \equiv \langle\mathbf{k}|\hat{g}|\mathbf{k}'\rangle$  has strength  $g < 0$  and is taken constant up to a large ultraviolet cutoff  $\Lambda \sim 1/R_e$ . The reduced mass in this two-component system is  $m_r = m_\uparrow m_\downarrow / (m_\uparrow + m_\downarrow)$ . As we are considering low-energy  $s$ -wave scattering, interactions between the same species of fermion are suppressed by Pauli exclusion.



Fig. 1. The sum of all possible repeated scattering processes of two atoms, resulting in the  $T$  matrix (black square). The circles represent the interaction  $\hat{g}$ .

The interaction between two atoms is conveniently described in terms of a  $T$  matrix, illustrated in Fig. 1, which describes the sum of repeated scattering processes between two atoms. In the center of mass frame, with incoming (outgoing) momenta of  $\pm\mathbf{k}_i$  ( $\pm\mathbf{k}_f$ ), the  $T$  matrix takes the form

$$\langle\mathbf{k}_f|\hat{T}(E+i0)|\mathbf{k}_i\rangle = \langle\mathbf{k}_f|\hat{g} + \hat{g} \frac{1}{E - \hat{H}_0 + i0} \hat{g} + \dots|\mathbf{k}_i\rangle = \frac{1}{g^{-1} - \Pi(E)}, \quad (11)$$

where the notation  $+i0$  indicates an infinitesimal positive imaginary part. Here  $\hat{H}_0$  is the non-interacting part of the Hamiltonian. The one loop polarization bubble takes the form

$$\Pi(E) = \sum_{\mathbf{q}}^{\Lambda} \langle\mathbf{q}|\frac{1}{E - \hat{H}_0 + i0}|\mathbf{q}\rangle = \sum_{\mathbf{q}}^{\Lambda} \frac{1}{E - q^2/2m_r + i0}. \quad (12)$$

Considering scattering at negative energies, it is immediately clear that the attractive contact interaction in 2D always admits a bound diatomic molecule (dimer) state in contrast to the 3D case. The energy of the bound state,  $-\varepsilon_b$  (we define  $\varepsilon_b$  positive), is determined through the pole of the  $T$  matrix, *i.e.*

$$\frac{1}{g} = \Pi(-\varepsilon_b). \quad (13)$$

This relation acts to renormalize the interaction: the integral logarithmically diverges at fixed  $\varepsilon_b$  if we take  $\Lambda \rightarrow \infty$ , however, the physics beyond the two-body problem becomes independent of  $\Lambda$  once Eq. (13) is used to replace  $g$  with the binding energy. Thus we arrive at the renormalized  $T$  matrix

$$T(E) \equiv \langle \mathbf{k}_f | \hat{T}(E + i0) | \mathbf{k}_i \rangle = \frac{1}{\Pi(-\varepsilon_b) - \Pi(E)} = \frac{2\pi}{m_r} \frac{1}{\ln(\varepsilon_b/E) + i\pi}. \quad (14)$$

As the  $T$  matrix does not depend on incoming momenta in the center of mass frame, we will simply denote it  $T(E)$ .

The on-shell scattering of two atoms at momenta  $\pm \mathbf{k}_i$  into momenta  $\pm \mathbf{k}_f$  with  $k = |\mathbf{k}_i| = |\mathbf{k}_f|$  yields the scattering amplitude through the relation  $f(\mathbf{k}) = 2m_r \langle \mathbf{k}_i | \hat{T}(k^2/2m_r) | \mathbf{k}_f \rangle$ . Then, using Eq. (7), we find that the two-body phase shift with this contact interaction takes the form  $\cot \delta_s(k) = -\frac{2}{\pi} \ln(1/ka_{2D})$ , which defines the 2D atom-atom scattering length  $a_{2D}$ .<sup>a</sup> The relation between the binding energy and the 2D scattering length is then simply

$$\varepsilon_b = \frac{1}{2m_r a_{2D}^2}. \quad (15)$$

### 2.3. Quasi-two-dimensional Fermi gases

Under realistic experimental conditions, the extent of the gas perpendicular to the plane is necessarily finite. The quasi-two-dimensional (quasi-2D) regime occurs when the confinement width is much smaller than both the interparticle spacing and the thermal wavelength, such that transverse degrees of freedom are frozen out. However, the length scale associated with the confinement to the quasi-2D geometry is necessarily much larger than the range of the van der Waals type interactions, and thus at short distances the two-body interactions are unaffected by the confinement. The

<sup>a</sup>In the literature, the alternative definition  $2e^{-\gamma} a_{2D}$  of the 2D scattering length is often employed, with  $\gamma$  the Euler gamma constant. This definition arises naturally when considering scattering from a hard disc of radius  $a_c$ , in which case  $a_{2D} = (e^\gamma/2)a_c$ .

relationship between the 2D scattering theory detailed above, and the realistic interatomic potential was considered in detail in Ref. 23. Here we present an alternative derivation of the quasi-2D scattering amplitude, and arrive at a form which is closer to that in Ref. 24.

We thus consider the experimentally relevant harmonic confinement  $V_\sigma(z) = \frac{1}{2}m_\sigma\omega_z^2z^2$  acting in the direction perpendicular to the 2D plane. While for the heteronuclear gas the confining frequency  $\omega_z$  is not necessarily the same for both species, this choice in general allows a separation of the center of mass from the relative motion and provides a major simplification of the formalism. In relative coordinates, the non-interacting two-body problem in the  $z$  direction reduces to the harmonic oscillator equation

$$\left(-\frac{1}{2m_r}\frac{d^2}{dz^2} + \frac{1}{2}m_r\omega_z^2z^2\right)\phi_n(z) = \left(n + \frac{1}{2}\right)\omega_z\phi_n(z). \quad (16)$$

Here, the motion along the  $z$  direction is clearly quantized, with a constant spacing  $\omega_z$  between energy levels. The non-interacting part of the quasi-2D Hamiltonian is thus

$$\hat{H}_0 = \sum_{\mathbf{kn}} \left[ \frac{k^2}{2m_r} + \left(n + \frac{1}{2}\right)\omega_z \right] |\mathbf{kn}\rangle\langle\mathbf{kn}|, \quad (17)$$

where  $n$  is the harmonic oscillator quantum number for the  $z$  direction. The gas is considered to be kinematically 2D if motion is restricted to the  $n = 0$  level.

To investigate two-body scattering in the quasi-2D geometry, we need to consider the bare interaction in three-dimensional space. For convenience, *in this section only*, we consider a separable 3D interaction of the form

$$g(\mathbf{k}_{3D}, \mathbf{k}'_{3D}) = \langle\mathbf{k}_{3D}|\hat{g}|\mathbf{k}'_{3D}\rangle \equiv ge^{-(k^2+k'^2+k_z^2+k_z'^2)/\Lambda^2}. \quad (18)$$

where  $k_z$  is the  $z$ -component of the 3D momentum and  $k$  is the magnitude of the inplane momentum  $\mathbf{k}$  as above. Letting the incoming (outgoing) atoms have momenta  $\pm\mathbf{k}_i$  ( $\pm\mathbf{k}_f$ ) in the plane and relative motion in the harmonic potential described by the index  $n_i$  ( $n_f$ ), the matrix elements of the 3D interaction in the quasi-2D basis are

$$\begin{aligned} \langle\mathbf{k}_fn_f|\hat{g}|\mathbf{k}_in_i\rangle &= \sum_{\mathbf{q}_{3D}\mathbf{q}'_{3D}} \langle\mathbf{k}_fn_f|\mathbf{q}_{3D}\rangle\langle\mathbf{q}_{3D}|\hat{g}|\mathbf{q}'_{3D}\rangle\langle\mathbf{q}'_{3D}|\mathbf{k}_in_i\rangle \\ &= gf_{n_f}f_{n_i}e^{-(k_i^2+k_f^2)/\Lambda^2}, \end{aligned} \quad (19)$$

where  $f_n \equiv \sum_{q_z} \tilde{\phi}_n(q_z) e^{-q_z^2/\Lambda^2}$  and  $\tilde{\phi}_n(q_z)$  is the Fourier transform<sup>b</sup> of the harmonic oscillator wave function. For the  $f$  coefficients, we then find

$$f_{2n} = (-1)^n \frac{1}{(2\pi l_z^2)^{1/4}} \frac{\sqrt{(2n)!}}{2^n n!} \frac{1}{\sqrt{1+\lambda}} \left( \frac{1-\lambda}{1+\lambda} \right)^n, \quad (20)$$

and  $f_{2n+1} = 0$ . Here  $l_z \equiv 1/\sqrt{2m_r\omega_z}$  is the harmonic oscillator length.<sup>c</sup>  $\lambda \equiv 1/(\Lambda l_z)^2$  is the (squared) ratio between the length scale of the short distance physics and the harmonic oscillator length, and is very small in typical experiments. Indeed, our approach of using a 3D interaction would be invalid if this were not the case.

We then evaluate the  $T$  matrix in a manner similar to the 2D case above:

$$\begin{aligned} \langle \mathbf{k}_f n_f | \hat{T}(E+i0) | \mathbf{k}_i n_i \rangle &= \langle \mathbf{k}_f n_f | \hat{g} + \hat{g} \frac{1}{E - \hat{H}_0 + i0} \hat{g} + \dots | \mathbf{k}_i n_i \rangle \\ &= e^{-(k_i^2 + k_f^2)/\Lambda^2} f_{n_i} f_{n_f} \frac{1}{g^{-1} - \Pi_{\text{Q2D}}(E)}. \end{aligned} \quad (21)$$

The quasi-2D polarization bubble takes the form

$$\Pi_{\text{Q2D}}(E) = \sum_{\mathbf{q}, n} |f_n|^2 \frac{e^{-2q^2/\Lambda^2}}{E - (n+1/2)\omega_z - q^2/2m_r + i0}. \quad (22)$$

The sum over  $n$  may be evaluated by changing variables to  $u = -2\lambda \frac{q^2/2m_r}{E - (n+1/2)\omega_z}$  and using<sup>d</sup>

$$\sum_{n=0}^{\infty} \frac{(2n)!}{(n!)^2} x^n = \frac{1}{\sqrt{1-4x}}. \quad (23)$$

<sup>b</sup> The harmonic oscillator wave function is

$$\phi_n(z) = \sqrt{\frac{1}{2^n n!}} \left( \frac{m_r \omega_z}{\pi} \right)^{1/4} \exp\left(-\frac{m_r \omega_z z^2}{2}\right) H_n(\sqrt{m_r \omega_z} z),$$

where  $H_n(x)$  are the Hermite polynomials.  $\phi_n(z)$  also happens to be an eigenfunction of the Fourier transform, so in momentum space it is simply

$$\tilde{\phi}_n(k_z) = (-i)^n \sqrt{\frac{2}{2^n n!}} \left( \frac{\pi}{m_r \omega_z} \right)^{1/4} \exp\left(-\frac{k_z^2}{2m_r \omega_z}\right) H_n\left(\sqrt{\frac{1}{m_r \omega_z}} k_z\right).$$

<sup>c</sup>For equal masses,  $l_z$  reduces to the usual harmonic oscillator length for the motion of the individual atoms. For a general mass ratio it differs by a factor  $\sqrt{2}$  from the usual definition of the harmonic oscillator length of the relative motion.

<sup>d</sup>While formally this approach is valid only for  $-1/4 \leq x < 1/4$ , by the analytic continuation  $E \rightarrow E + i0$  the result can be extended to all energies.

We then find

$$\Pi_{\text{Q2D}}(E) = -\frac{m_r}{(2\pi)^{3/2}l_z} \int_0^\infty \frac{du}{u+2\lambda} \frac{e^{-(-E/\omega_z+1/2)u}}{\sqrt{(1+\lambda)^2 - (1-\lambda)^2 e^{-2u}}}. \quad (24)$$

Finally, we relate this result back to the 3D physics: The interaction (18) is renormalized using the relationship<sup>e</sup> between the  $T$  matrix at vanishing energy and the 3D scattering length,  $a_s$ . Thus we arrive at the  $T$  matrix

$$\langle \mathbf{k}_f n_f | \hat{T}(E+i0) | \mathbf{k}_i n_i \rangle = e^{-(k_i^2+k_f^2)/\Lambda^2} f_{n_i} f_{n_f} \frac{2\pi l_z}{m_r} \frac{1}{\frac{l_z}{a_s} - \mathcal{F}_\lambda(-E/\omega_z + 1/2)}, \quad (25)$$

with

$$\mathcal{F}_\lambda(x) = \int_0^\infty \frac{du}{\sqrt{4\pi(u+2\lambda)^3}} \left[ 1 - \frac{e^{-xu}}{\sqrt{[(1+\lambda)^2 - (1-\lambda)^2 e^{-2u}]/(2u+4\lambda)}} \right]. \quad (26)$$

This expression reduces to that of Ref. 24 in the limit  $\lambda \rightarrow 0$ . In this case, the  $T$  matrix only depends on  $E$  and the quantum numbers in the harmonic potential, and we write

$$\langle \mathbf{k}_f n_f | \hat{T}(E+i0) | \mathbf{k}_i n_i \rangle \equiv \sqrt{2\pi} l_z f_{n_i} f_{n_f} \mathcal{T}(E), \quad (27)$$

where  $\mathcal{T}(E) \equiv \frac{\sqrt{2\pi}}{m_r} \frac{1}{\frac{l_z}{a_s} - \mathcal{F}_0(-E/\omega_z+1/2)}$  contains the entire energy dependence.

### 2.3.1. Low-energy scattering

At energies close to the scattering threshold, the function  $\mathcal{F}$  may be expanded. Specializing to the case  $\lambda = 0$ , this results in

$$\mathcal{F}_0(x) \approx \frac{1}{\sqrt{2\pi}} \ln(\pi x/B) + \frac{\ln 2}{\sqrt{2\pi}} x - \frac{\pi^2 - 12 \ln^2 2}{48\sqrt{2\pi}} x^2 + \mathcal{O}(x^3), \quad |x| \ll 1, \quad (28)$$

with  $B \approx 0.905$ ; see Refs. 23,24. This in turn yields the 2D scattering length

$$a_{2\text{D}} = l_z \sqrt{\pi/B} \exp(-\sqrt{\pi/2} l_z/a_s). \quad (29)$$

We emphasize that this result is valid across the 3D resonance, as it only requires the scattering energy to be negligible compared with the strength

<sup>e</sup>The 3D scattering length is related to the  $T$  matrix at vanishing energy by  $a_s = (m_r/2\pi) \langle \mathbf{0} | T(0) | \mathbf{0} \rangle = (m_r/2\pi) / (g^{-1} + m_r \Lambda / (2\pi)^{3/2})$ .

of the confinement. In particular, if  $|l_z/a_s| \gg 1$ , then for a large range of energies in the continuum close to the threshold, *i.e.* for  $|E - \omega_z/2| \ll \omega_z$ , the scattering amplitude may simply be approximated by

$$f(\mathbf{k}) \approx 2\sqrt{2\pi} a_s/l_z. \quad (30)$$

Thus, in this regime, the two-body interaction is approximately independent of energy, and the system may be considered scale invariant. This can have important consequences for the many-body system.

### 2.3.2. Bound state

The binding energy of the dimer is the solution of

$$\frac{l_z}{a_s} = \mathcal{F}_\lambda(\varepsilon_b/\omega_z), \quad (31)$$

where we measure the binding energy from the threshold of free relative motion of the two atoms. In contrast to the situation in 3D, where a bound state only exists for  $a_s > 0$ , under a harmonic confinement a bound state exists for a zero-range interaction of arbitrary strength. In this sense, for negative 3D scattering length, the dimer in the quasi-2D geometry is confinement induced. This may be viewed as resulting from the increase of the continuum by  $\frac{1}{2}\omega_z$ , as illustrated in Fig. 2. In the following, we focus on the case  $\lambda = 0$ , but similar behavior should hold for  $\lambda \ll 1$ .

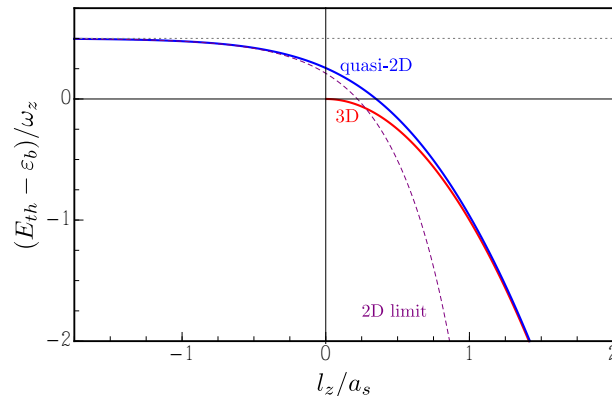


Fig. 2. The binding energy of the quasi-2D dimer with  $\lambda = 0$  (blue, solid). Also shown is the 3D dimer (red, solid), and the 2D expression  $\varepsilon_b = \frac{1}{2m_r a_{2D}^2}$  (dashed). The threshold energy  $E_{th}$  is 0 in the 3D case, and  $\omega_z/2$  in quasi-2D.

For small positive scattering length,  $l_z/a_s \gg 1$ , the 3D dimer with size  $\sim a_s$  fits well within the confining potential and is only weakly perturbed by the harmonic confinement, as illustrated in Fig. 2. As the scattering length is increased, eventually the dimer energy becomes strongly modified; for instance at the 3D resonance the binding energy takes the universal value<sup>23</sup>  $\varepsilon_b = 0.244\omega_z$ . On the other hand, in the limit of a small negative 3D scattering length,  $l_z/a_s \ll -1$ , the dimer spreads out in the 2D plane and the binding energy follows from the expansion Eq. (28). Taking only the first term, the result is seen to match the 2D expression  $\varepsilon_b = \frac{1}{2m_r a_{2D}^2}$ , *i.e.*

$$\varepsilon_b \approx \omega_z \frac{B}{\pi} \exp(\sqrt{2\pi} l_z/a_s), \quad l_z/a_s \ll -1 \quad (32)$$

as is also seen in Fig. 2. However, this expression breaks down when  $l_z/a_s > -1$ . The fact that in general  $\varepsilon_b \neq \frac{\hbar^2}{2m_r a_{2D}^2}$ , should not come as a surprise. It simply follows from the introduction of an extra length scale,  $l_z$ , into the problem, and is analogous to the problem of a narrow Feshbach resonance in the 3D gas.<sup>25</sup>

The dimer binding energy has been measured using radio-frequency (RF) spectroscopy in experiments on ultracold  ${}^6\text{Li}$  (Ref. 11) and  ${}^{40}\text{K}$  (Ref. 13) atoms subjected to a tight optical confinement. The results are shown in Fig. 3, and both experiments agree well with theory<sup>23,24</sup> across the Feshbach resonance.

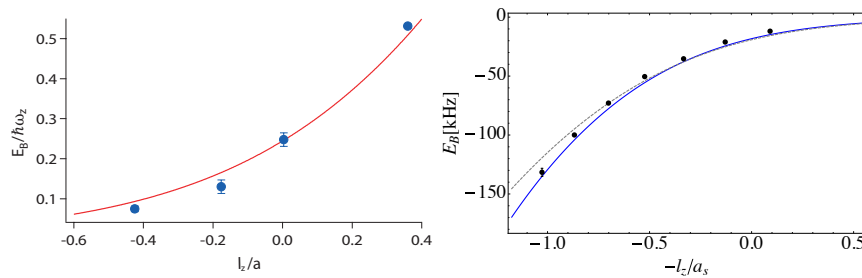


Fig. 3. (a) Experimental (blue circles) and theoretical (solid line) binding energy of a fermion pair in a gas of  ${}^6\text{Li}$  atoms.<sup>11</sup> (b) Binding energy in a  ${}^{40}\text{K}$  gas<sup>13</sup> at a confinement of  $\omega_z = 2\pi \times 75\text{kHz}$ . The experimental result (black circles) is compared with the theoretical prediction at zero effective range (gray, dashed), and finite effective range (blue, solid), according to the equation for the binding energy modified by the 3D effective range  $r_{\text{eff}}$ ,  $\frac{l_z}{a_s} + \frac{r_{\text{eff}}}{2l_z} (\varepsilon_b/\omega_z - 1/2) = \mathcal{F}_0(\varepsilon_b/\omega_z)$ .

Reprinted figure in (a) with permission from: A. T. Sommer, L. W. Cheuk, M. J. H. Ku, W. S. Bakr, and M. W. Zwierlein, *Phys. Rev. Lett.* **108**, 045302 (2012). Copyright 2012 by the American Physical Society.

#### 2.4. Confinement induced resonances

One consequence of confining the gas to lower dimensions is the appearance of so-called *confinement induced resonances*. At the simplest level, these refer to any region of resonantly enhanced two-body scattering resulting from the confinement. However, the situation in 2D is slightly more subtle, given that the purely 2D system (where we effectively have  $l_z = 0$ ) already exhibits an enhancement of the scattering amplitude for energy  $E \sim \varepsilon_b$ , as can be seen from the  $T$  matrix  $T(E) = \frac{2\pi}{m_r} \frac{1}{\ln(\varepsilon_b/E) + i\pi}$ . Thus, it is important to make a distinction between enhanced scattering that can arise from 2D kinematics, and resonances that only result from the finite extent of the gas in the confined direction.

An example of the latter case is the confinement induced resonance associated with quasi-1D systems.<sup>26,27</sup> Here, a resonance occurs when a virtual bound state (arising from the excited levels of the transverse confinement) crosses the 1D atom-atom scattering threshold. This process can be captured with a simplified two-channel model<sup>27</sup>

$$\mathcal{H}_{\text{Q1D}} = \sum_k \frac{k^2}{2m_r} |k\rangle\langle k| + \nu |b\rangle\langle b| + \alpha \sum_k (|k\rangle\langle b| + |b\rangle\langle k|), \quad (33)$$

where  $|b\rangle$  corresponds to the virtual “closed channel” bound state associated with the excited states in the harmonic confinement,  $\nu$  is the energy of this state with respect to the continuum threshold, and  $\alpha$  is the coupling between  $|b\rangle$  and the scattering states  $|k\rangle$  in 1D. Here, we neglect the interactions between the 1D scattering states and we take  $\alpha$  and  $\nu$  to be independent parameters.<sup>f</sup> In general, this model leads to energy-dependent interactions, but for zero-energy scattering we have an effective 1D contact potential  $g_{\text{1D}}\delta(x)$  with interaction strength  $g_{\text{1D}} = -\alpha^2/\nu$ . Thus, we obtain a scattering resonance where  $g_{\text{1D}} \rightarrow \pm\infty$  when  $\nu \rightarrow 0^\mp$ . Note that this does not signal the appearance of a two-body bound state like in the 3D case where the scattering length diverges ( $1/a_s = 0$ ). Instead, Eq. (33) always yields a two-body bound state with binding energy  $\varepsilon_b$  satisfying the condition  $\sqrt{2}(\nu + \varepsilon_b)/\alpha^2 = \sqrt{m_r/\varepsilon_b}$ . Moreover, we see that  $\varepsilon_b$  is finite at the resonance  $\nu = 0$ , thus illustrating how this resonance is a feature of confinement that goes beyond the behaviour in a purely 1D system.

On the other hand, such a confinement induced resonance does not exist in the quasi-2D system. If we consider the two-channel model (33) in 2D,

<sup>f</sup>In the real quasi-1D system,  $\alpha$  and  $\nu$  are not independent, as is apparent from the two-channel model in Ref. 27.

where we have  $|\mathbf{k}\rangle$  instead of  $|k\rangle$ , then we obtain the modified  $T$  matrix

$$T(E) = \frac{2\pi}{m_r} \left[ \ln \left( \frac{1}{2m_r a_{2D}^2 E} \right) + \frac{2\pi E}{m_r \alpha^2} + i\pi \right]^{-1}, \quad (34)$$

with  $a_{2D} = \Lambda^{-1} \exp(\pi\nu/m_r\alpha^2)$ . This is essentially the quasi-2D  $T$  matrix  $\mathcal{T}(E)$  expanded up to linear order in  $E/\omega_z$ . Comparing with the terms in the expansion (28) yields  $\omega_z = m_r\alpha^2 \ln(2)/2\pi$ . However, this modification to the  $T$  matrix only shifts the scattering enhancement away from  $E \sim \varepsilon_b$  (where  $T(-\varepsilon_b)^{-1} = 0$ ). The resonance still remains strongly energy dependent like in the purely 2D case. However, it can still be characterized experimentally: For a Boltzmann gas in the 2D limit, the scattering is enhanced for temperature  $T \sim \varepsilon_b$ . The requirement  $T \ll \omega_z$  then implies that  $\varepsilon_b \ll \omega_z$  and thus the resonance occurs on the attractive side of the 3D Feshbach resonance,  $a_s < 0$ , according to Fig. 2.

Additional resonances will appear when there are anharmonicities in the confining potential, as is usually the case in experiments employing an optical lattice. Any anharmonicity inevitably leads to coupling between two-body states with different center-of-mass harmonic quantum numbers  $N$ . In particular, there will (for instance) be a coupling between scattering states  $|\mathbf{k}\rangle$  with  $N = 0$  and two-body bound states with  $N = 2$ , due to the selection rules. This leads to increased molecule formation when  $\varepsilon_b$  is close to  $2\hbar\omega_z$ , which in turn leads to enhanced losses due to subsequent collisions with other particles. Such an ‘‘inelastic’’ confinement induced resonance was recently observed experimentally in low-dimensional geometries.<sup>28-30</sup> In the absence of effective range corrections, the inelastic resonance in the quasi-2D geometry arising from the above mentioned coupling occurs when  $l_z/a_s \simeq 1.2$ , in contrast to the resonance derived from 2D kinematics.

### 3. Universal few-body physics in a 2D Fermi gas

Recent years have brought a wealth of experiments exploring few- and many-body physics in ultracold atomic gases — see, for instance, Refs. 24,25 and references therein. In particular, it has enabled the study of *universal* few-body physics, since the low-energy scattering is insensitive to the details of the short-range interactions, and this in turn has major consequences for the many-body system. For instance, in the regime where a dimer exists, a knowledge of the dimer-dimer<sup>31</sup> and atom-dimer<sup>32</sup> scattering lengths is necessary for a complete description of the balanced<sup>33</sup> and polarized<sup>34</sup> Fermi gases. The properties of few-body inelastic processes furthermore explains

the exceptional stability of 3D Fermi gases close to the unitary limit.<sup>31</sup> The experimental exploration of 2D Fermi gases is still ongoing, but few-body physics has already played an important role in understanding many-body phenomena, as can be seen in Secs. 4 and 5.

While experiments have thus far focussed on the equal-mass case, heteronuclear Fermi-Fermi mixtures with mass imbalance promise to provide even richer few-body phenomena. For instance, in 1D it has been shown that when the mass ratio exceeds one, trimers (bound states of 1 light atom, 2 heavy atoms) can form.<sup>35</sup> This can lead to a Luttinger liquid of trimers in the polarized gas, while more exotic bound states such as tetramers (1,3), pentamers (2,3), etc., can also exist at higher mass ratios.<sup>36</sup> Similarly, in 2D<sup>37</sup> and 3D,<sup>38</sup> trimers are predicted to exist above a mass ratio of 3.3 and 8.2, respectively, which can lead to a trimer phase in the highly polarized Fermi gas.<sup>39</sup> Additionally, tetramers have been predicted in 1D,<sup>36,40</sup> 2D,<sup>41</sup> and 3D.<sup>42</sup> These bound states all share the property of being universal, in the sense that their binding energy is a multiple of the dimer binding energy without the need for additional parameters. For a recent review of bound few-body states, we refer the reader to Ref. 43.

Thus far, the only heteronuclear Fermi-Fermi mixture where tunable short-range interactions have been experimentally demonstrated<sup>44–46</sup> is  $^{40}\text{K}$ - $^6\text{Li}$  with a mass ratio of 6.64. However, the periodic table offers ample opportunity for exploring additional mass ratios, while the possibility to tune the effective mass ratio using optical lattices also exists. Thus, for the theoretical approach employed in this section, we may consider the mass ratio to be a free parameter.

Finally, we note that there is a special class of states — the well-known Efimov states — where the 3D physics is manifestly different from the situation in confined geometries.<sup>47</sup> Efimov states have been observed experimentally as sharp peaks in the loss rate in both bosonic<sup>48</sup> and (three-component) fermionic<sup>49</sup> systems. In the heteronuclear fermionic system in 3D, the Efimov effect occurs for (2,1) trimers above a mass ratio of 13.6 and for (3,1) tetramers<sup>50</sup> for mass ratios exceeding 13.4. On the other hand, it is known that Efimov's scenario does not occur in the 1D and 2D geometries.<sup>51</sup> Very recently it was shown that under realistic experimental conditions, if Efimov trimers exist in 3D, these will impact the few-body physics in a strongly confined geometry.<sup>52</sup> However, in the following we ignore this effect and focus either on the idealized 2D scenario and/or on mass ratios for which the Efimov effect is absent.

### 3.1. Equal mass fermions



Fig. 4. Illustration of the Skorniakov–Ter-Martirosian equation which governs the interaction of an atom (straight line) with a dimer (wavy line).  $\tilde{f}$  is the atom-dimer scattering amplitude.

We now discuss the three- and four-body problem in a homonuclear gas. The first of these plays an important role in accurately determining the energy of an impurity atom immersed in a Fermi sea — see Sec. 6. It is also of practical importance when considering inelastic processes such as three-body recombination,<sup>53</sup> the process whereby three atoms collide to produce an atom and a dimer. The dimer-dimer scattering length, on the other hand, is important in describing the many-body system in the limit of tightly bound pairs, as shown in Sec. 4. In the present discussion we confine ourselves to on-shell scattering properties.

The interaction between a spin- $\uparrow$  atom with an  $\uparrow\downarrow$  dimer may be investigated with the Skorniakov–Ter-Martirosian (STM) equation introduced in the context of neutron-deuteron scattering.<sup>32</sup> The atom-dimer scattering arises from the repeated exchange between identical spin- $\uparrow$  atoms of the spin- $\downarrow$  atom, and the STM integral equation yields the sum of diagrams with any number of such exchanges as illustrated in Fig. 4. We are interested in the on-shell scattering amplitude, and thus we let the incoming [outgoing] atom and dimer have four-momentum  $(\mathbf{k}, \epsilon_{\mathbf{k}\uparrow})$  and  $(-\mathbf{k}, E - \epsilon_{\mathbf{k}\uparrow})$  [ $(\mathbf{p}, \epsilon_{\mathbf{k}\uparrow})$  and  $(-\mathbf{p}, E - \epsilon_{\mathbf{k}\uparrow})$ ], respectively, with  $E = k^2/2m_{\text{ad}} - \epsilon_b$  such that the incoming dimer is on shell. Here the single particle kinetic energy is  $\epsilon_{\mathbf{k},\sigma} = k^2/2m_\sigma$ , where  $m_\sigma$  is the mass.  $m_{\text{ad}}$  is the atom-dimer reduced mass  $m_{\text{ad}}^{-1} = m_\uparrow^{-1} + M^{-1}$ , with  $M = m_\uparrow + m_\downarrow$ . The on-shell condition  $|\mathbf{k}| = |\mathbf{p}|$  is taken at the end of the calculation. With these definitions, the STM equation takes the form of an integral equation<sup>53</sup>

$$\tilde{f}_\ell(k, p) = -h(k, p) \left[ g_\ell(k, p) - \int \frac{q dq}{2\pi} \frac{g_\ell(p, q) \tilde{f}_\ell(k, q)}{q^2 - k^2 - i0} \right], \quad (35)$$

where we note that the atom-dimer scattering preserves angular momentum, allowing a decoupling of  $\tilde{f}(\mathbf{k}, \mathbf{p})$  into its partial wave components. The scattering amplitude then follows from taking the on-shell condition  $f_\ell(k) = \tilde{f}_\ell(k, k)$ .  $g_\ell$  is the partial wave projection of the spin- $\downarrow$  propagator

and  $h$  is proportional to the two-body  $T$  matrix.<sup>8</sup>

From the resulting scattering amplitude, the low-energy scattering properties such as the  $s$ -wave scattering length and the  $p$ -wave scattering area (see Sec. 2.1) may be extracted. For equal masses, we find:<sup>53</sup>

$$a_{\text{ad}} \approx 1.26a_{2\text{D}}, \quad s_{\text{ad}} \approx -2.92a_{2\text{D}}^2. \quad (37)$$

Thus, the  $s$ -wave scattering is repulsive at low energies while the  $p$ -wave scattering is attractive in this case. The scattering amplitude furthermore gives access to the partial wave cross sections, which are shown for  $s$ - and  $p$ -waves in Fig. 5(c). While the  $s$ -wave cross section is apparently completely described in terms of the scattering length, interestingly we note that the  $s$ - and  $p$ -wave cross sections are comparable for collision energies of the order of the binding energy. This is unlike the 3D case,<sup>54</sup> and is due to the weaker centrifugal barrier between identical fermions in 2D. Thus three-body correlations are likely to be more important in 2D than in 3D.

Both the atom-dimer and the dimer-dimer scattering lengths have been extracted from a quantum Monte Carlo (QMC) calculation of the excitation gap in the BEC regime.<sup>55</sup> The result was  $a_{\text{ad}} = 1.7(1)a_{2\text{D}}$  and  $a_{\text{dd}} = 0.55(4)a_{2\text{D}}$ . Note that these relations do not depend on the definition of the scattering length. The discrepancy between the exact result in Eq. (37) and the QMC result is likely to be due to the fact that the extraction of  $a_{\text{ad}}$  from the data relied on an equation of state that was only logarithmically accurate. On the other hand, the dimer-dimer scattering length is in perfect agreement with the exact few-body calculation of Petrov et al.:<sup>56</sup>  $a_{\text{dd}} \approx 0.56a_{2\text{D}}$ .

### 3.2. Heteronuclear Fermi gas

The three-body problem in a heteronuclear 2D Fermi gas with short-range interparticle interactions was first studied by Pricoupenko and Pedri.<sup>37</sup> Remarkably, even in the absence of Efimov physics, they still found that two heavy fermionic atoms and a light atom can form an ever increasing number of trimers as the mass ratio is increased. However, at any given mass ratio,

<sup>8</sup>The projection of the propagator of the spin- $\downarrow$  fermion onto the  $\ell$ 'th partial wave is

$$g_\ell(p, q) = \int_0^{2\pi} \frac{d\phi}{2\pi} \frac{\cos(\ell\phi)}{E - \epsilon_{\mathbf{k}\uparrow} - \epsilon_{\mathbf{q}\uparrow} - \epsilon_{\mathbf{p}+\mathbf{q}\downarrow} + i0}, \quad (36)$$

with  $\phi$  the angle between  $\mathbf{p}$  and  $\mathbf{q}$ . We also define  $h(k, p) \equiv (k^2 - p^2)T(E - p^2/2m_{\text{ad}})$  [see Eq. (14)] in order to separate out the simple pole of the two-particle propagator occurring at  $|\mathbf{k}| = |\mathbf{p}|$ .

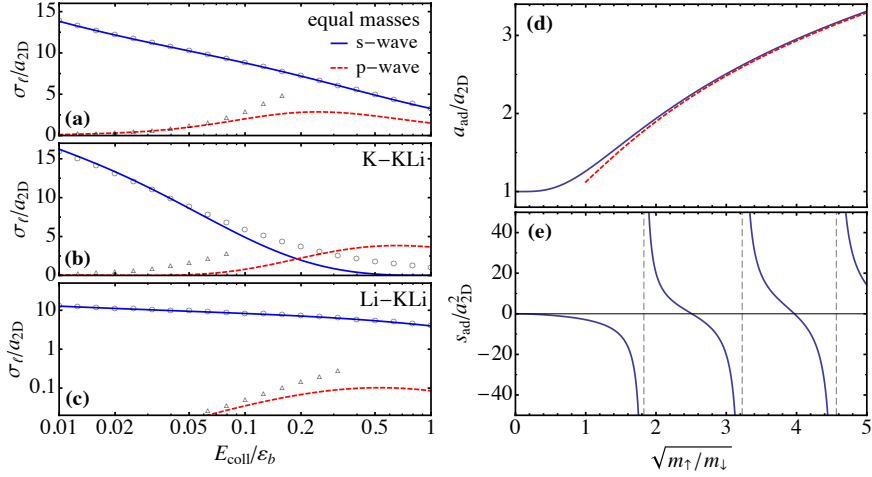


Fig. 5. (a,b,c)  $s$ - and  $p$ -wave atom-dimer cross sections as a function of collision energy  $E_{\text{coll}} \equiv k^2/2M + k^2/2m_\uparrow$  for equal masses and for the K-Li mixture. The circles [triangles] correspond to the low-energy expansion, see Sec. 2.1, using the atom-dimer scattering length [area]. Note the log-scale used in (c). (d) Atom-dimer scattering length and (e) area as a function of mass ratio. In (d) the dashed line is the asymptotic behavior at large mass ratio<sup>53</sup> and in (e) the vertical dashed lines indicate the appearance of trimers. The figure is taken from Ref. 53.

the number of trimers in the spectrum was found to be finite. In Refs. 53,57 it was argued that the appearance of trimers was due to an effective  $1/R$  potential in odd partial waves between heavy atoms at a separation  $R$ , mediated by the light atom.<sup>h</sup> Consequently, at large mass ratios, the spectrum of bound states is hydrogen-like.

Signatures of trimer formation are clearly seen in the atom-dimer scattering properties, Fig. 5. Here the  $p$ -wave scattering surface diverges at the mass ratios<sup>37</sup>  $m_\uparrow/m_\downarrow = 3.33, 10.41, \text{etc.}$ , when a trimer state crosses the atom-dimer scattering threshold. Thus, the  $p$ -wave interaction becomes resonant at the crossing, and while the K-Li mass ratio of 6.64 is in-between the appearance of bound states in 2D, we still observe that the  $p$ -wave cross section in K-KLi scattering dominates at a collision energy comparable to  $\varepsilon_b$ . On the other hand, the scattering length increases monotonically with

<sup>h</sup>As the heavy atoms are identical fermions, the wavefunction of the light atom is necessarily antisymmetric (symmetric) for scattering in even (odd) partial waves. The antisymmetric state suppresses tunneling of the light atom between heavy atoms, and as a result the effective potential between the heavy atoms is repulsive (attractive) in even (odd) partial waves. Consequently, trimers only form in odd partial waves.

mass ratio.

The strong atom-dimer scattering in higher partial waves due to the proximity of trimers may be investigated using a mixture of heavy atoms and heavy-light dimers, as in a recent experiment using a K-Li mixture in 3D.<sup>58</sup> In such a mixture, the energy shift of an atom due to the interaction with dimers is proportional to the real part of the atom-dimer scattering amplitude, and may be directly accessed by radiofrequency spectroscopy.

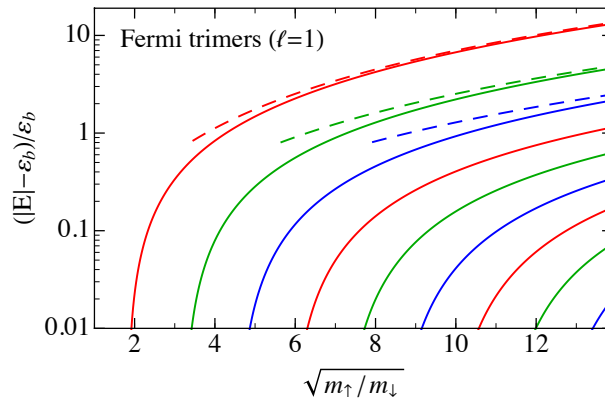


Fig. 6. The spectrum of  $p$ -wave trimers<sup>37</sup> as a function of mass ratio, taken from Ref. 53. The dashed lines are the large mass ratio asymptotic hydrogen-like energy levels (40).

Turning now to trimers, in Fig. 6 we show their spectrum obtained from Eq. (35).<sup>37,53</sup> To shed light on the appearance of trimers at large mass ratio, it is instructive to turn to the Born-Oppenheimer approximation (in the following discussion we follow Ref. 53, but see also Ref. 57): Assume that the wavefunction of the light atom at position  $\mathbf{r}$  adiabatically adjusts itself to the positions of the heavy atoms,  $\pm \mathbf{R}/2$ . Then the wavefunction of the light atom is

$$\psi_{\mathbf{R}}(\mathbf{r}) \propto K_0(\kappa_{\mp}(R)|\mathbf{r} - \mathbf{R}/2|) \mp K_0(\kappa_{\mp}(R)|\mathbf{r} + \mathbf{R}/2|), \quad (38)$$

where the upper (lower) sign describes even (odd) partial wave scattering. The modified Bessel function of the second kind  $K_0(\kappa_{\mp}(R)r)$  is the decaying solution of the free single-particle Schrödinger equation with energy  $\epsilon_{\mp}(R) = -\kappa_{\mp}(R)^2/2m_{\downarrow}$ . The energy of the light atom as a function of separation of heavy atoms is determined from the Bethe-Peierls boundary condition in 2D:  $[\tilde{r}\psi'(\tilde{r})/\psi]_{\tilde{r}\rightarrow 0} = 1/\ln(\tilde{r}/(2e^{-\gamma}a_{2D}))$  where  $\tilde{\mathbf{r}} = \mathbf{r} \pm \mathbf{R}/2$ .

This leads to the implicit equation

$$\ln \left( -\frac{\epsilon_{\mp}(R)}{\epsilon_b} \right) = \mp 2K_0 \left( \sqrt{-\frac{\epsilon_{\mp}(R)}{\epsilon_b} \frac{R}{a_{2D}}} \right). \quad (39)$$

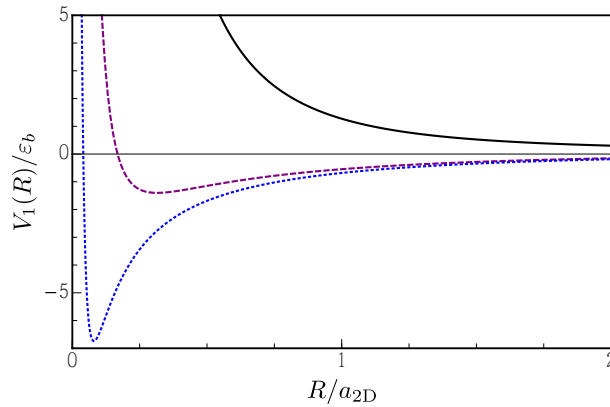


Fig. 7. Born-Oppenheimer effective  $p$ -wave potential between two heavy fermions mediated by a light atom. Top to bottom are the potentials for mass ratios  $m_{\uparrow}/m_{\downarrow} = 1, 3.33$  (critical mass ratio for the appearance of trimers), and 6.64 (the  $^{40}\text{K}$ - $^6\text{Li}$  mass ratio).

The energy levels of the light atom act as potential surfaces for the motion of the heavy atoms. In the case of  $p$ -wave scattering, the effective potential  $V_p(R) = \epsilon_+(R) - \epsilon(\infty) + 1/(m_{\uparrow}R^2)$  including the centrifugal barrier is shown in Fig. 7. The potential is measured from the limiting value of the potential at large separation,  $\epsilon(\infty)$ , which reduces to  $-\epsilon_b$  at large mass ratios. We see that when the mass ratio is small, the effective potential is always repulsive. On the other hand, the potential develops an attractive well as the mass ratio is increased and it is in this well that trimers can form. For a large mass ratio, the odd partial wave potential becomes  $\epsilon_+(R) \approx -\frac{2\epsilon_b}{e^{\gamma}} \frac{a_{2D}}{R}$  at short distances,  $R \ll a_{2D}$ . This potential is hydrogen-like and thus the spectrum of the deepest bound trimers is<sup>59</sup> (appropriately shifted by the dimer binding energy)

$$E_n = -\frac{m_{\uparrow}}{e^{2\gamma}m_{\downarrow}} \frac{\epsilon_b}{2(n+1/2)^2} - \epsilon_b, \quad (40)$$

with integer quantum number  $n \geq \ell$ . In Fig. 6 this asymptotic expression is shown to agree well with the exact results for the deepest bound trimers. The expression (40) makes it clear that deeply bound trimers in

different partial wave channels are quasi-degenerate<sup>i</sup>, as observed in Ref. 37. Remarkably, at very short distances, the  $1/R^2$  behavior of the centrifugal barrier always dominates. This has the important consequence that the trimers may be expected to be quite long-lived, as they are large (of size  $a_{2D}$ ) and the constituent atoms do not approach each other easily. This is completely unlike the 3D case, where the mediated potential also goes as  $1/R^2$  and the Efimov effect occurs at large mass ratio.

The number of bound states at any given mass ratio may be approximated<sup>53</sup> by noting that it is proportional to the number of nodes of the zero-energy wavefunction. The trimers exist in the hydrogen-like part of the effective potential,  $R \lesssim a_{2D}$ , and in this regime the relative wavefunction of the heavy particles is proportional to the Bessel function  $J_{2\ell}(2\sqrt{e^{-\gamma}(m_{\uparrow}/m_{\downarrow})R/a_{2D}})$ . The wavefunction acquires an additional node each time the argument increases by  $\pi$ , and consequently the number of trimers is proportional to  $\sqrt{m_{\uparrow}/m_{\downarrow}}$ . This feature is clearly observed in Figs. 5(b) and 6. Using a semi-classical approximation, Ref. 57 found that in the limit of a large mass ratio the number of bound states is approximately  $0.73\sqrt{m_{\uparrow}/m_{\downarrow}}$ .

### 3.2.1. Bound states of three identical fermions and a light atom

In fact, it is also possible for three identical fermionic atoms to bind together owing to the attractive interaction mediated by a light atom.<sup>41</sup> The critical mass ratio for the binding of this tetramer is  $m_{\uparrow}/m_{\downarrow} \approx 5.0$ , and like the trimer, the tetramer binds in the  $p$ -wave state. It remains to be seen whether more tetramers bind with increasing mass ratio, as in the case of trimers, and whether they also form in higher partial waves. These questions may presumably be answered within the Born-Oppenheimer approximation. Interestingly, the tetramer is very close in energy to a trimer plus a free atom, and this should lead to strong atom-trimer interactions in the 2D heteronuclear Fermi gas for species close to the critical mass ratio. A similar bound state has been predicted in 3D above a mass ratio of 9.5 (Ref. 42) and in 1D above the mass ratio 2.0 (Ref. 40). It is likely that these states are continuously connected as the system is tuned between the different geometries.

<sup>i</sup>In fact, as the spectrum of even partial wave trimers consisting of two identical (non-interacting) heavy bosons and a light atom are determined from the same effective potential, these are also quasi-degenerate with the fermionic trimers arising in odd partial waves.

### 3.3. Universal bound states in realistic experiments: Going beyond the 2D limit

As discussed previously, realistic experiments on 2D Fermi gases involve the presence of a tight confinement and the length scale corresponding to this confinement always greatly exceeds the range of the interatomic interactions. Thus, it is important to relate the universal 2D few-body physics presented above to realistic experiments, taking into account the 3D nature of the interactions.

In Sec. 2.3, the effects of confinement on the two-body interaction were described. As should be clear from that discussion, the 2D limit of the universal bound states described thus far constitutes the regime where the 3D scattering length is negative and much smaller than the confinement length, *i.e.*  $l_z/a \ll -1$ ; in this limit we have a dimer whose binding energy  $\varepsilon_b$  is much smaller than the level spacing in the harmonic trap,  $\omega_z$ , and as the energies of the universal bound states scale with  $\varepsilon_b$  we may be in a regime where these are also negligible compared with  $\omega_z$ .

It is natural to ask what happens to the bound trimers and tetramers described above, once the confinement is relaxed. This question was investigated in Ref. 41 under the assumption that both species of atoms are confined by a harmonic trap of the same frequency. It was shown that the minimum energy  $E$  in the problem of  $N$  spin- $\uparrow$  atoms and a single spin- $\downarrow$  atom in the center of mass frame corresponds to a non-trivial solution of

$$\chi_{\mathbf{k}_2 \dots \mathbf{k}_N}^{n_0 \dots n_N} = - \sum_{\mathbf{k}'_1, n'_0, n'_1} \frac{T_{n_0 n_1}^{n'_0 n'_1}(\mathbf{k}_0 + \mathbf{k}_1, E_0 + \epsilon_{\mathbf{k}_1 n_1 \uparrow})}{E_0 + \epsilon_{\mathbf{k}_1 n_1 \uparrow} - \epsilon_{\mathbf{k}_0 + \mathbf{k}_1 - \mathbf{k}'_1, n'_0 \downarrow} - \epsilon_{\mathbf{k}'_1, n'_1 \uparrow}} \times \left\{ \chi_{\mathbf{k}'_1 \mathbf{k}_3 \dots \mathbf{k}_N}^{n'_0 n_2 n'_1 n_3 \dots n_N} + \dots + \chi_{\mathbf{k}_2 \dots \mathbf{k}_{N-1} \mathbf{k}'_1}^{n'_0 n_N n_2 \dots n_{N-1} n'_1} \right\}. \quad (41)$$

Here the single particle energies are  $\epsilon_{\mathbf{k}n\sigma} = k^2/2m_\sigma + n\omega_z$ ,  $\mathbf{k}_1, \dots, \mathbf{k}_N$  are the initial momenta of the spin- $\uparrow$  atoms, while  $\mathbf{k}_0$  and  $E_0 \equiv E - \sum_{i=1}^N \epsilon_{\mathbf{k}_i n_i \uparrow}$  are the initial momentum and energy of the spin- $\downarrow$  atom. Since we consider scattering in the center of mass frame of the 2D motion, we have  $\mathbf{k}_0 = -\sum_i^N \mathbf{k}_i$ . The energy is measured from the  $N+1$  atom threshold ( $N+1$ ) $\omega_z/2$ .  $T_{n_0 n_1}^{n'_0 n'_1}$  is related to the quasi-two-dimensional  $T$  matrix<sup>j</sup> Eq. (25)

<sup>j</sup> Specifically,

$$T_{n_0 n_1}^{n'_0 n'_1}(\mathbf{q}, \epsilon) = \sum_{n_r, n'_r} C_{nn_r}^{n_0 n_1}(m_\downarrow, m_\uparrow) C_{nn'_r}^{n'_0 n'_1}(m_\downarrow, m_\uparrow) \times \sqrt{2\pi} l_z f_{n_r} f_{n'_r} \mathcal{T} \left( \epsilon - n\omega_z + \frac{1}{2}\omega_z - \frac{q^2}{2M} \right).$$

via a change of basis to the relative and center of mass motion in the two-atom problem. The minus sign on the *r.h.s.* arises from the antisymmetry of the vertex  $\chi$  under exchange of identical fermions.

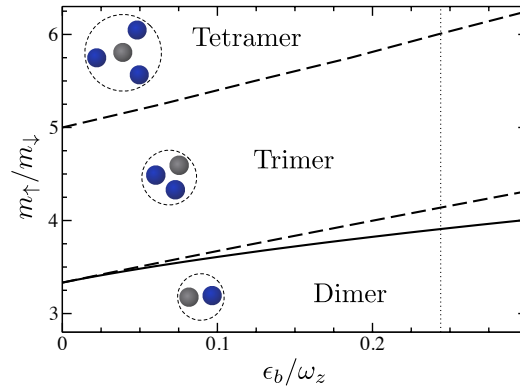


Fig. 8. The critical mass ratio for the formation of trimers and tetramers away from the 2D limit of  $\varepsilon_b/\omega_z = 0$ , assuming the two species are confined by a harmonic potential characterized by the same frequency  $\omega_z$ . The solid line is the result of exact calculations, while the dashed lines employ a two-channel model for the confinement. The vertical dotted line corresponds to the position of the 3D resonance. The figure is taken from Ref. 41.

While Eq. (41) is quite compact and in principle allows one to capture the crossover from 2D to 3D physics, its numerical solution quickly becomes prohibitive with increasing number of atoms. Instead, the departure from the 2D limit of the few-body bound states described above may be considered in a perturbative expansion<sup>41</sup> in the parameter  $\varepsilon_b/\omega_z$ . This amounts to expanding the function  $\mathcal{F}$  in Eq. (26) to linear order in  $|E|/\omega_z$  while setting all harmonic oscillator quantum numbers to zero in Eq. (41), and follows from the antisymmetry of the vertex  $\chi$  under exchange of any of the  $N$  spin- $\uparrow$  atoms. For definiteness we write down here the resulting equation which determines the trimer binding energy in the 3-body problem in the limit of strong confinement:

$$\begin{aligned} & \frac{m_r}{2\pi} \left( \ln \left[ \frac{-E + k_2^2/2m_{\text{ad}}}{\varepsilon_b} \right] - \ln(2) \frac{\varepsilon_b + E - k_2^2/2m_{\text{ad}}}{\omega_z} \right) \chi_{\mathbf{k}_2} \\ &= \sum_{\mathbf{k}_1} \frac{\chi_{\mathbf{k}_1}}{E - \epsilon_{\mathbf{k}_1\uparrow} - \epsilon_{\mathbf{k}_2\uparrow} - \epsilon_{\mathbf{k}_1+\mathbf{k}_2\downarrow}}. \end{aligned} \quad (42)$$

The Clebsch-Gordan coefficients  $C_{nn_r}^{n_0n_1}(m_\downarrow, m_\uparrow) \equiv \langle n_0n_1 | nn_r \rangle$  were obtained in Ref. 60 and vanish unless  $n_0 + n_1 = n + n_r$ .

Figure 8 shows the behavior of the critical mass ratio of the trimer and tetramer as the system is tuned away from the strict 2D limit. We observe that the critical mass ratio increases, consistent with the corresponding results in 3D.<sup>38,42</sup> This behavior is likely due to the increased centrifugal barrier for  $p$ -wave pairing in 3D. Interestingly, at unitarity the critical mass ratio for tetramer formation in this quasi-2D geometry is below the K-Li mass ratio.

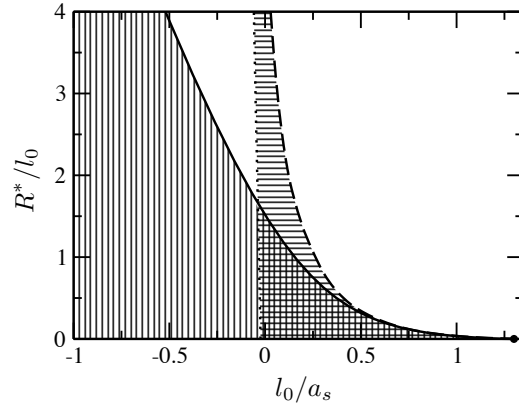


Fig. 9. Confinement induced trimers for the K-K-Li system: The solid line corresponds to the trimer formation threshold when both species are confined by a harmonic potential of the same frequency, while the dashed line assumes confinement of the heavy atom only. Three atoms bind to a trimer in the shaded regions.  $l_0 = 1/\sqrt{m\uparrow\omega\uparrow}$  is the confinement length of the heavy atoms, while  $R^* = -r_e/2 > 0$  is a length scale parameterizing the width of the Feshbach resonance ( $r_e$  is the effective range). The figure is taken from Ref. 54.

From the point of view of experiment, it is useful to determine the precise conditions under which K and Li atoms will form such stable few-body bound states. In the above we assumed that the confinement frequencies of the two atomic species were identical, and while this can be engineered using species dependent optical lattices this need not be the case. However, even in the case where the frequencies are species dependent, few-body properties may only be weakly affected by this dependence; for instance, once the light atom oscillator length greatly exceeds the two-body bound state, the light atom is essentially confined by its interaction with the heavy atoms. This is clearly illustrated in Fig. 9 which shows the critical confinement length needed to confine two K atoms and a Li atom into a trimer, and thus to make the atom-dimer interaction resonant in the  $p$ -wave channel.<sup>54</sup>

This result additionally takes into account the fact that Li-K interspecies Feshbach resonances are narrow in magnetic field width, associated with a weak coupling to the closed channel molecular state. This latter effect tends to suppress the attraction mediated by the light atom, and introduces an additional complication in the quest to obtain these few-body states.

### **3.4. Identical fermions with $p$ -wave interactions — Super Efimov states**

Finally, we mention that the three-body problem of identical fermions in 2D interacting via a  $p$ -wave Feshbach resonance has also been investigated.<sup>61,62</sup> Ref. 61 studied the atom-dimer scattering problem and found that the  $T$ -matrix at a momentum  $\mathbf{p}$  is  $T(p) \propto \cos \left[ \frac{4}{3} \ln \ln \Lambda/p + \phi \right]$  where  $\phi$  is a phase and  $\Lambda$  a momentum cutoff. Remarkably, this  $T$ -matrix displays a discrete scale invariance reminiscent of the Efimov effect, with a three-body parameter set by the momentum cutoff. However, unlike the standard Efimov effect, the scaling is here characterized by a double exponential factor, which quickly becomes enormous. More recently, Ref. 62 studied the bound state problem and found the existence of trimers with a doubly exponential scaling of the binding energy, naming these super Efimov states.

## **4. Ground state of the many-body system**

### **4.1. The BCS-BEC crossover**

We now turn to the behavior of the many-body system, where one has a finite density of spin-up and spin-down fermions, denoted  $n_{\uparrow} = N_{\uparrow}/A$  and  $n_{\downarrow} = N_{\downarrow}/A$ , respectively. At zero temperature, in the absence of interactions, each type of fermion forms a filled Fermi sea with radius in momentum space given by the Fermi wave vector  $k_{F\sigma} = \sqrt{4\pi n_{\sigma}}$  in 2D. For an attractive interspecies interaction, such as the short-range potential described in Eq. (10), a variety of pairing phenomena is expected to occur in the Fermi system. In particular, for the case of equal densities,  $k_{F\uparrow} = k_{F\downarrow} \equiv k_F$ , the ground state can smoothly evolve from the BCS regime of Cooper pairing to a Bose-Einstein condensate (BEC) of tightly bound dimers with increasing interaction strength. This constitutes the celebrated BCS-BEC crossover, which was theoretically predicted several decades ago,<sup>63,64</sup> and first successfully realised in 3D cold-atom experiments in 2004 (Refs. 65,66).

The different regimes of pairing are generally parameterized by the dimensionless quantity  $k_F l$ , where  $l$  is a typical length scale that defines the

strength of the interaction. For short-range  $s$ -wave interactions in 3D,  $l$  is simply the  $s$ -wave scattering length  $a_s$ , while in 2D it corresponds to  $a_{2D}$ , which is related to the size of the two-body bound state and is defined in Sec. 2.2. Thus, in 2D, the BCS and BEC regimes correspond, respectively, to  $k_F a_{2D} \gg 1$  and  $k_F a_{2D} \ll 1$ , where the pair size is much greater than the inter-particle spacing in the former case, and much smaller in the latter. The dimensionless parameter  $k_F a_{2D}$  automatically implies that there are two ways of achieving the BCS-BEC crossover: by varying the interactions or by varying the density. Note, however, that this is not the case for 3D contact interactions, since a two-body bound state does not exist for arbitrarily weak attraction, and the scattering length can change sign. Thus, in 3D, one cannot traverse the entire crossover by varying density alone.

This section will focus on the situation where the masses are equal, i.e.,  $m_\uparrow = m_\downarrow \equiv m$ . In any case, we do not expect the qualitative picture of the BCS-BEC crossover to change for a small mass imbalance. However, we can see from Fig. 6 in Sec. 3 that once  $m_\uparrow/m_\downarrow \gtrsim 25$  (or equivalently when  $m_\uparrow/m_\downarrow \lesssim 1/25$ ), the trimer state has a lower energy than two dimers and therefore, in the BEC regime, the system will prefer to form a mixed gas of trimers and light atoms. It remains an open question what happens deep in the BCS regime, where the size of the trimer becomes larger than the inter-particle distance.

#### 4.2. Mean-field description

To gain insight into the BCS-BEC crossover, it is instructive to employ a mean-field approach to the problem. We start by considering the full quasi-2D problem as exists in experiment, and then we specialize to the 2D limit in later sections. The quasi-2D Fermi gas was first considered within the mean-field approximation in Ref. 67, but only a few harmonic oscillator levels were included. Here, we follow the approach in Ref. 68, which can in principle account for an infinite number of levels.

Building on the formalism in Sec. 2, the many-body grand-canonical Hamiltonian in the quasi-2D geometry is (setting the system area  $A = 1$ ):

$$\begin{aligned} \hat{H} = & \sum_{\mathbf{k}, n, \sigma} (\epsilon_{\mathbf{k}n} - \mu) c_{\mathbf{k}n\sigma}^\dagger c_{\mathbf{k}n\sigma} \\ & + \sum_{\substack{\mathbf{k}, n_1, n_2 \\ \mathbf{k}', n_3, n_4 \\ \mathbf{q}}} \langle n_1 n_2 | \hat{g} | n_3 n_4 \rangle c_{\mathbf{k}n_1\uparrow}^\dagger c_{\mathbf{q}-\mathbf{k}n_2\downarrow}^\dagger c_{\mathbf{q}-\mathbf{k}'n_3\downarrow} c_{\mathbf{k}'n_4\uparrow}, \end{aligned} \quad (43)$$

where  $\epsilon_{\mathbf{k}n} = k^2/2m + n\omega_z$  are the single particle energies relative to the zero-point energy of the  $n = 0$  state. Note that since we have assumed that the masses and particle densities are equal, the chemical potential must be the same for each spin  $\sigma$ , i.e.,  $\mu_\uparrow = \mu_\downarrow \equiv \mu$ .

The 3D attractive short-range interaction is set by the constant  $g$  like in Sec. 2. In the many-body system, it is convenient to work in the basis of the individual atoms rather than only considering the relative pair motion as in the two-body problem. However, since the interaction only depends on the relative motion, the interaction matrix elements  $\langle n_1 n_2 | \hat{g} | n_3 n_4 \rangle$  are best determined by switching to relative and center of mass harmonic oscillator quantum numbers,  $\nu$  and  $N$  respectively. This yields

$$\begin{aligned} \langle n_1 n_2 | \hat{g} | n_3 n_4 \rangle &= g \sum_{N\nu\nu'} f_\nu \langle n_1 n_2 | N\nu \rangle f_{\nu'} \langle N\nu' | n_3 n_4 \rangle \\ &\equiv g \sum_N V_N^{n_1 n_2} V_N^{n_3 n_4}, \end{aligned} \quad (44)$$

where  $f_\nu = \sum_{k_z} \tilde{\phi}_\nu(k_z)$ , and  $\tilde{\phi}_\nu$  is the Fourier transform of the  $\nu$ -th harmonic oscillator eigenfunction. These correspond to the  $f$  coefficients defined previously in Sec. 2, but with momentum cut-off  $\Lambda \rightarrow \infty$ , i.e., for even  $\nu$ , we obtain Eq. (20) with  $\lambda = 0$ . In this case,  $f_\nu$  reduces to the harmonic oscillator wave function evaluated at  $z = 0$ . The Clebsch-Gordan coefficients in the matrix elements are given by<sup>60,69</sup>

$$\langle n_1 n_2 | N\nu \rangle = \delta_{N+\nu, n_1+n_2} \sqrt{\frac{N!\nu!}{2^{n_1+n_2} n_1! n_2!}} \sum_{i+j=\nu} (-1)^j \binom{n_1}{i} \binom{n_2}{j}, \quad (45)$$

with  $i = 0, 1, \dots, n_1$  and  $j = 0, 1, \dots, n_2$ . Note that the scattering process conserves parity since  $\nu, \nu'$  must be even; namely, if  $n_1 + n_2$  is even (odd), then the matrix element is only non-zero when  $n_3 + n_4$  is also even (odd). The 3D contact interaction parameter  $g$  can be written in terms of the quasi-2D two-body binding energy  $\epsilon_b$ :

$$-\frac{1}{g} = \sum_{\mathbf{k}, n_1, n_2} \frac{f_{n_1+n_2}^2 |\langle n_1 n_2 | 0 \ n_1 + n_2 \rangle|^2}{\epsilon_{\mathbf{k}n_1} + \epsilon_{\mathbf{k}n_2} + \epsilon_b}. \quad (46)$$

Here, we simply take  $N = 0$  since  $\epsilon_b$  is independent of the two-body center of mass motion. One can also connect  $\epsilon_b$  to the 3D scattering length  $a_s$  using Eq. (31) with  $\lambda = 0$ .

Following Ref. 68, we define the pairing order parameter

$$\Delta_{\mathbf{q}N} = g \sum_{\mathbf{k}, n_1, n_2} V_N^{n_1 n_2} \langle c_{\mathbf{q}-\mathbf{k}n_2\downarrow} c_{\mathbf{k}n_1\uparrow} \rangle, \quad (47)$$

and assume that fluctuations around this are small, thus obtaining the mean-field Hamiltonian,

$$\begin{aligned} \hat{H}_{\text{MF}} = & \sum_{\mathbf{k}, n, \sigma} (\epsilon_{\mathbf{k}n} - \mu) c_{\mathbf{k}n\sigma}^\dagger c_{\mathbf{k}n\sigma} \\ & + \sum_{\mathbf{q}, N} \left( \Delta_{\mathbf{q}N} \sum_{\mathbf{k}, n_1, n_2} V_N^{n_1 n_2} c_{\mathbf{k}n_1\uparrow}^\dagger c_{\mathbf{q}-\mathbf{k}n_2\downarrow}^\dagger \right. \\ & \left. + \Delta_{\mathbf{q}N}^* \sum_{\mathbf{k}', n_3, n_4} V_N^{n_3 n_4} c_{\mathbf{q}-\mathbf{k}'n_3\downarrow} c_{\mathbf{k}'n_4\uparrow} - \frac{|\Delta_{\mathbf{q}N}|^2}{g} \right). \end{aligned} \quad (48)$$

If we further assume that the ground state has a uniform order parameter without nodes so that  $\Delta_{\mathbf{q}N} = \delta_{\mathbf{q}\mathbf{0}} \delta_{N0} \Delta_0$ , then Eq. (48) only contains a single unknown parameter  $\Delta_0$ . Thus  $\hat{H}_{\text{MF}}$  can be diagonalized to yield

$$\hat{H}_{\text{MF}} = \sum_{\mathbf{k}, n} (\epsilon_{\mathbf{k}n} - \mu - E_{\mathbf{k}n}) - \frac{\Delta_0^2}{g} + \sum_{\mathbf{k}, n, \sigma} E_{\mathbf{k}n} \gamma_{\mathbf{k}n\sigma}^\dagger \gamma_{\mathbf{k}n\sigma}, \quad (49)$$

where  $E_{\mathbf{k}n}$  are the quasiparticle excitation energies. The quasiparticle creation and annihilation operators are respectively given by

$$\gamma_{\mathbf{k}n\uparrow}^\dagger = \sum_{n'} (u_{\mathbf{k}n'n} c_{\mathbf{k}n'\uparrow}^\dagger + v_{\mathbf{k}n'n} c_{-\mathbf{k}n'\downarrow}) \quad (50)$$

$$\gamma_{-\mathbf{k}n\downarrow} = \sum_{n'} (u_{\mathbf{k}n'n} c_{-\mathbf{k}n'\downarrow} - v_{\mathbf{k}n'n} c_{\mathbf{k}n'\uparrow}^\dagger), \quad (51)$$

where the amplitudes  $u, v$  only depend on the magnitude  $k \equiv |\mathbf{k}|$  and satisfy  $\sum_{n'} (|u_{\mathbf{k}n'n}|^2 + |v_{\mathbf{k}n'n}|^2) = 1$ . Without loss of generality, we can choose  $u, v$  to be real. Note that while the quasiparticles have a well defined spin and momentum, they involve a superposition of different harmonic oscillator levels. Since the ground state corresponds to the vacuum state for the quasiparticles, the ground-state wave function can be written

$$|\Psi_{\text{MF}}\rangle \propto \prod_{\mathbf{k}n\sigma} \gamma_{\mathbf{k}n\sigma} |0\rangle, \quad (52)$$

where  $|0\rangle$  is the vacuum state for the bare operators  $c_{\mathbf{k}n\sigma}$ . In the 2D limit where  $\omega_z \gg \mu, \varepsilon_b$  and we only have the lowest level  $n = 0$ , we recover the standard BCS wave function

$$|\Psi_{\text{MF}}\rangle = \prod_{\mathbf{k}} \left( u_{\mathbf{k}00} + v_{\mathbf{k}00} c_{\mathbf{k}0\uparrow}^\dagger c_{-\mathbf{k}0\downarrow}^\dagger \right) |0\rangle. \quad (53)$$

In general, we must minimize  $\langle \hat{H}_{\text{MF}} \rangle = \sum_{\mathbf{k}, n} (\epsilon_{\mathbf{k}n} - \mu - E_{\mathbf{k}n}) - \frac{\Delta_0^2}{g}$  with respect to  $\Delta_0$  at fixed  $\mu$  to obtain the ground state. For the 2D limit, this

yields the usual form  $E_{\mathbf{k}} \equiv E_{\mathbf{k}0} = \sqrt{(\epsilon_{\mathbf{k}} - \mu)^2 + \Delta^2}$ , with  $\epsilon_{\mathbf{k}} \equiv \epsilon_{\mathbf{k}0}$  and  $\Delta \equiv \Delta_0 V_0^{00}$ . Using the density  $2n_\sigma = -\partial\langle\hat{H}_{\text{MF}}\rangle/\partial\mu$  and the 2D Fermi energy  $\varepsilon_F = k_F^2/2m$ , we also obtain  $\mu = \varepsilon_F - \varepsilon_b/2$  and  $\Delta = \sqrt{2\varepsilon_F\varepsilon_b}$ , as derived previously.<sup>18,19</sup> For the quasi-2D system, one must use the general expression for the density  $n_\sigma = \sum_{\mathbf{k},n',n} |v_{\mathbf{k}n'n}|^2$  and define  $\varepsilon_F$  to be the chemical potential of an ideal Fermi gas with the same density.

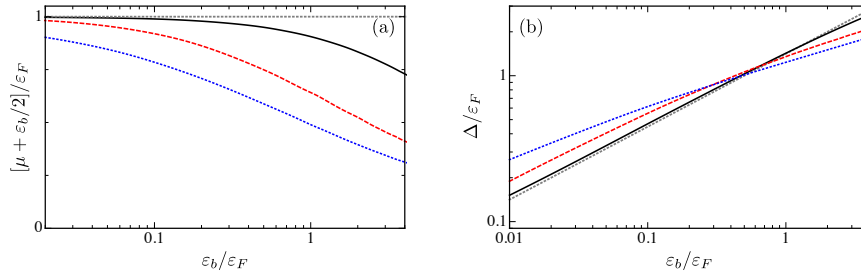


Fig. 10. Behaviour of the chemical potential (a) and the order parameter (b) as a function of the interaction parameter  $\varepsilon_b/\varepsilon_F$  for different confinement strengths. The solid (black), dashed (red), and dotted (blue) lines correspond to  $\varepsilon_F/\omega_z = 0.1, 0.5$  and  $1$ , respectively. The thin dotted lines are the results in the 2D limit,  $\mu = \varepsilon_F - \varepsilon_b/2$  and  $\Delta = \sqrt{2\varepsilon_b\varepsilon_F}$ . In (a), the term from two-body binding,  $-\varepsilon_b/2$ , has been subtracted from  $\mu$  in order to expose the many-body corrections. The data is taken from Ref. 68.

As the interactions are varied in the quasi-2D Fermi gas, the chemical potential always evolves from  $\varepsilon_F$  in the weakly interacting BCS limit  $\varepsilon_b/\varepsilon_F \ll 1$ , to  $-\varepsilon_b/2$  in the BEC limit  $\varepsilon_b/\varepsilon_F \gg 1$ . However, the precise evolution in the BCS-BEC crossover is dependent on the quasi-2D confinement frequency  $\omega_z$  once we are away from the 2D limit  $\omega_z \gg \varepsilon_F, \varepsilon_b$ , and this has implications for current 2D experiments, as we discuss later. If we take the limit of weak confinement  $\omega_z \rightarrow 0$ , there will be a crossover to 3D pairing, albeit with a modified density of states due to the trapping potential in the  $z$ -direction. For instance, in the BEC regime, we should recover “3D bosons” with  $\varepsilon_b \simeq 1/ma_s^2$  in the limit  $\varepsilon_b \gg \omega_z$  — see the discussion in Sec. 2.3. For strong confinement, one might naively expect to observe 2D behaviour once  $\varepsilon_b, \varepsilon_F < \omega_z$ . However, the chemical potential can be dramatically reduced from the 2D result even in this regime, as shown in Fig. 10 (a), and the deviation from 2D involves multiple harmonic oscillator levels.<sup>68</sup> Moreover, once we approach  $\varepsilon_F \simeq \omega_z$ , the chemical potential is strongly modified even when the interactions are weak,  $\varepsilon_b \ll \omega_z$ . This is analogous to the behaviour of the quasi-2D two-body  $T$  matrix (27), which

only resembles the 2D expression when the collision energy  $E \ll \omega_z$ , and is substantially different when  $E \simeq \omega_z$ . The pairing order parameter  $\Delta$  is also modified by the presence of  $\omega_z$ , with  $\Delta$  being increased in the BCS regime with increasing  $\varepsilon_F/\omega_z$ , as seen in Fig. 10 (b). This suggests that pairing is enhanced by perturbing away from the 2D limit and this therefore impacts the critical temperature for superfluidity (see Sec. 5).

### 4.3. Perturbative regimes

In order to go beyond mean-field theory, we restrict ourselves to the 2D limit  $\omega_z \gg \varepsilon_F, \varepsilon_b$ , so that the different regimes are completely parameterized by  $k_F a_{2D}$ . In this case, the Hamiltonian in Eq. (43) reduces to

$$\hat{H} = \sum_{\mathbf{k}, \sigma} (\varepsilon_{\mathbf{k}} - \mu) c_{\mathbf{k}\sigma}^\dagger c_{\mathbf{k}\sigma} + g \sum_{\mathbf{k}, \mathbf{k}', \mathbf{q}} c_{\mathbf{k}\uparrow}^\dagger c_{\mathbf{q}-\mathbf{k}\downarrow}^\dagger c_{\mathbf{q}-\mathbf{k}'\downarrow} c_{\mathbf{k}'\uparrow}, \quad (54)$$

where  $g$  is now an effective 2D contact interaction like in Eq. (10), which gives rise to the required scattering length  $a_{2D}$  (or two-body binding energy  $\varepsilon_b$ ). While mean-field theory provides an appealingly simple and intuitive picture of the BCS-BEC crossover in 2D, it is not expected to be quantitatively accurate and it at best provides an upper bound on the energy, being in essence a variational approach. In particular, it substantially overestimates the effective dimer-dimer interaction in the BEC regime. Even in the BCS regime where interactions are weak, it fails to capture the leading order dependence of the energy on  $1/\ln(k_F a_{2D})$  since it neglects the interaction energy of the normal Fermi liquid phase. However, one can extract accurate analytic expressions for the behaviour in the limits  $|\ln(k_F a_{2D})| \gg 1$  by performing a proper perturbative expansion in the interaction.

In the regime of weak attraction  $\ln(k_F a_{2D}) \gg 1$ , the gas behaves as a Fermi liquid in the normal state.<sup>70–72</sup> One can show using perturbation theory in  $g$  that the energy per particle in this limit is<sup>71,73</sup>

$$\frac{E}{N} = \frac{\varepsilon_F}{2} \left( 1 - \frac{1}{\eta} + \frac{\mathcal{A}}{\eta^2} \right), \quad (55)$$

where  $N = N_\uparrow + N_\downarrow$  and  $\eta = \ln(k_F a_{2D})$ . Of course, in the ground state, the gas will be a paired superfluid rather than a Fermi liquid, but the energy due to pairing scales as  $\Delta^2/\varepsilon_F \sim \varepsilon_b$  in this limit, which tends to zero faster than  $\varepsilon_F/\ln(k_F a_{2D})$  as  $\varepsilon_b \rightarrow 0$ . While the structure of the perturbative expansion is clear, there is some discrepancy in the literature regarding the constant  $\mathcal{A}$ . A thorough calculation for the repulsive Fermi gas using second-order

perturbation theory<sup>71,72</sup> gives  $\mathcal{A} = 3/4 - \ln(2) \simeq 0.06$ . However, a recent QMC calculation<sup>55</sup> finds a larger value:  $\mathcal{A} \simeq 0.17$ .

In the opposite limit  $\ln(k_F a_{2D}) \ll -1$ , the system can be regarded as a weakly interacting gas of bosonic dimers. In this case, the effective dimer-dimer interaction  $g_d$  in the low-energy limit is parameterized by the scattering length  $a_{dd} \simeq 0.56a_{2D}$ , as noted in Sec. 3. Moreover, the total energy of the system can be written as  $E = -\varepsilon_b N_d + E_d$ , where  $N_d = N_\sigma = N/2$  and  $E_d$  is the energy of a repulsive gas of  $N_d$  bosons. We can likewise introduce a boson chemical potential  $\mu_d = 2\mu + \varepsilon_b$ . Note that in the limit  $a_{dd} \rightarrow 0$  (or, equivalently, when  $\varepsilon_b \rightarrow \infty$ ), we have  $\mu_d \rightarrow 0^+$ , as expected for a non-interacting BEC. However, this behavior is not captured by BCS mean-field theory, which predicts  $\mu_d = 2\varepsilon_F$ . This corresponds to an effective dimer-dimer interaction that only scales with the density, as one might expect from a classical theory of interacting dimers in 2D rather than an appropriately renormalized quantum one (see Sec. 7).

To extract the behaviour of the weakly repulsive Bose gas, we consider the grand potential according to Bogoliubov theory:

$$\Omega = -\frac{\mu_d^2}{2g_d} - \frac{1}{2} \sum_{\mathbf{k} \neq 0} \left( \epsilon_{\mathbf{k}d} + \mu_d - \sqrt{\epsilon_{\mathbf{k}d}(\epsilon_{\mathbf{k}d} + 2\mu_d)} \right), \quad (56)$$

where  $\epsilon_{\mathbf{k}d} = \frac{k^2}{2M}$  and  $M = m_\uparrow + m_\downarrow = 2m$ . After regularizing the momentum sum, we obtain (see, also, Ref. 74)

$$\Omega = \frac{M\mu_d^2}{16\pi} \left[ 1 - 2 \ln \left( \frac{1}{Ma_{dd}^2 \mu_d} \right) \right]. \quad (57)$$

To relate this back to the Fermi system, we consider the density of dimers:

$$n_d \equiv \frac{N_d}{A} = -\frac{\partial \Omega}{\partial \mu_d} = \frac{M\mu_d}{4\pi} \ln \left( \frac{1}{Ma_{dd}^2 \mu_d} \right). \quad (58)$$

Assuming that  $\ln \left( \frac{1}{4\pi n_d a_{dd}^2} \right) \gg 1$ , this can then be rearranged to obtain the leading order expression for  $\mu_d$  in terms of the density  $n_d$ , i.e.,

$$\mu_d \simeq \frac{4\pi n_d}{M} \frac{1}{\ln \left( \frac{1}{4\pi n_d a_{dd}^2} \right)} \left[ 1 - \frac{\ln \ln \left( \frac{1}{4\pi n_d a_{dd}^2} \right)}{\ln \left( \frac{1}{4\pi n_d a_{dd}^2} \right)} \right]. \quad (59)$$

This finally gives us the energy density  $E/N_d = -\varepsilon_b + E_d/N_d$ , with

$$\frac{E_d}{N_d} \simeq \frac{2\pi n_d}{M} \frac{1}{\ln\left(\frac{1}{4\pi en_d a_{dd}^2}\right)} \left[ 1 - \frac{\ln \ln\left(\frac{1}{4\pi en_d a_{dd}^2}\right)}{\ln\left(\frac{1}{4\pi en_d a_{dd}^2}\right)} - \frac{1}{2 \ln\left(\frac{1}{4\pi en_d a_{dd}^2}\right)} \right], \quad (60)$$

where we have used the fact that  $E_d = \Omega + \mu_d N_d$  at zero temperature. This agrees with the expression used in Ref. 55.

#### 4.4. Equation of state

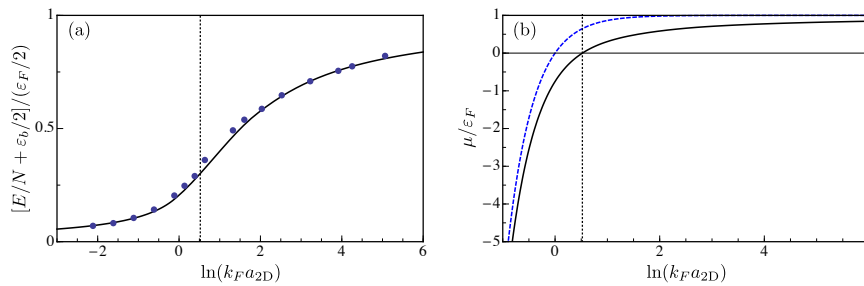


Fig. 11. (a) Energy per particle in units of  $\varepsilon_F/2$  (the energy per particle in the non-interacting gas) as a function of interaction strength. The trivial two-body binding energy has been subtracted. The data points are the results of the QMC calculation,<sup>55</sup> while the solid line is an interpolation between the known weak coupling results in the BCS and BEC limits. (b) Chemical potential in units of the Fermi energy. The solid (black) line is an interpolation between the known limiting behaviors, while the dashed (blue) line is the mean-field result  $\mu = \varepsilon_F - \varepsilon_b/2$ . In both plots, the vertical dotted line indicates the point at which the chemical potential is zero.

In order to obtain an accurate equation of state throughout the BCS-BEC crossover, one must resort to numerical approaches such as the fixed node diffusion QMC method mentioned previously.<sup>55</sup> The QMC result for the energy per particle is displayed in Fig. 11(a).<sup>k</sup> As expected, the energy matches the known results in the BCS and BEC limits (taking the QMC value for  $\mathcal{A}$  in Eq. (55)). Indeed, by interpolating between the known weak-coupling results in the BCS and BEC regimes, we can obtain a reasonable curve for the energy throughout the crossover that matches the QMC data. This also allows us to easily extract other thermodynamic quantities such

<sup>k</sup>Note that we have used a different definition of  $a_{2D}$  compared with the original QMC paper – see the discussion in Sec. 2.2.

as the chemical potential and the pressure — one simply takes the appropriate derivative of the expressions in the perturbative regimes and then interpolates between the results. In particular, the chemical potential in the BEC regime can be taken from Eq. (59), while in the BCS limit it corresponds to

$$\mu = \frac{\partial E}{\partial N} = \varepsilon_F \left( 1 - \frac{1}{\eta} + \frac{4\mathcal{A} + 1}{4\eta^2} \right). \quad (61)$$

Referring to Fig. 11(b), we find that the interpolated  $\mu$  is lower than that from mean-field theory, but it still evolves from  $\varepsilon_F$  to  $-\varepsilon_b/2$  with increasing attraction (decreasing  $\ln(k_F a_{2D})$ ). The point  $\mu = 0$  may be regarded as the “crossover point” that approximately separates Fermi and Bose regimes, as we discuss in Sec. 4.5.

The pressure as a function of interaction has recently been measured experimentally in a quasi-2D Fermi gas.<sup>17</sup> As shown in Fig 12, the comparison with the QMC prediction is reasonable, aside from the BCS side of the crossover (or Fermi regime), where the pressure is significantly higher. Indeed, this is in the limit where the weak-coupling result becomes accurate and the pressure should simply correspond to:

$$P \simeq \frac{(2n_\uparrow)^2 \pi}{2m} \left( 1 - \frac{1}{\eta} + \frac{2\mathcal{A} + 1}{2\eta^2} \right). \quad (62)$$

However, the experiment was performed at finite temperature, while the theory is for zero temperature. Indeed, a recent self-consistent  $T$ -matrix (or Luttinger-Ward) calculation<sup>75</sup> for the normal state finds that the deviations in this regime are consistent with a temperature of  $T \simeq 0.15T_F$ , where  $T_F = \varepsilon_F/k_B$ . Another factor that complicates the analysis is the quasi-2D nature of the gas. The experiment is never in the 2D limit since  $\varepsilon_b > \omega_z$  in the Bose regime and  $\varepsilon_F \gtrsim 0.5\omega_z$  throughout. This may account for the smaller but arguably more striking deviation from the QMC prediction in the strongly interacting regime (Fig 12). Here, the pressure is consistently below the QMC curve, whereas one would generally expect the pressure to be higher at finite temperature when  $k_F a_{2D}$  is fixed. However, perturbing away from the 2D limit (which is equivalent to relaxing the quasi-2D confinement) is expected to reduce the pressure in the plane since the atoms can spread out in the transverse direction.<sup>76</sup> This suggests that there are two competing effects in the experiment: finite temperature tends to raise the pressure, as evident in the Fermi regime, while quasi-2D effects act to reduce it, particularly for strong interactions where both  $\varepsilon_b/\omega_z$  and  $\varepsilon_F/\omega_z$  are sizeable.

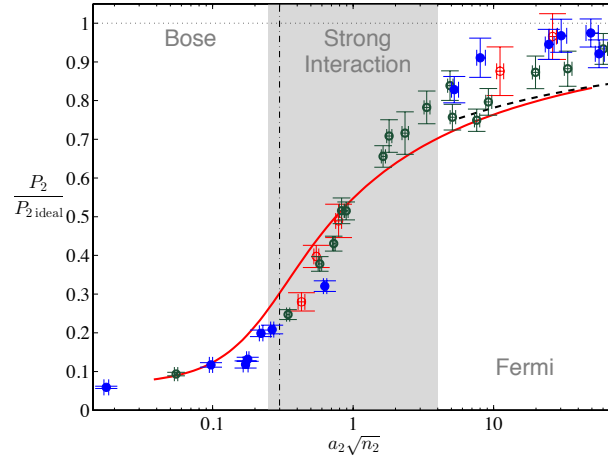


Fig. 12. The experimentally measured pressure  $P_2$  in a quasi-2D Fermi gas.<sup>17</sup> The pressure is scaled with respect to that of an ideal 2D Fermi gas,  $P_{2,\text{ideal}}$ . Note that the experiment is not purely 2D since  $\varepsilon_F = 2\pi n_2/m \gtrsim 0.5\omega_z$ , and  $\varepsilon_b > \omega_z$  in the Bose limit. Therefore, the scattering length (denoted  $a_2$ ) is not always simply related to  $\varepsilon_b$ , and must be defined via the quasi-2D  $T$  matrix. The solid red curve is obtained from a fit to the 2D QMC data<sup>55</sup> while the dashed line approximately corresponds to the weak-coupling result in the Fermi regime.

Reprinted figure with permission from: V. Makhhalov, K. Martiyanov, and A. Turlapov, *Phys. Rev. Lett.* **112**, 045301 (2014). Copyright 2014 by the American Physical Society.

#### 4.4.1. Contact

Another important thermodynamic quantity is the contact density  $C$ , which fixes the tail of the momentum distribution:  $n(\mathbf{k}) \sim C/k^4$  as  $k \rightarrow \infty$ . This is related to the 2D equation of state by the adiabatic theorem<sup>77,78</sup>

$$C = 2\pi m \frac{dE}{d \ln a_{2D}}. \quad (63)$$

Since the contact determines the short-distance behavior of the gas (i.e., it essentially gives the probability of finding a pair of  $\uparrow$  and  $\downarrow$  fermions close together), it can also be related to the high-frequency and large-momentum limits of other correlation functions in 2D such as the current response function.<sup>79</sup> Mean-field theory simply gives  $C = m^2 \Delta^2$ , which is consistent with the fact that  $C$  should monotonically increase with increasing attraction, and it yields the correct two-body contact in the Bose limit. However, the mean-field result is not quantitatively accurate in the Fermi regime since it does not capture the leading order dependence on the interaction, as discussed in Sec. 4.3.

The 2D contact may be experimentally determined from the high-

frequency tail of the RF spectrum,<sup>80</sup> as well as from the momentum profile. In contrast to the pressure, the contact appears to be surprisingly insensitive to temperature in the degenerate regime  $T < T_F$ . Figure 13 shows that there is good agreement between the experimentally measured contact density<sup>15</sup> at  $T/T_F = 0.27$  and the  $T = 0$  QMC result.<sup>55</sup> The contact determined using the Luttinger-Ward approach at the same temperature ( $T/T_F = 0.27$ ) confirms that it is relatively unchanged for low temperatures.<sup>75</sup>

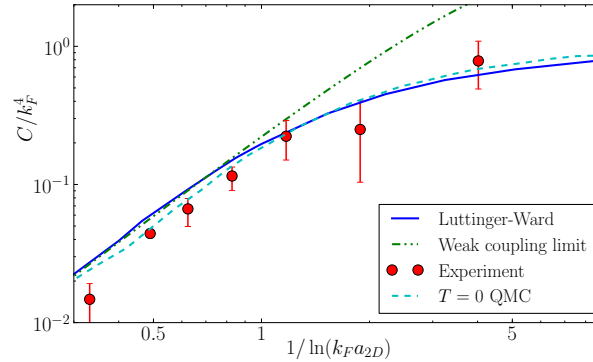


Fig. 13. Contact density  $C$  in the regime  $\ln(k_F a_{2D}) > 0$ . The filled circles correspond to the data in Ref. 15 at  $T/T_F = 0.27$ , the dashed line is a fit to the 2D QMC result,<sup>55</sup> and the solid line is determined from a Luttinger-Ward, or self-consistent  $T$ -matrix, approach described in Ref. 75. The  $T = 0$  weak-coupling limit is extracted from Eq. (55). The figure is adapted from Ref. 75.

#### 4.5. The 2D crossover “point”

Finally, we turn to the crossover from Fermi to Bose behavior in the regime of strong interactions  $|\ln(k_F a_{2D})| \lesssim 1$ . From the point of view of mean-field theory, the natural crossover point is at  $\mu = 0$ , since this marks a qualitative change in the quasiparticle excitation spectrum  $E_{\mathbf{k}} = \sqrt{(\epsilon_{\mathbf{k}} - \mu)^2 + \Delta^2}$ . When  $\mu > 0$ , the minimum energy gap  $\Delta$  occurs at finite momentum,  $k = \sqrt{2m\mu}$ , corresponding to the remnants of a Fermi surface. However, for  $\mu < 0$ , the minimum gap occurs at  $k = 0$  and no longer corresponds to  $\Delta$ . Indeed, for sufficiently strong attraction, the gap in the single-particle spectrum becomes  $-\varepsilon_b/2$ , as expected. Thus, the  $\mu < 0$  regime resembles the behavior of a gas of bosonic dimers. According to mean-field theory, the point where  $\mu = 0$  corresponds to  $\ln(k_F a_{2D}) = 0$ , and this is generally

viewed as playing a role analogous to the unitarity point  $1/a_s = 0$  in the 3D BCS-BEC crossover.<sup>1</sup>

However, if we go beyond mean-field theory and consider the more accurate QMC calculations,<sup>55</sup> then we find<sup>81</sup> that the point where  $\mu = 0$  instead occurs at much weaker attraction, with  $\ln(k_F a_{2D}) \simeq 0.5$ , as shown in Fig. 11. This suggests that the Fermi side of the crossover occurs at larger  $\ln(k_F a_{2D})$  than previously assumed, and is consistent with the observation in QMC simulations<sup>55</sup> that a variational wave function based on dimers outperforms the one for a Fermi liquid once  $\ln(k_F a_{2D}) \lesssim 1$ . Of course, it remains an open question how  $\mu$  is connected to the quasiparticle dispersion beyond the mean-field approximation, but a negative  $\mu$  already indicates strong deviations from fermionic behavior.

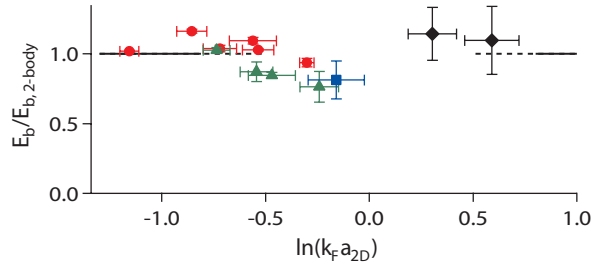


Fig. 14. Experimental measurement of the pairing gap  $E_b$  in the 2D Fermi gas using RF spectroscopy, taken from Ref. 11. The straight line corresponds to the mean-field result, which is simply the two-body binding energy (denoted here by  $E_{b,2\text{-body}}$ ).

Reprinted figure in (a) with permission from: A. T. Sommer, L. W. Cheuk, M. J. H. Ku, W. S. Bakr, and M. W. Zwierlein, *Phys. Rev. Lett.* **108**, 045302 (2012). Copyright 2012 by the American Physical Society.

A recent experiment<sup>11</sup> on pairing in the 2D Fermi gas also suggests that the Bose regime extends beyond  $\ln(k_F a_{2D}) = 0$ . Figure 14 shows the pairing gap  $E_b \equiv E_{\mathbf{k}=0} - \mu$ , corresponding to the onset of the pairing peak in the RF spectrum. At first glance, this measurement appears to validate mean-field theory, which simply predicts  $E_b = \varepsilon_b$  throughout the crossover. However, this result is also expected for a gas of dimers; thus an alternative explanation is that the experiment only probes the Bose limit of the crossover, with  $\ln(k_F a_{2D}) \lesssim 0.5$ .

<sup>1</sup>Note that the analogy between  $1/a_s = 0$  in 3D and  $\ln(k_F a_{2D}) = 0$  in 2D is far from perfect, since we have  $\mu > 0$  at  $1/a_s = 0$  and thus the unitarity point lies on the Fermi side of the crossover.

## 5. Finite-temperature phenomenology

The behaviour of the 2D Fermi gas at finite temperature is even richer than at zero temperature, since we have the possibility of superfluid phase transitions and pairing without superfluidity. Above the critical temperature  $T_c$  for superfluidity, the normal phase is also markedly different in the two perturbative limits, with a Fermi liquid for  $\ln(k_F a_{2D}) \gg 1$  and a Bose liquid for  $\ln(k_F a_{2D}) \ll -1$ . This raises the question of whether the normal gas within the crossover can display features intermediate between Fermi and Bose behavior. In particular, there may exist a so-called “pseudogap” regime in the normal phase, where there is a suppression of spectral weight at the Fermi surface that is reminiscent of a pairing gap.<sup>82</sup> Such a phenomenon has been observed in the quasi-2D cuprate superconductors, but its origin still remains a mystery.<sup>83</sup> By investigating its existence in attractive Fermi gases, cold-atom experiments may help settle the question of whether or not a pseudogap can be produced by pairing alone, in principle.

In this section, we will review our current understanding of the normal phase of the 2D Fermi gas, including the transition to superfluidity at low temperatures. We will also briefly discuss how the behavior is affected by the quasi-2D nature of the gas and the in-plane trapping potential present in experiment. To simplify the equations, we set  $k_B = 1$  in the following.

### 5.1. Critical temperature for superfluid transition

Two-dimensional gases are marginal in the sense that true long-range order (i.e. condensation) only exists at  $T = 0$ . Instead, the superfluid phase at finite temperature exhibits quasi-long-range order where the correlations decay algebraically.<sup>84</sup> Increasing temperature further eventually results in a Berezinskii-Kosterlitz-Thouless (BKT) transition to the normal phase.<sup>84–86</sup>

In the limit  $\ln(k_F a_{2D}) \ll -1$ , the system corresponds to a weakly interacting Bose gas and the BKT transition temperature is:<sup>56</sup>

$$\frac{T_c}{T_F} = \frac{1}{2} \left[ \ln \left( \frac{\mathcal{B}}{4\pi} \ln \left( \frac{4\pi}{k_F^2 a_{2D}^2} \right) \right) \right]^{-1}, \quad (64)$$

where  $\mathcal{B} \simeq 380$ . Note that  $T_c \rightarrow 0$  in the limit  $\ln(k_F a_{2D}) \rightarrow -\infty$ , but since the dependence on  $\ln(k_F a_{2D})$  is logarithmic, in practice we obtain  $T_c/T_F \simeq 0.1$  for the interaction regime accessible in experiment (see Fig. 15).

In the BCS limit  $\ln(k_F a_{2D}) \gg 1$ , the critical temperature is set by the energy required to break pairs, which is the lowest energy scale in the problem. Thus, one can estimate  $T_c$  by taking the mean-field Hamiltonian

(49) and determining the point at which  $\Delta$  vanishes.<sup>87</sup> From the resulting linearized gap equation (or Thouless criterion) one obtains<sup>88</sup>

$$\frac{T_c}{T_F} = \frac{2e^\gamma}{\pi k_F a_{2D}}. \quad (65)$$

A more thorough calculation that includes Gorkov–Melik-Barkhudarov corrections<sup>56</sup> yields the BCS result above reduced by a factor of  $e$ .

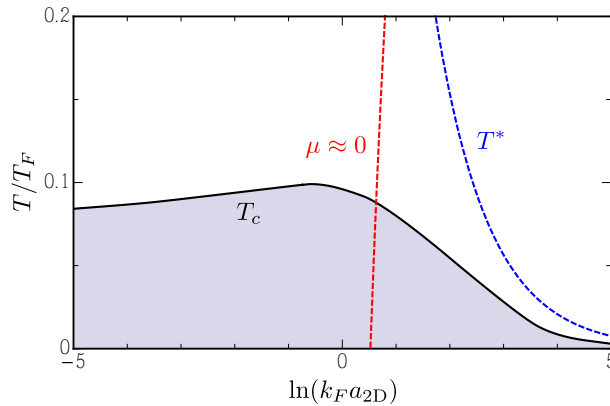


Fig. 15. Schematic phase diagram throughout the BCS-Bose crossover. The critical temperature for superfluidity is represented by the solid line, and corresponds to an interpolation between the known limits. The dashed lines correspond to  $\mu \approx 0$  and the onset of pairing  $T^*$ , which approximately bound the pseudogap region above  $T_c$ . The  $\mu(T) \approx 0$  line is obtained by setting  $T = \mu(0)$ , while  $T^*$  is estimated from the Thouless criterion (64).

Referring to Fig. 15, we see that the results for  $T_c$  in the BCS and Bose limits can be smoothly interpolated, suggesting that  $T_c/T_F$  never exceeds 0.1. Note that  $T_c$  has a maximum in the regime  $|\ln(k_F a_{2D})| < 1$ . As yet, there is no experimental observation of  $T_c$  in the 2D Fermi gas.

#### 5.1.1. Quasi-2D case

Given that experiments deal with quasi-2D Fermi gases, it is important to understand the effect of a finite confinement length on  $T_c$ . This is in general a challenging problem to address throughout the BCS-Bose crossover, but it is possible to estimate the dependence on  $\varepsilon_F/\omega_z$  in the BCS limit. Using the mean-field approach for the quasi-2D system described in Sec. 4.2, one

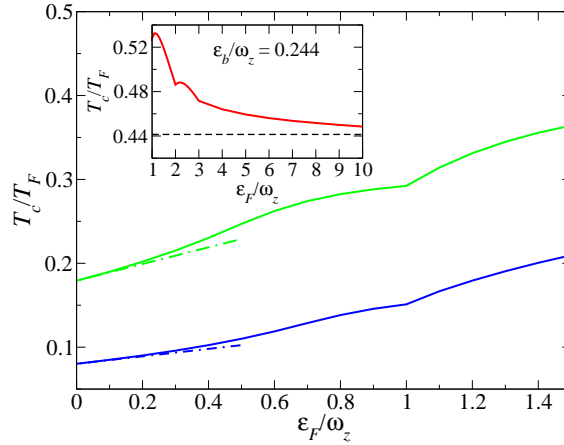


Fig. 16. Evolution of the mean-field critical temperature as the system is perturbed away from the 2D limit, taken from Ref. 76. The blue (bottom) and red (top) solid curves correspond to  $\varepsilon_b/\varepsilon_F = 0.01$  and  $\varepsilon_b/\varepsilon_F = 0.05$ , respectively. The dash-dotted lines are the leading order behavior in  $\varepsilon_F/\omega_z$ . Inset: The critical temperature at unitarity for large  $\varepsilon_F/\omega_z$ . The line tends towards the 3D result (dashed line) as  $\varepsilon_F/\omega_z \rightarrow \infty$ .

obtains a natural generalization of the Thouless criterion to quasi-2D:<sup>76</sup>

$$-\frac{1}{g} = \sum_{\mathbf{k}, n_1, n_2} (V_0^{n_1 n_2})^2 \frac{\tanh(\beta_c \xi_{\mathbf{k}n_1}/2) + \tanh(\beta_c \xi_{\mathbf{k}n_2}/2)}{2(\xi_{\mathbf{k}n_1} + \xi_{\mathbf{k}n_2})}, \quad (66)$$

where  $g$  is the 3D contact interaction,  $\beta_c = 1/T_c$ , and  $\xi_{\mathbf{k}n} = \epsilon_{\mathbf{k}n} - \mu$ . Solving for  $T_c$ , we arrive at the result plotted in Fig. 16. While the mean-field approach will overestimate  $T_c$ , it should be qualitatively accurate in the BCS regime and we clearly see that  $T_c/T_F$  increases as we perturb away from 2D at fixed  $\varepsilon_b/\varepsilon_F$ . Indeed, the leading order behavior in  $\varepsilon_F/\omega_z$  is<sup>76</sup>

$$\frac{T_c}{T_F} = \frac{2e^\gamma}{\pi k_F a_{2D}} \left[ 1 + \frac{\varepsilon_F}{\omega_z} \ln \left( \frac{7 + 4\sqrt{3}}{8} \right) \right]. \quad (67)$$

This suggests that experiments will have a better chance of observing  $T_c$  and superfluidity if they are not purely 2D. For intermediate values of the confinement, we clearly see the presence of cusps at integer values of  $\varepsilon_F/\omega_z$ , which correspond to discontinuities in the density of states every time the Fermi energy crosses a harmonic oscillator level. In the limit  $\omega_z \rightarrow 0$ , Eq. (66) yields the 3D expression for the Thouless criterion, as expected.<sup>m</sup> An interesting possibility is that  $T_c/T_F$  is maximized at in-

<sup>m</sup>The correct 3D expression is obtained by treating the confining potential in the  $z$ -direction within the local density approximation — see, also, Sec. 5.4.

intermediate confinement strengths, where the geometry is between two and three dimensions, but one would need to go beyond mean-field theory to assess this.

## 5.2. High temperature limit

For high temperatures  $T \gg T_F$ , the gas is no longer quantum degenerate and the behavior tends towards that of a classical Boltzmann gas where the particle statistics are unimportant. In this limit, one may exploit the virial expansion described below, which has the advantage of being a controlled approach at high temperatures throughout the Fermi-Bose crossover. As such, the virial expansion can be used to investigate pairing phenomena at finite temperature and thus provide a benchmark for both theory and experiment.

### 5.2.1. Virial expansion

In the following, we outline the basic idea of the virial expansion, as applied to the uniform 2D Fermi gas. Working in the grand canonical ensemble, we define the virial coefficients  $b_j$  such that the grand potential  $\Omega(T, \mu)$  is given by:

$$\Omega = -2T\lambda^{-2} \sum_{j \geq 1} b_j z^j, \quad (68)$$

where the thermal wavelength  $\lambda = \sqrt{2\pi/mT}$ , the fugacity  $z = e^{\beta\mu}$ , and  $\beta \equiv 1/T$ . In the high-temperature limit, the thermodynamics of the system can be accurately described by just the first few terms in the above power series. For a typical Fermi gas,  $z$  is the relevant expansion parameter, but this is not the case in the Bose limit of the crossover where  $k_F a_{2D} \ll 1$ . In this limit,  $\mu \simeq -\varepsilon_b/2$  at low temperatures so that  $z \simeq e^{-\beta\varepsilon_b/2} \rightarrow 0$  as  $T \rightarrow 0$ , which naively suggests that the virial expansion is valid at arbitrarily low temperatures. However, it can be shown that the coefficients  $b_j$  also contain powers of  $e^{\beta\varepsilon_b/2}$  that cancel the contribution from the binding energy in  $z$  when  $j$  is even.<sup>81</sup> Thus, the relevant expansion parameter in the Bose limit is instead  $z^{(\text{Bose})} = ze^{\beta\varepsilon_b/2}$ , with corresponding coefficients  $b_j^{(\text{Bose})} = e^{-j\beta\varepsilon_b/2} b_j$ .

The virial expansion effectively amounts to a cluster expansion, whereby one determines the correlations between particles in a cluster of a given size, and then increases the size of the cluster at each order. For instance,  $b_2$  only contains contributions from the one- and two-body problems,  $b_3$

further includes three-body scattering, and so on. As such, one can make use of the few-body results described in Sec. 3. For a recent review of the virial expansion in cold gases, see Ref. 89.

The first calculation of the virial coefficients in a 2D Fermi gas was for the trapped system.<sup>90</sup> Indeed, one typically determines each virial coefficient by solving the relevant few-body problem in a harmonic trap. The coefficients for the trapped gas can be straightforwardly mapped to those in the uniform case using the relation:  $b_j = j b_j^{\text{trap}}$  (Ref. 81). The lowest order coefficients are plotted in Fig. 17. We see that the correction to the second virial coefficient due to interactions is attractive, as expected, since it lowers the grand potential at fixed  $\mu$  and  $T$ . However, this lowest order term is expected to overestimate the attraction at lower temperatures and thus the third-order correction acts to increase the energy.

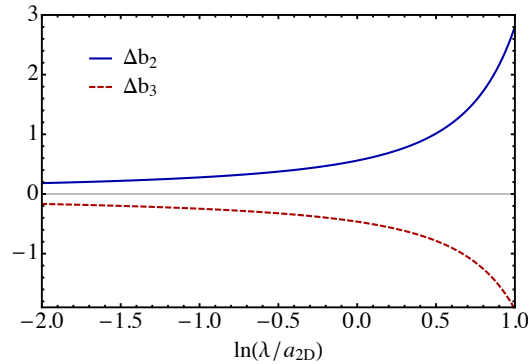


Fig. 17. The contribution from interactions to the second and third virial coefficients of the uniform 2D Fermi gas, taken from Ref. 81. The coefficients for the non-interacting gas are  $b_j^{(\text{free})} = (-1)^{j-1} j^{-2}$  for  $j \geq 1$ , and  $\Delta b_j \equiv b_j - b_j^{(\text{free})}$ . Note that the virial coefficients are functions of  $\ln(\lambda/a_{2D})$ , or equivalently  $\beta\varepsilon_b$ , only. In the limit  $\beta\varepsilon_b \rightarrow \infty$ , both  $\Delta b_2$  and  $\Delta b_3$  are dominated by the two-body bound state and thus they both go like  $e^{\beta\varepsilon_b}$  (but with different signs).

One can also determine  $b_j$  directly using a diagrammatic approach<sup>91</sup> where the single-particle propagator  $G$  is expanded in  $z$ , and this was first performed in 2D in Ref. 81. This approach also makes it straightforward to determine the virial expansion for the spectral function  $A_\sigma(\mathbf{k}, \omega) = -2\text{Im}G_\sigma(\mathbf{k}, \omega)$ , which is related to the probability of extracting an atom in state  $\sigma$  with momentum  $\mathbf{k}$  and frequency  $\omega$ . This allows one to investigate pairing gaps in the spectrum at high temperature, as we now discuss.

### 5.3. Pseudogap

The pseudogap regime is often synonymous with “pairing above  $T_c$ ” in the cold-atom literature. However, such a scenario is trivially achieved in a classical gas of diatomic molecules, where the gap in the spectrum corresponds to the dimer binding energy. To reproduce the phenomenology of high- $T_c$  superconductors, one requires the presence of a Fermi surface, since the pseudogap in these systems manifests itself as a loss of spectral weight at the Fermi surface.<sup>83</sup> Indeed, it is not a priori obvious that such a phenomenon can be replicated with an attractive Fermi gas: a large attraction will surely lead to a pronounced pairing gap above  $T_c$ , but it will also destroy the Fermi surface. It is therefore reasonable to assume that any pseudogap regime must have  $\mu > 0$  in addition to pairing, as schematically depicted in Fig. 15.

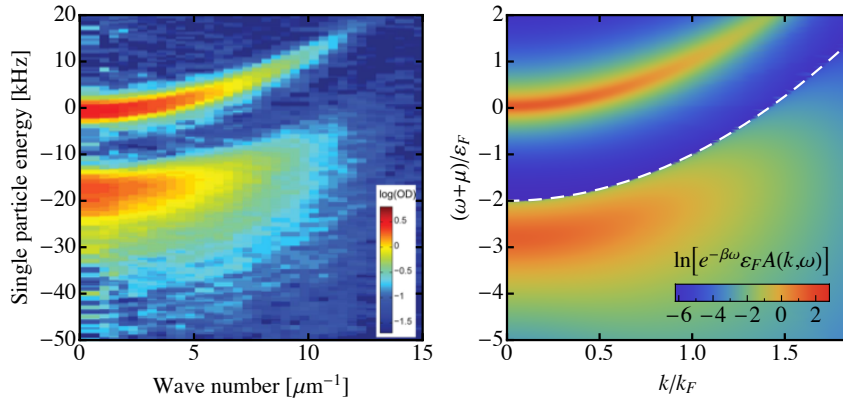


Fig. 18. The occupied part of the spectral function at  $\ln(k_F a_{2D}) = 0$ . (left) Measured momentum-resolved photoemission signal, taken from Ref. 10. (right) Theoretical prediction at  $T/T_F = 1$  from the virial expansion up to second order.<sup>81</sup> The white dotted line marks the edge of the band of bound dimers (the incoherent part of the spectrum) and corresponds to the free atom dispersion shifted by the two-body binding energy, i.e.,  $\epsilon_{\mathbf{k}} - \epsilon_b$ . (left) Reprinted by permission from Macmillan Publishers Ltd: Nature **480**, 75 (2011) copyright 2011.

The possibility of a pseudogap regime has been investigated in 3D Fermi gases,<sup>92–95</sup> but its existence is still under debate. In 2D, the pseudogap regime is expected to be much more pronounced than in 3D, since quantum fluctuations suppress superfluid long-range order, and the system more readily forms two-body bound states. Already, a recent measurement<sup>10</sup> of the spectral function in 2D has found indications of a pairing gap above  $T_c$ . However, a similar pairing gap is found using the lowest order virial expansion

sion of the spectral function, which only includes two-body correlations, i.e., no Fermi surface.<sup>81,96</sup> In Fig. 18, the agreement between experiment and theory suggests that the observed pairing effectively arises from two-body physics only and therefore does not correspond to a pseudogap. Furthermore, most of the experimental measurements of the spectral function were apparently performed in the regime where  $\mu < 0$  (see Fig. 15 and Ref. 81). Thus, it is likely that lower temperatures and lower attraction are required to observe a pseudogap. In particular, both non-self-consistent<sup>97</sup> and self-consistent<sup>75</sup>  $T$ -matrix approximations predict the existence of a pseudogap in the regime  $T/T_F \lesssim 0.2$  for  $\ln(k_F a_{2D}) \simeq 1$ .

#### 5.4. Equation of state in a trapped gas

The fact that the interaction parameter  $\ln(k_F a_{2D})$  can be tuned by varying the density has important consequences for the trapped 2D gas. Specifically, it implies that  $\ln(k_F a_{2D})$  decreases as we move from the high-density region at the center of the trapped gas to the low-density region at the edge. Thus, we can in principle observe the entire Fermi-Bose crossover in a single experiment. This argument relies on the local density approximation (LDA), where the in-plane trapping potential can be incorporated into the chemical potential,  $\mu(r) = \mu - V(r)$ , and thus each point in the trap corresponds to a different  $\ln(k_F(r) a_{2D})$ . For a harmonic potential with frequency  $\omega_\perp$ , we require  $\omega_\perp \ll T, \varepsilon_F$  in order for LDA to be valid.

One can make a direct connection with trapped-gas experiments by considering the density  $n(\beta\mu, \beta\varepsilon_b)$  as a function of  $\beta\mu$  for different values of the interaction parameter  $\beta\varepsilon_b$  (see Fig. 19). Such an equation of state can be straightforwardly extracted from the measured density profile in a trap.<sup>98</sup> To reveal the effects of interactions, we normalize the density  $n$  by that of the ideal Fermi gas,  $n_0 = 2 \ln(1 + e^{\beta\mu})/\lambda^2$ . In the high-temperature (low-density) limit where  $\beta\mu \rightarrow -\infty$ , the behaviour approaches that of an ideal Boltzmann gas, as expected. However, with decreasing temperature,  $n/n_0$  eventually exhibits a maximum around  $\beta\mu \simeq 0$ , implying that interactions are strongest at intermediate rather than low temperatures. This results from the fact that decreasing  $T/T_F$  at fixed  $\beta\varepsilon_b$  corresponds to an increasing  $\ln(k_F a_{2D})$ . Thus, we likewise expect the system to approach a weakly interacting gas in the low temperature regime. This behavior is qualitatively different from that observed in 3D,<sup>98</sup> and is a direct consequence of the fact that one can traverse the Fermi-Bose crossover in 2D by only varying the density.

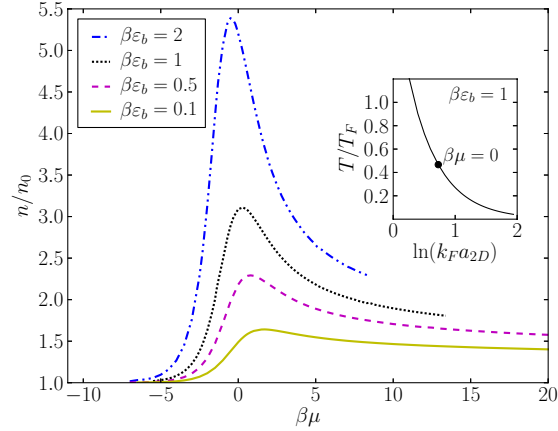


Fig. 19. The equation of state for the density at finite temperature, taken from Ref. 75. The density  $n$  is normalized by  $n_0(\beta\mu)$ , the density of the non-interacting Fermi gas. The curves for large  $\beta\epsilon_b$  are shown up to the critical value  $\mu_c(\beta\epsilon_b)$  where the system is expected to enter the BKT phase. The inset shows a typical trajectory corresponding to fixed  $\beta\epsilon_b$  in the phase space of  $T/T_F$  versus  $\ln(k_F a_{2D})$ . Along this line,  $\beta\mu$  increases with decreasing  $T/T_F$ .

## 6. The 2D polaron problem

The properties of an impurity immersed in a quantum-mechanical medium constitutes a fundamental problem in many-body physics. A classic example in the solid state is the Fröhlich polaron, an electron moving in a crystal and interacting with the resulting bosonic lattice vibrations. Due to the interactions, the system of impurity plus lattice vibrations is better described in terms of a quasiparticle, the polaron, which has modified effective mass, chemical potential, charge, etc., compared with the free electron. The quasiparticle thus encompasses both the electron and the cloud of excitations of the medium.

In the context of two-component Fermi gases, the spin components may be imbalanced straightforwardly, leading naturally to a polaron problem in the limit of a large spin polarization, i.e., the problem of a single spin-down impurity. However, in contrast to the case of the Fröhlich polaron, the medium is now fermionic, and this can strongly modify the character of the impurity quasiparticle, as we discuss below. Furthermore, the properties of the polaron will directly impact the topology of the whole phase diagram for the spin-imbalanced Fermi gas. It is well known that BCS pairing is very sensitive to mismatched Fermi surfaces, and such a spin imbalance can

thus lead to more exotic superfluid phases. For instance, the formation of Cooper pairs at finite momentum may occur, giving rise to the so-called Fulde-Ferrell-Larkin-Ovchinnikov (FFLO) state.<sup>99,100</sup> For sufficiently large spin imbalance, the system encounters the Chandrasekhar-Clogston limit and ceases to display paired-fermion superfluidity. This limit has recently been experimentally investigated in the strongly interacting Fermi gas in both 3D<sup>101–104</sup> and 1D,<sup>105</sup> but it remains to be seen how the breakdown of superfluidity occurs in the 2D Fermi gas. For a further discussion of the polarized Fermi gas in 3D, we refer the reader to, e.g., the reviews of Refs. 106 and 107.

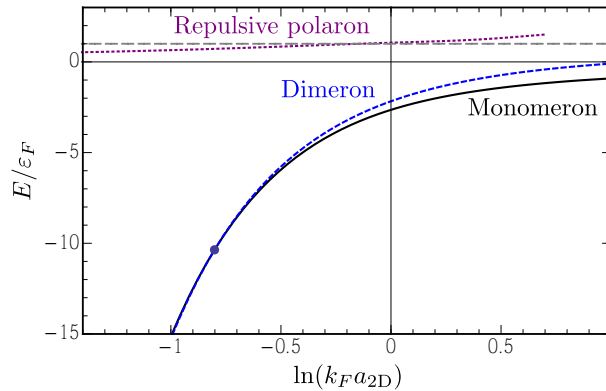


Fig. 20. The relevant quasiparticle branches in 2D for  $m_{\uparrow} = m_{\downarrow}$ : The monomeron (black, solid),<sup>108</sup> the dimeron (blue, dashed),<sup>109</sup> and the repulsive polaron (purple, dotted).<sup>110,111</sup> The filled circle marks the monomeron-dimeron transition in the ground state. The dot-dashed marks the Fermi energy. All quasiparticle energies displayed follow from variational wavefunctions limited to one particle-hole pair excitation (see text).

An important question concerns the nature of the ground state of a spin-down impurity atom in a spin-up Fermi sea. For weak attractive interactions, the quasiparticle has properties similar to that of the bare impurity and will be termed the “monomeron”.<sup>11</sup> However, as the interaction strength is increased, the impurity can bind a majority particle to form

<sup>11</sup>In this work we use the terminology monomeron, dimeron, trimeron, and tetrameron to denote the impurity bound to 0, 1, 2, and 3 majority atoms, respectively, in the presence of interactions with the Fermi sea. This replaces previous terminology (attractive polaron, molecule, dressed trimer, and dressed tetramer, respectively). As there is only one repulsive branch (see below) this is referred to as the repulsive polaron.

a two-body bound state dressed by particle-hole fluctuations of the Fermi sea.<sup>112–114</sup> This is illustrated in Fig. 20, which shows the quasiparticle branches for equal masses. Interestingly, in the fermionic problem, the impurity can undergo a sharp transition in the ground state and effectively change its statistics by binding fermions from the majority fermions, an effect absent in the classic Fröhlich polaron example above. Quasiparticles in a 2D Fermi gas have been investigated in two experiments: Fermi polarons have been observed,<sup>14</sup> while radio-frequency spectra of the unpolarized Fermi gas have been interpreted in terms of monomers.<sup>12</sup>

The polaron problem also has relevance to the phenomenon of *itinerant ferromagnetism*. Here, a two-component equal-mass Fermi gas with repulsive short-range interactions is predicted to spontaneously undergo a transition to spin-polarized domains for sufficiently strong repulsion. This classic Stoner transition received renewed interest when its observation was reported in a recent MIT experiment on the repulsive branch in 3D Fermi gases.<sup>115</sup> Subsequently, however, it was shown that the experiment had instead only observed a fast decay into pairs;<sup>116</sup> this realization led to the assertion that the Fermi gas with strong short-range repulsive interactions can never undergo a ferromagnetic transition.<sup>117</sup> The central issue is that strongly repulsive interactions can only be truly short-ranged if the underlying potential is attractive, and thus any magnetic phase in such a system will be metastable at best. As we describe below, the properties of the repulsive polaron (see Fig. 20) are crucial for determining whether saturated ferromagnetism may exist in the 2D Fermi gas, and it, in fact, appears that the fast decay into the attractive branch also precludes saturated ferromagnetism in 2D.<sup>111</sup> For a recent review on polaron physics in ultracold gases with an emphasis on the relation to itinerant ferromagnetism, we refer the reader to Ref. 118.

### 6.1. Variational approach

An intuitive way to describe the Fermi polaron theoretically is through variational wavefunctions. The simplest is Chevy's ansatz:<sup>119</sup>

$$|P\rangle = \alpha_0^{(\mathbf{p})} c_{\mathbf{p}\downarrow}^\dagger |FS\rangle + \sum_{\mathbf{k}\mathbf{q}} \alpha_{\mathbf{k}\mathbf{q}}^{(\mathbf{p})} c_{\mathbf{p}+\mathbf{q}-\mathbf{k}\downarrow}^\dagger c_{\mathbf{k}\uparrow}^\dagger c_{\mathbf{q}\uparrow} |FS\rangle. \quad (69)$$

Here and in the following we assume that  $|\mathbf{k}| > k_F$  ( $|\mathbf{q}| < k_F$ ) describes a particle (hole). For simplicity, we define  $k_F$  as the Fermi momentum of the spin- $\uparrow$  atoms. The wavefunction describes the spin- $\downarrow$  impurity as a quasiparticle at momentum  $\mathbf{p}$  using two terms: the first is simply the

bare impurity on top of the non-interacting majority Fermi sea, denoted by  $|FS\rangle$ , while the second incorporates how the impurity can distort the Fermi sea by exciting a particle out of it, leaving a hole behind.

The energy of the polaron state is obtained by minimizing the expectation value  $\langle P|\mathcal{H} - E|P\rangle$  with respect to the variational parameters  $\alpha_0^{(P)}$  and  $\alpha_{\mathbf{kq}}^{(P)}$ , where  $\mathcal{H}$  is the 2D Hamiltonian (54). This yields the equation

$$E - \epsilon_{\mathbf{p}\downarrow} = \sum_{\mathbf{q}} \left[ \frac{1}{g} - \sum_{\mathbf{k}} \frac{1}{E - \epsilon_{\mathbf{k}\uparrow} + \epsilon_{\mathbf{q}\uparrow} - \epsilon_{\mathbf{p}+\mathbf{q}-\mathbf{k}\downarrow}} \right]^{-1}. \quad (70)$$

Formally, the variational approach as introduced here only admits one solution: the monomeron,<sup>119</sup> which has energy less than the impurity in vacuum. However, the variational approach may be extended to include metastable states where the energy is allowed to have a finite imaginary part — see Ref. 120. In this case, one also obtains a second solution, the “repulsive polaron”,<sup>121,122</sup> which has an energy  $E_{\text{rep}}$  exceeding that of the impurity in vacuum and potentially even exceeding the Fermi energy for strong interactions. The wavefunction (69) may straightforwardly be extended by considering further excitations; however the present approximation of one particle-hole pair excitation gives a surprisingly good estimate of the energy and the residue  $Z = \left| \alpha_0^{(P)} \right|^2$ . This is due to an approximate cancellation of higher order terms in the expansion in particle-hole pairs.<sup>123</sup> A recent work in 3D has demonstrated an impressive agreement between the variational approach and experiment.<sup>124</sup>

In addition to the states described by Eq. (69), the impurity may also (depending on the  $\uparrow$ - $\downarrow$  mass ratio) form dimeron, trimeron, and tetramer states by binding one or several majority particles, in a natural analogy to the possible vacuum bound states such as the dimer, trimer, and tetramer described in Sec. 3. Remarkably, these states may be the ground states even when they do not bind in vacuum. The variational wavefunctions for such states can be generated in a similar fashion to Eq. (69) above, but rather than displaying them here, we instead refer the reader to the original works on the dimeron<sup>109,125–127</sup> and trimeron.<sup>39,120</sup>

## 6.2. The repulsive polaron and itinerant ferromagnetism

Following the observation that recombination processes preclude itinerant ferromagnetism in the 3D atomic Fermi gas,<sup>117</sup> it is pertinent to ask the question whether the Stoner transition can take place in a 2D Fermi gas.<sup>128</sup>

The main difference between the 2D and 3D Fermi gases with short-range interactions is that in 3D the vacuum two-body bound state appears in the regime of strongest interactions,  $1/k_F a_s = 0$ , whereas in 2D, the bound state only approaches the continuum in the limit of weak attraction. Thus, one may speculate that the pairing mechanism that prevented the appearance of itinerant ferromagnetism in 3D could be suppressed. Indeed, the three-body recombination mechanism by which three atoms recombine into an atom and a dimer takes completely different forms in 3D<sup>129</sup> and in 2D.<sup>53</sup> However, despite this difference, the decay into the attractive branch is still strong enough to exclude fully polarized itinerant ferromagnetism, as we now discuss.

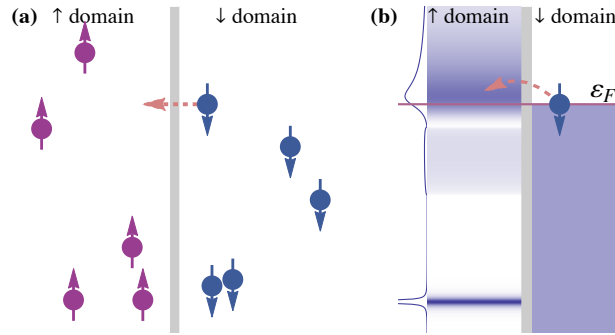


Fig. 21. Illustration of the stability condition for stable spin-polarized domains, taken from Ref. 130. (a) A spin- $\downarrow$  atom can tunnel across the interface and become an impurity in the spin- $\uparrow$  domain. (b) Density plot of the energy levels available to the fermion at  $\ln(k_F a_{2D}) = 0.5$ . The spectral function at  $\mathbf{k} = \mathbf{0}$  of the impurity in the  $\uparrow$  domain is evaluated in the one particle-hole pair dressing approximation.

Following Ref. 111, we investigate the stability of *fully polarized* domains. To preserve  $SU(2)$  symmetry and make a direct connection with ferromagnetism, we confine the discussion to equal-mass fermions. The fully polarized domains are illustrated in Fig. 21(a), and the central question is whether there is an energy cost associated with moving a spin- $\downarrow$  atom from its domain to that of the spin- $\uparrow$  atoms. Assuming purely repulsive interactions, this is the case if the energy of the dressed impurity exceeds the Fermi energy in the spin- $\uparrow$  region. If one further assumes mechanical equilibrium, where the pressures of the domains are equal, then the Fermi energies  $\varepsilon_F^\uparrow = \varepsilon_F^\downarrow$ . Thus, referring to Fig. 20 and assuming that the impurity would tunnel into the repulsive polaron state, the domains appear mechanically stable if  $\ln(k_F a_{2D}) > -0.15$  and one concludes that

itinerant ferromagnetism is possible.

However, we must consider two other effects: The first is the finite lifetime of the repulsive polaron, as the quasiparticle decay rate is predicted to be a significant fraction of the Fermi energy in the strongly interacting regime<sup>111</sup> (the decay rate may also be investigated as a pairing instability — see Ref. 131). This in turn leads to a large uncertainty in the energy of the repulsive state, allowing atoms to tunnel across the interface and depolarize the domains. Eventually, in the weakly interacting regime  $\ln(k_F a_{2D}) \gg 1$ , the quasiparticle decay rate becomes suppressed; however, as the tunneling probability is proportional to the residue  $Z$  of the corresponding quasiparticle, and the residue of the repulsive branch is strongly suppressed in this regime,<sup>110,111</sup> the atoms will tunnel directly into the attractive branch. Combining the knowledge of the residue and the lifetime of the repulsive polaron allows one to conclude that even if spin polarized domains were to be artificially created, these would not be dynamically stable.<sup>111</sup>

The repulsive polaron has been observed in a recent experiment<sup>14</sup> and, in accordance with the theory, no ferromagnetic transition was observed. In fact, the experiment<sup>o</sup> was limited to the regime  $-2.5 < \ln(k_F a_{2D}) < -1.3$ , i.e., away from the limit where the variational approach predicts  $E_{\text{rep}} > \varepsilon_F$ . In this regime, it may be expected that  $E_{\text{rep}} \gtrsim 0.3\varepsilon_F$  (see Fig. 20), whereas the experimentally observed energies ranged from 10% to 20% of the Fermi energy. The discrepancy may in part be due to the trap averaging<sup>110</sup> and finite temperature effects. However, in agreement with the theory,<sup>111</sup> the lifetime was severely suppressed, preventing the detection of a coherent repulsive quasiparticle for stronger interactions.

### 6.3. Ground state of an impurity in a 2D Fermi gas

In the following, we initially focus on the equal-mass case. For a single impurity attractively interacting with a 3D Fermi gas of identical atoms, the existence of a sharp quasiparticle transition from the monomeron to the dimeron state has been predicted.<sup>112–114</sup> Such a transition was recently observed experimentally for a finite density of impurities.<sup>133</sup> On the other hand, in the 1D case, the exact Bethe ansatz solution<sup>134</sup> implies that no

<sup>o</sup>In the experiment, the 2D scattering length was taken directly from the quasi-2D dimer binding energy, i.e.,  $a_{2D}^* = 1/\sqrt{m\varepsilon_b}$ . The relation between the present definition of  $a_{2D}$  and the one used in experiment is:  $a_{2D} = a_{2D}^* \sqrt{\frac{\pi}{B} \frac{\varepsilon_b}{\omega_z} e^{-\sqrt{\frac{\pi}{2}} \mathcal{F}_0(\varepsilon_b/\omega_z)}}$ , where  $\mathcal{F}_0$  was introduced in Eq. (26). As argued in Ref. 132, the convention used for  $a_{2D}$  in this review yields a better agreement between the results of the quasi-2D experiments and the strict 2D theory presented here.

such transition takes place. It is therefore natural to ask whether a transition in the ground state occurs for an impurity in a 2D Fermi gas, where quantum fluctuations are expected to be stronger than in 3D. The existence or otherwise of such a transition will impact the overall phase diagram for the spin-imbalanced 2D Fermi gas.<sup>135–138</sup>

The first work on this subject<sup>108</sup> did not find any ground-state transition, the issue being that the authors did not consider the monomeron and dimeron on an equal footing in terms of particle-hole pair dressing of the variational wavefunctions. Later, one of us<sup>109</sup> included a particle-hole pair excitation in the dimeron variational wavefunction to show that there is indeed a ground state transition. We recently extended this analysis to argue that, under a minimal set of assumptions, the critical interaction strength for the monomeron-dimeron transition must lie in the interval<sup>120</sup>

$$-0.97 < \ln(k_F a_{2D})_{\text{crit}} < -0.80. \quad (71)$$

The lower (upper) bound corresponds to comparing the dimeron dressed by one particle-hole pair excitation with the monomeron dressed by two (one) excitations. As seen in Fig. 22(a), our result agrees with the critical interaction found in two recent diagrammatic Monte Carlo studies:  $\ln(k_F a_{2D})_{\text{crit}} = -0.95(0.15)$  [Ref. 139] and  $\ln(k_F a_{2D})_{\text{crit}} = -1.1(0.2)$  [Ref. 140].

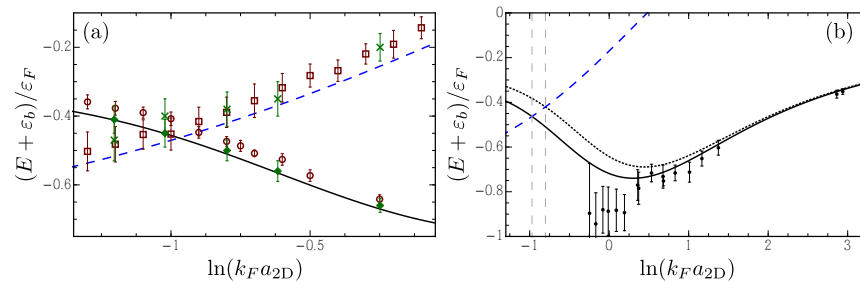


Fig. 22. Energy of the impurity measured from the two-body binding energy. The dotted line corresponds to the energy of the monomeron within the Chevy ansatz,<sup>108</sup> Eq. (70), while the solid line is within the two particle-hole pair approximation.<sup>120</sup> The dashed line is the energy of the dimeron within the one particle-hole pair approximation.<sup>109</sup> (a) The data points are from the two recent Monte Carlo simulations: for the monomeron (dimeron) these are marked by red open squares (circles)<sup>139</sup> and by green diamonds (crosses).<sup>140</sup> Note that the variational approach provides an upper bound on the energy. (b) The ground state transition within the two approximations for the monomeron energy are illustrated by vertical dashed lines, while the experimental data<sup>o</sup> is taken from Ref. 14.

The monomeron was investigated in a recent experiment,<sup>14</sup> and Fig. 22(b) shows that for  $\ln(k_F a_{2D}) \geq 0.3$  the comparison between theory and experiment is excellent. For stronger attraction, the agreement becomes progressively worse until at  $\ln(k_F a_{2D}) \simeq -0.6$  the measured effective mass appears to diverge, which was taken to be a signature of the monomeron-dimeron transition.<sup>14</sup> However, if one extrapolates the measured residue to zero,<sup>141</sup> one instead obtains a critical interaction strength of  $\ln(k_F a_{2D})_{\text{crit}} = -0.88(0.20)$ , which is in good agreement with theory.<sup>109,120</sup> As mentioned previously, the experimental investigation of the polaron problem can be complicated by temperature effects and trap averaging. In addition, one must consider the fact that the high polarization limit typically corresponds to a *finite density* of spin- $\downarrow$  impurities.<sup>142</sup> Thus, we are faced with the question of whether the single-impurity transitions are thermodynamically stable, i.e., whether they are preempted by first-order transitions in the thermodynamic limit. We have recently shown<sup>120</sup> that a first-order superfluid-normal phase transition preempts the single-impurity transition at zero temperature, similarly to the situation in 3D.<sup>39</sup> However, this result requires the presence of a superfluid, and thus it is an open question whether single-impurity transitions may exist at higher temperatures.

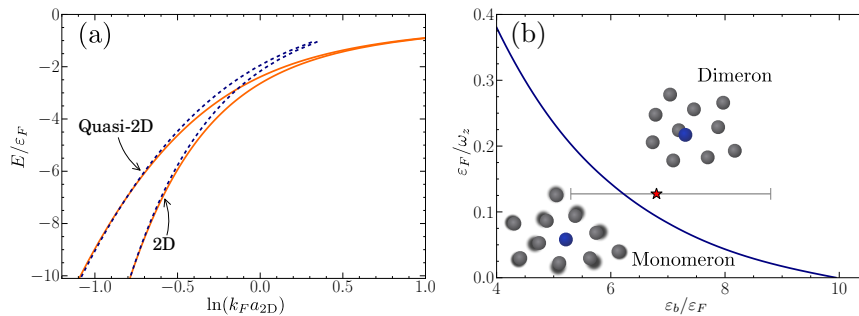


Fig. 23. The behavior of the quasi-2D polaron taken from Ref. 132. (a) Monomeron (solid lines) and dimeron (dashed) energies in 2D and in quasi-2D at  $\varepsilon_F/\omega_z = 1/10$ . (b) The single impurity phase diagram. The ground state of the impurity is a monomeron (dimeron) to the left (right) of the line. The theory lines are all within the one particle-hole pair approximation. The star shows the experimental transition point with error bars.<sup>141</sup>

In the present discussion, we have mapped<sup>o</sup> the results of the experiment onto a pure 2D theory. However, let us now discuss the validity of such an approach.<sup>132</sup> The transverse confinement applied in the experiment<sup>14</sup> was

$\omega_z = 2\pi \times 78.5\text{kHz}$ , while the Fermi energy of the majority component was  $2\pi \times 10\text{kHz}$ . This in turn means that the pure 2D theory<sup>109,120</sup> predicts the transition to occur when  $\varepsilon_b \geq 2\pi \times 100\text{kHz}$ , *i.e.* when the binding energy exceeds the transverse confinement strength. In this regime, the binding energy is strongly modified from the 2D prediction — see Fig. 2 and the discussion in Sec. 2. On the other hand, the ground state transition is governed by interactions that take place at the typical energy scale  $\sim \varepsilon_F$ . Since  $\varepsilon_F \ll \omega_z$  the low-energy quasi-2D theory described by Eqs. (28) and (29) is still approximately valid, explaining our choice of using a definition of  $a_{2D}$  which derives from low-energy scattering rather than the binding energy.

The deviation from the pure 2D limit of the monomeron-dimeron transition may be further investigated<sup>132</sup> by including harmonic oscillator levels in the variational wavefunction and using the full quasi-2D Hamiltonian (43). The results of such an analysis are shown in Fig. 23, where we see how the transition point indeed changes very little in  $\ln(k_F a_{2D})$  for  $\varepsilon_F/\omega_z \lesssim 1/10$ , while on the other hand the change is rather large in terms of the parameter  $\varepsilon_b/\varepsilon_F$ .

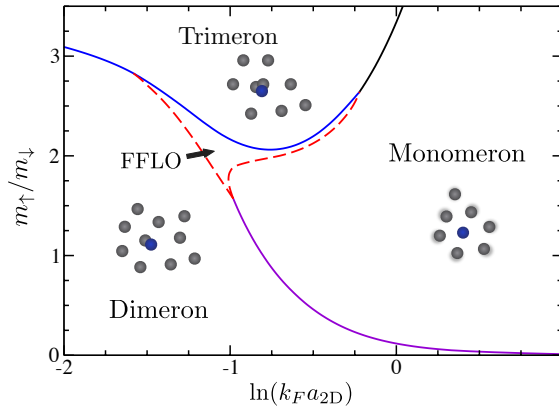


Fig. 24. Ground-state phase diagram for a single impurity atom of mass  $m_\downarrow$  immersed in a gas of fermions of mass  $m_\uparrow$ , adapted from Ref. 120. The phase boundaries are derived within the one particle-hole pair dressing approximation. The single-impurity analog of the FFLO phase corresponds to a ground state dimeron at non-zero momentum.

We finally turn to the mass-imbalanced system, where the single impurity phase diagram<sup>120</sup> as a function of interaction strength takes the form displayed in Fig. 24. In Sec. 3 we discussed how in vacuum the  $\uparrow\downarrow$  trimer

appears<sup>37</sup> when  $m_{\uparrow}/m_{\downarrow} = 3.33$ . Remarkably it is seen that the presence of a Fermi sea favors trimer formation: within the approximation used, the trimeron is predicted to be the ground state for mass ratios  $m_{\uparrow}/m_{\downarrow} \geq 2.1$ . This lower critical mass ratio may be understood as a consequence of the kinetic energy cost involved in forming a dimeron at rest: in the simplest approximation, the impurity at momentum  $+\mathbf{k}_F$  binds a majority atom at  $-\mathbf{k}_F$  and, if the impurity is sufficiently light, it may be energetically favorable to instead form a dimeron at finite momentum or a trimeron. The same effect was predicted in 3D.<sup>39</sup> While the trimeron is favored by the Fermi sea, we found<sup>120</sup> that the tetramer appears disfavored, i.e., the critical mass ratio for tetramer formation in the strongly interacting regime increases from its vacuum value<sup>41</sup> of  $m_{\uparrow}/m_{\downarrow} = 5.0$ .

The possibility of a dimeron at finite momentum is of considerable interest, since it is a single-particle analog of the FFLO phase — for a small but finite density of impurities this has been shown to lead to a spatially-modulated superfluid.<sup>143,144</sup> We see in Fig. 24 that the FFLO dimeron occupies a considerable part of the phase diagram, making it possible that FFLO physics may be observed in the strongly spin-imbalanced 2D Fermi gas.

## 7. Dynamics

Dynamical properties provide a powerful probe into the nature of interactions in strongly correlated quantum systems. For instance, it has been predicted that the harmonically trapped 2D quantum gas features an  $SO(2,1)$  dynamical scaling symmetry due to the (classical) scale invariance of the uniform gas with contact interactions. A consequence of this symmetry is the existence of an undamped monopole breathing mode with frequency exactly twice that of the trap.<sup>145</sup> While true in the absence of interactions, the scale invariance which exists at the classical level is broken by the procedure of renormalization,<sup>145</sup> the so-called *quantum anomaly*.<sup>146</sup> Thus, the shift of the breathing mode frequency probes the breaking of scale invariance in the interacting 2D quantum gas. Another dynamical phenomenon is that of spin diffusion, the process that evens out differences in spin polarization across the gas. Here the diffusivity in the strongly interacting and degenerate regime is naturally of order  $\hbar/m$  and an interesting possibility is that there is a universal lower bound set by quantum mechanics.

As of now, there have been experiments on the collective modes in a harmonic trap<sup>16</sup> and on spin transport.<sup>147</sup> The results of the experiments

have indicated several surprising features of the 2D Fermi gas: an undamped breathing mode with a frequency compatible with no shift from the classical (non-interacting) result; a quadrupole mode strongly damped even in the weakly interacting regime; and a transverse spin diffusivity three orders of magnitude smaller than in any other system. The strong damping of the quadrupole mode may be explained,<sup>148</sup> at least in part,<sup>149</sup> by the anisotropy of the trapping potential used. However at first sight the other two features appear contradictory, as the results of the breathing mode experiment indicate that the effect of interactions is much weaker than expected by theories, while the spin diffusivity experiment indicates the opposite. Ultimately, further experiments as well as possibly finite temperature QMC calculations will likely be needed to shed light on the discrepancy.

In this section we assume a purely 2D geometry, such that the transverse confinement frequency  $\omega_z$  drops out of the problem. The experiments described here are indeed all in the regime where  $T \leq T_F \lesssim 0.1\omega_z$ , so this approximation is reasonable.

### **7.1. Classical scale invariance, a hidden $SO(2, 1)$ symmetry, and the breathing mode**

It has been predicted<sup>145</sup> that a 2D quantum gas in a harmonic transverse trapping potential features an undamped monopole breathing mode with frequency exactly twice that of the trap. The origin of this surprising result is the (classical) scale invariance of the Hamiltonian with a short-range  $\delta$ -function interaction. Define the  $2N$  dimensional vector  $\mathbf{X} = (\boldsymbol{\rho}_1, \dots, \boldsymbol{\rho}_N)$ , with  $\boldsymbol{\rho}_i$  the positions of the atoms  $i = 1, \dots, N$ , and the hyperradius  $X \equiv |\mathbf{X}|$ . In real space, both terms in the Hamiltonian

$$H_0 = -\frac{\Delta_{\mathbf{X}}^2}{2m} + g \sum_{i < j} \delta(\boldsymbol{\rho}_i - \boldsymbol{\rho}_j) \quad (72)$$

scale as  $\lambda^{-2}$  under the scale transformation  $\mathbf{X} \rightarrow \lambda\mathbf{X}$ , and consequently the Hamiltonian is scale invariant. While this is true classically, the procedure of renormalization of the quantum theory introduces a scale, the 2D scattering length  $a_{2D}$ , as discussed in Section 2; the absence of a scale in the classical theory and the introduction of one through renormalization is known as a quantum anomaly. The scale invariance is still approximately valid in the limits  $a_{2D} \rightarrow 0$  and  $a_{2D} \rightarrow \infty$  where the following results

apply.<sup>P</sup>

The presence of a harmonic trapping potential

$$H_{\text{trap}} = \frac{1}{2}m\omega_0 X^2 \quad (73)$$

in the 2D plane obviously breaks the scale invariance as it scales as  $\lambda^2$  under  $\mathbf{X} \rightarrow \lambda\mathbf{X}$ . However, it leads to a very interesting algebra:<sup>145</sup> using the usual commutation relations for  $\mathbf{X}$  and  $\mathbf{P} \equiv i\partial_{\mathbf{X}}$ , one may easily show  $[H_{\text{trap}}, H] = i\omega_0^2 Q$ . Here  $Q \equiv \frac{1}{2}(\mathbf{P} \cdot \mathbf{X} + \mathbf{X} \cdot \mathbf{P})$ ,  $e^{-\ln(\lambda)Q}$  is the generator of scale transformations,<sup>151</sup> and  $H = H_0 + H_{\text{trap}}$  is the total Hamiltonian. Then defining the operators

$$L_1 = \frac{1}{2\omega_0}(H_0 - H_{\text{trap}}), \quad L_2 = Q/2, \quad L_3 = \frac{1}{2\omega_0}(H_0 + H_{\text{trap}}), \quad (74)$$

these satisfy

$$[L_1, L_2] = -iL_3, \quad [L_2, L_3] = iL_1, \quad [L_3, L_1] = iL_2, \quad (75)$$

which is the algebra of the Lorentz group in 2D,  $SO(2,1)$ . As usual, one may then define raising and lowering operators  $L_{\pm} = \frac{1}{\sqrt{2}}(L_1 \pm iL_2)$ . From the commutation relations  $[H, L_{\pm}] = \pm 2\omega_0 L_{\pm}$  it follows that if  $|\Psi_g\rangle$  is the ground state with energy  $E_g$ , the state  $L_+|\Psi_g\rangle$  has energy  $E_g + 2\omega_0$  while  $L_-|\Psi_g\rangle = 0$ . Thus the repeated action of  $L_+$  generates a tower of states, separated by  $2\omega_0$  and these may be identified with the breathing modes of the system. For instance, if the system is initially in a stationary state with a constant trap frequency  $\omega_0$  at time  $t < 0$ , the trap frequency is slightly perturbed during the interval  $0 < t < t_f$ , and returns to its initial value at time  $t > t_f$ , one finds<sup>150</sup> that the final state scale oscillates around unity with frequency  $2\omega_0$ . That is, the lowest breathing mode has been excited.

In the above scale invariant (and non-interacting) regimes, the breathing mode is undamped and its frequency is independent of amplitude. On the other hand, in the interacting quantum system, the breathing mode is shifted to  $\omega_B = 2\omega_0 + \delta\omega_B$  from its non-interacting value, as discussed in the Bose case in Ref. 146. In the 2D Fermi gas,<sup>q</sup> this shift has been modelled<sup>153</sup> (see also Refs. 152,154,155) by assuming a hydrodynamic description of the strongly interacting regime, and a polytrope  $P \sim n^{\gamma+1}$  for the dependence of pressure on density. These assumptions allow for

<sup>P</sup>Whereas the scale invariance in 2D is only exact in the trivial non-interacting limits, it is, in fact, quantum mechanically exact for the 3D unitary Fermi gas<sup>150</sup> as well as for the 1D gas in the Tonks limit, both strongly interacting systems.

<sup>q</sup>In fact, within mean-field theory, the breathing mode has frequency  $2\omega_0$  in the entire BCS-BEC crossover.<sup>152</sup>

a solution of the linearized hydrodynamic equations, and in turn for the breathing mode frequency,  $\omega_B = \omega_0 \sqrt{2 + 2\gamma}$ .  $\gamma$  itself was obtained by comparing with the zero-temperature QMC data<sup>55</sup> discussed in Section 4. The resulting frequency shift is shown in Fig. 25, and is seen to be of order 10% in the regime of strong interactions,  $\ln(k_F a_{2D}) \sim 0$ .

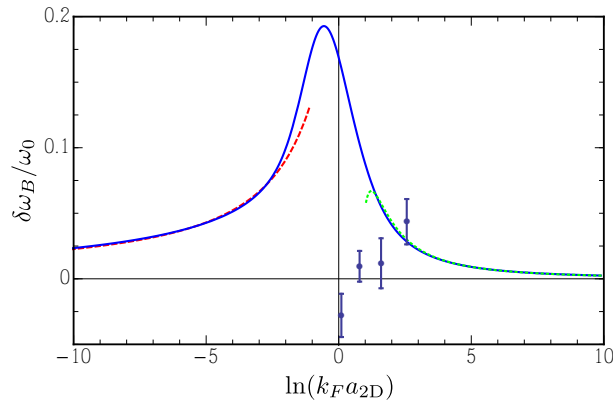


Fig. 25. Shift of the breathing mode as a function of interaction parameter. The solid line (full theory), dashed (BEC limit), and dotted (BCS limit) are the theory curves from Ref. 153 while the data points are from the experiment.<sup>16</sup>

Experimentally, the breathing mode was investigated<sup>16</sup> using a procedure essentially as described above: The two-dimensional confinement was adiabatically lowered from the initial configuration and then abruptly returned to its original configuration. After a variable wait time, the confinement was switched off and the density distribution was revealed by an absorption image after time of flight. The experiment investigated a large range of interaction strengths,  $0 \lesssim \ln k_F a_{2D} \lesssim 500$ . Surprisingly, the results of the experiment were consistent with the scale invariant assumption above, i.e., no significant frequency shift was observed, even in the regime of strong interactions (see Fig. 25). The results beg the question whether the zero-temperature equation of state<sup>55</sup> is appropriate for the comparison with the experiment at  $T/T_F = 0.4$ , i.e., whether the apparent scale invariance arises due to finite temperature effects.<sup>153</sup> Indeed, in the high temperature limit the shift of the breathing mode may be analyzed by combining the virial expansion of the equation of state with a variational method in the hydrodynamic regime.<sup>156</sup> The results of this analysis are consistent with the experiment and the theoretical curve in Fig. 25 in the regime of validity

of the approach,  $\ln(k_F a_{2D}) \gtrsim 1.75$ .

The damping of the breathing mode is related to the bulk viscosity. In particular both the bulk viscosity and the damping are expected to vanish in the normal phase in the regime where the  $SO(2,1)$  symmetry is exact, as first pointed out in the context of the unitary Fermi gas.<sup>157</sup> Using a sum rule, the bulk viscosity has been argued<sup>152</sup> to vanish in the weakly interacting limits  $|\ln(k_F a_{2D})| \gg 1$ . However, in the intermediate strongly interacting regime one expects a non-vanishing bulk viscosity and related damping of the breathing mode. Therefore it is surprising that the experiment<sup>16</sup> measures a damping consistent with vanishing bulk viscosity across the entire interaction range.

## 7.2. Quadrupole mode

In addition to the breathing mode, the experiment<sup>16</sup> considered the quadrupole mode, corresponding to an excitation with velocity field  $\mathbf{x} - \mathbf{y}$  oscillating with frequency  $\omega_Q$ . The excitation procedure was similar to the monopole mode described above: the radial trap was adiabatically made elliptical, followed by an abrupt return to the original configuration, a short free oscillation, and an absorption image after time of flight. The results of the experiment are shown in Fig. 26(a). Two regimes are immediately identifiable: the collisionless regime, where  $\ln(k_F a_{2D}) \gg 1$  and  $\omega_Q \approx 2\omega_0$ , and the hydrodynamic regime, where  $\omega_Q \approx \sqrt{2}\omega_0$ . The theory curves<sup>148</sup> (see also Ref. 158) are calculated using kinetic theory and correctly identify the onset of the hydrodynamic regime. The theory is not expected to be valid when  $\ln(k_F a_{2D}) \lesssim 0.5$ , where the (zero-temperature) chemical potential is negative<sup>81</sup> (see the discussion in Sec. 4.4) and pairing becomes significant.

The damping of the quadrupole mode is shown in Fig. 26(b): it is seen that this is a sizeable fraction of the trap frequency, and curiously this is the case even in the weakly interacting regime  $\ln(k_F a_{2D}) \gg 1$  — in fact, the experiment<sup>16</sup> showed that the large damping persists up to very large  $\ln(k_F a_{2D}) \sim 500$ , far into the collisionless regime where the damping is expected to vanish, and kinetic theory is valid. Ref. 148 argued that the large damping in the weakly interacting regime arises mainly from systematic effects, which generate an approximately constant damping across all interaction strengths (indeed a smaller constant damping was also observed in the breathing mode experiment described above). The anisotropy of the trap before time of flight may then account for the remaining discrepancy in this limit.<sup>148</sup> However, a recent analysis using a realistic trapping potential

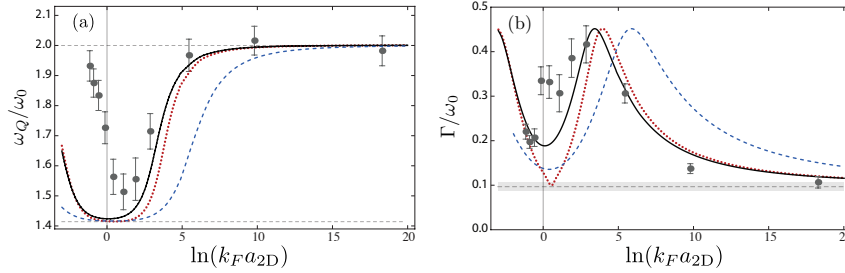


Fig. 26. (a) Quadrupole frequency and (b) damping as a function of interaction parameter. The lines are the theoretical curves<sup>148</sup> in the Boltzmann limit (blue, dashed), with Pauli blocking only (black, solid), and with additional medium effects (red, dotted). The black dots are the results of the experiment.<sup>16</sup> The trap frequency here is  $\omega_0 = \sqrt{\omega_x \omega_y}$ . In (b) a constant shift has been applied to the theory to account for systematic effects. Figure adapted with permission from Ref. 148. Copyrighted by the American Physical Society.

and including even the effect of gravity concluded that the damping of the quadrupole mode in the weakly interacting regime could not be explained by the specific geometry of the trap.<sup>149</sup> In the strongly interacting hydrodynamic regime, the damping may be related to the shear viscosity of the gas.<sup>159–161</sup>

### 7.3. Spin diffusion

An interesting application of fermionic quantum gases is the study of spin transport. These systems may provide particularly clean experimental realizations compared with, e.g.,  $^3\text{He}$ - $^4\text{He}$  solutions, since in the quantum gases the interactions are tunable and spin states may be manipulated in a coherent manner by radio-frequency pulses. One basic transport process is that of spin diffusion, recently investigated in the context of ultracold atomic gases.<sup>147,162</sup> This process acts to even out differences in polarization. Writing the magnetization as a product of the magnitude and the direction,  $\mathcal{M} = \mathcal{M}\hat{\mathbf{e}}$ , there are two contributions to the magnetization gradient  $\nabla\mathcal{M} = (\nabla\mathcal{M})\hat{\mathbf{e}} + \mathcal{M}\nabla\hat{\mathbf{e}}$ . The first of these, longitudinal diffusion, acts between regions of different magnitude of magnetization, while the second, transverse diffusion, acts between regions of different orientation.

In the light of the proposed quantum limit of the ratio of shear viscosity to entropy density,<sup>163</sup> it is interesting to ask the question whether quantum mechanics provides a lower bound for other transport phenomena such as spin diffusion in a strongly interacting Fermi gas. As decoherence is introduced by collisions, the resulting spin diffusivity may be expected to go as

the collision speed of two atoms multiplied by the mean free path. In the degenerate regime, the former may be taken to be  $\hbar k_F/m$ , while the mean free path is  $1/n\sigma \sim 1/k_F$ ; the density  $n \sim k_F^2$  and the cross section in the degenerate regime takes its strongest value allowed by quantum mechanics, *i.e.*  $k_F^{-1}$ . Thus the diffusivity may be expected to be of order  $\hbar/m$  in the degenerate regime and indeed the lowest spin diffusivity for longitudinal spin currents has been measured to be  $6.3\hbar/m$  in a 3D quantum degenerate Fermi gas at unitarity.<sup>162</sup> In general this argument is too simple; for instance it neglects the effect of Pauli blocking which causes the longitudinal spin diffusivity in the Fermi liquid to diverge as  $1/T^2$  at low temperature. Note that for the purpose of this discussion we have displayed  $\hbar$  explicitly.

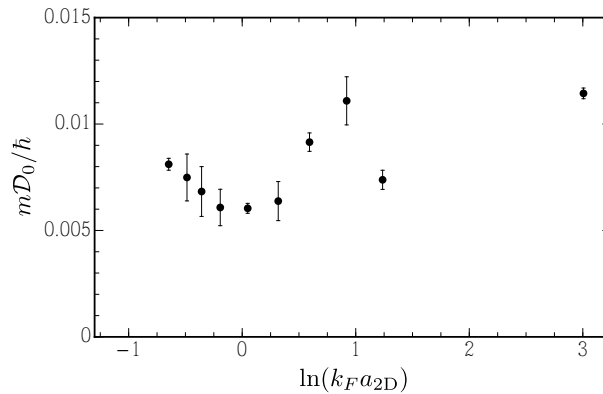


Fig. 27. Transverse spin diffusivity measured in experiment<sup>147</sup> across the strongly interacting regime.

Surprisingly, a recent experiment<sup>147</sup> has found a transverse spin diffusivity in the strongly interacting regime that is orders of magnitude smaller than  $\hbar/m$ . Starting from a fully polarized 2D gas of  $^{40}\text{K}$  atoms, the experiment used a spin-echo technique consisting of three consecutive radio-frequency pulses: First, a  $\pi/2$  pulse was applied to rotate the spin into a coherent superposition of  $\uparrow$  and  $\downarrow$  states. A magnetic field gradient ensured a transverse spin wave due to the difference in gyromagnetic ratio of the two spin states, thus lifting the spin polarization and allowing the different spin states to collide and diffuse. Trivial dephasing due to the magnetic field gradient was reversed by the application of a  $\pi$  pulse after a time  $\tau$ . This ensured that the spin state would refocus at time  $2\tau$  in the absence of decoherence, in which case the final  $\pi/2$  pulse would rotate the spin state

back to the original one. The experimental observable was the final magnetization  $\langle M \rangle \equiv (N_{\uparrow} - N_{\downarrow}) / (N_{\uparrow} + N_{\downarrow})$ , and by measuring this for different spin evolution times  $2\tau$ , the transverse spin diffusivity was extracted.<sup>r</sup> The results are shown in Fig. 27, and it is seen that  $\mathcal{D}_0$  has a shallow minimum around  $\ln(k_F a_{2D}) = 0$ , with values as low as  $0.006\hbar/m$ .

The transverse spin diffusivity in the 2D Fermi gas was recently investigated using a kinetic theory based on a many-body  $T$  matrix.<sup>164</sup> Indeed, it was found that medium effects could substantially suppress the spin diffusion below  $\hbar/m$ , see Fig. 28. As shown in the figure, the theory also predicts that at temperatures below  $T_F$ , the transverse spin diffusivity is quite sensitive to magnetization and gets suppressed as the magnetization decreases. The origin of the suppression lies in the enhanced cross section in the many-body system close to the Thouless pole and, as discussed in Sec. 4, the Thouless pole overestimates the critical temperature. However, it is likely that the theory captures the correct qualitative behavior; thus this feature may have implications for the interpretation of the experiment, which assumes a constant transverse spin diffusivity over the timescale  $2\tau$ .

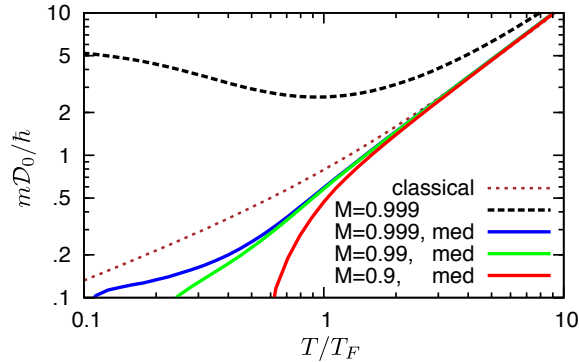


Fig. 28.  $\mathcal{D}_0$  as a function of temperature at  $\ln(k_F a_{2D}) = 0$  for various magnetizations.<sup>164</sup> The dashed (black) line includes Pauli blocking only, while the dotted line is the high-temperature Boltzmann limit. For comparison, the experiment<sup>147</sup> was carried out at  $T/T_F = 0.24(3)$ .

Reprinted figure with permission from: T. Enss, *Phys. Rev. A* **88**, 033630 (2013). Copyright 2013 by the American Physical Society.

<sup>r</sup> $\mathcal{D}_0$  was obtained from the magnetization using the time evolution  $\langle M_z \rangle \propto e^{-(2/3)\mathcal{D}_0(\delta\gamma B')^2\tau^3}$  with  $\delta\gamma$  the difference in gyromagnetic ratio between the two spin states and  $B' = \partial B_z / \partial x$  the magnetic field gradient.

## 8. Discussion and outlook

Low-dimensional Fermi gases are expected to feature stronger correlations and larger quantum fluctuations than their 3D counterparts. Yet, some of the first experiments on the 2D Fermi gas appear to have observed the opposite. The monopole breathing mode apparently displays no shift from the predicted value in the absence of interactions, indicating a scale invariant system.<sup>16</sup> Likewise, the energy of the repulsive branch of the polarized Fermi gas was found to be much smaller than that predicted theoretically.<sup>14</sup> This could imply one of two things: either our expectation of strong correlations in the 2D Fermi gas is incorrect, or there are additional factors present in 2D experiments that need to be taken into account. For instance, the apparent scale invariance may be influenced by finite temperature, the quasi-2D nature of the gas, or even the in-plane trapping potential and trap averaging. Thus, a detailed theoretical understanding of these effects is important.

Indeed, a major challenge currently facing experiments on 2D Fermi gases is to achieve ultracold temperatures under strong confinement. As such, superfluidity in the 2D Fermi gas has not yet been realized experimentally. Given that the BKT transition has already been observed in 2D Bose gases,<sup>86</sup> it is likely that superfluidity in the Bose regime of the crossover in Fermi gases will soon be realized. It may prove more difficult to observe the superfluid phase in the BCS regime because of the reduced  $T_c$  in this limit. However, as one of us has recently argued,<sup>76</sup> the quasi-2D nature of the gas could turn out to be advantageous here, since mean-field theory predicts that  $T_c/\varepsilon_F$  is increased as the confinement is relaxed at fixed  $\varepsilon_F/\varepsilon_b$  and the Fermi system is tuned away from 2D. This raises the tantalizing possibility of  $T_c$  being maximal in the regime intermediate between 2D and 3D.

Thus far, cold-atom experiments have only just begun to explore the behavior of fermions in 2D. Even above  $T_c$ , a pseudogap regime has not yet been conclusively observed: while a gap in the spectra has been nicely demonstrated,<sup>10</sup> it seems likely that this is due to two-body effects only, and any apparent reduction of the gap at finite temperature is due to thermal broadening.<sup>81</sup> Thus, the interaction strength *vs* temperature phase diagram requires further investigation. In the future, we expect an increasing array of tuning “knobs” to be added to the exploration of 2D Fermi gases. There is the prospect of varying the spin imbalance and achieving superfluid-normal transitions at zero temperature. Moreover, heteronuclear Fermi-Fermi mixtures promise a fascinating new playground, where novel bound

states become possible as the mass ratio is increased. Ultimately, one would like to fully uncover the fundamental differences between 2D and other dimensions.

### Acknowledgements

We gratefully acknowledge our collaborators on 2D Fermi gases and related subjects for many illuminating discussions. In particular, we thank Marianne Bauer, Stefan Baur, Georg Bruun, Nigel Cooper, Tilman Enss, Andrea Fischer, Peter Littlewood, Francesca Marchetti, Pietro Massignan, Vudtiwat Ngampruetikorn, Dmitry Petrov, and Gora Shlyapnikov. Michael Köhl is thanked for several very useful discussions on experiments in 2D Fermi gases, and for sharing the data of Refs. 14,16,147. We also wish to thank Stefan Baur, Georg Bruun, Pietro Massignan, and Vudtiwat Ngampruetikorn for helpful feedback on the manuscript. Stefan Baur and Vudtiwat Ngampruetikorn are also thanked for help with figures. We thank Johannes Hofmann for sharing the data of Ref. 153, Jonas Vlietinck for sharing the data of Ref. 139, and Peter Kroiß for sharing the data of Ref. 140. This work was supported in part by the National Science Foundation under Grant No. PHYS-1066293 and the hospitality of the Aspen Center for Physics. MMP acknowledges support from the EPSRC under Grant No. EP/H00369X/2.

### References

1. M. R. Norman, The challenge of unconventional superconductivity, *Science*. **332**, 196 (2011).
2. D. L. Smith and C. Mailhot, Theory of semiconductor superlattice electronic structure, *Rev. Mod. Phys.* **62**, 173–234 (1990).
3. J. Singleton and C. Mielke, Quasi-two-dimensional organic superconductors: A review, *Contemporary Physics*. **43**, 63–96 (2002).
4. N. D. Mermin and H. Wagner, Absence of ferromagnetism or antiferromagnetism in one- or two-dimensional isotropic heisenberg models, *Phys. Rev. Lett.* **17**, 1133–1136 (1966).
5. P. C. Hohenberg, Existence of long-range order in one and two dimensions, *Phys. Rev.* **158**, 383–386 (1967).
6. K. Günter, T. Stöferle, H. Moritz, M. Köhl, and T. Esslinger,  $p$ -wave interactions in low-dimensional fermionic gases, *Phys. Rev. Lett.* **95**, 230401 (2005).
7. K. Martiyanov, V. Makhalov, and A. Turlapov, Observation of a two-dimensional Fermi gas of atoms, *Phys. Rev. Lett.* **105**, 030404 (2010).

8. B. Fröhlich, M. Feld, E. Vogt, M. Koschorreck, W. Zwerger, and M. Köhl, Radio-frequency spectroscopy of a strongly interacting two-dimensional Fermi gas, *Phys. Rev. Lett.* **106**, 105301 (2011).
9. P. Dyke, E. D. Kuhnle, S. Whitlock, H. Hu, M. Mark, S. Hoinka, M. Lingham, P. Hannaford, and C. J. Vale, Crossover from 2D to 3D in a weakly interacting Fermi gas, *Phys. Rev. Lett.* **106**, 105304 (2011).
10. M. Feld, B. Fröhlich, E. Vogt, M. Koschorreck, and M. Köhl, Observation of a pairing pseudogap in a two-dimensional Fermi gas, *Nature*. **480**, 75 (2011).
11. A. T. Sommer, L. W. Cheuk, M. J. H. Ku, W. S. Bakr, and M. W. Zwierlein, Evolution of fermion pairing from three to two dimensions, *Phys. Rev. Lett.* **108**, 045302 (2012).
12. Y. Zhang, W. Ong, I. Arakelyan, and J. E. Thomas, Polaron-to-polaron transitions in the radio-frequency spectrum of a quasi-two-dimensional Fermi gas, *Phys. Rev. Lett.* **108**, 235302 (2012).
13. S. K. Baur, B. Fröhlich, M. Feld, E. Vogt, D. Pertot, M. Koschorreck, and M. Köhl, Radio-frequency spectra of Feshbach molecules in quasi-two-dimensional geometries, *Phys. Rev. A*. **85**, 061604 (2012).
14. M. Koschorreck, D. Pertot, E. Vogt, B. Fröhlich, M. Feld, and M. Köhl, Attractive and repulsive Fermi polarons in two dimensions, *Nature*. **485**, 619 (2012).
15. B. Fröhlich, M. Feld, E. Vogt, M. Koschorreck, M. Köhl, C. Berthod, and T. Giamarchi, Two-dimensional Fermi liquid with attractive interactions, *Phys. Rev. Lett.* **109**, 130403 (2012).
16. E. Vogt, M. Feld, B. Fröhlich, D. Pertot, M. Koschorreck, and M. Köhl, Scale invariance and viscosity of a two-dimensional Fermi gas, *Phys. Rev. Lett.* **108**, 070404 (2012).
17. V. Makhlov, K. Martinyanov, and A. Turlapov, Ground-state pressure of quasi-2D Fermi and Bose gases, *Phys. Rev. Lett.* **112**, 045301 (2014).
18. M. Randeria, J.-M. Duan, and L.-Y. Shieh, Bound states, Cooper pairing, and Bose condensation in two dimensions, *Phys. Rev. Lett.* **62**, 981 (1989).
19. M. Randeria, J.-M. Duan, and L.-Y. Shieh, Superconductivity in a two-dimensional Fermi gas: Evolution from Cooper pairing to Bose condensation, *Phys. Rev. B*. **41**, 327 (1990).
20. S. Schmitt-Rink, C. M. Varma, and A. E. Ruckenstein, Pairing in two dimensions, *Phys. Rev. Lett.* **63**, 445–448 (1989).
21. L. D. Landau and E. M. Lifshitz, *Quantum Mechanics*. Butterworth-Heinemann, Oxford, UK (1981).
22. S. K. Adhikari, Quantum scattering in two dimensions, *American Journal of Physics*. **54**, 362 (1986).
23. D. S. Petrov and G. V. Shlyapnikov, Interatomic collisions in a tightly confined Bose gas, *Phys. Rev. A*. **64**, 012706 (2001).
24. I. Bloch, J. Dalibard, and W. Zwerger, Many-body physics with ultracold gases, *Rev. Mod. Phys.* **80**, 885 (2008).
25. D. S. Petrov, Few-atom problem. In ed. L. C. C. Salomon, G. V. Shlyapnikov, *Many-body physics with ultra-cold gases: Lecture Notes of the Les*

- Houches Summer Schools, vol. 94.* Oxford University Press, Oxford, England (2012).
26. M. Olshanii, Atomic scattering in the presence of an external confinement and a gas of impenetrable bosons, *Phys. Rev. Lett.* **81**, 938 (1998).
  27. T. Bergeman, M. G. Moore, and M. Olshanii, Atom-atom scattering under cylindrical harmonic confinement: Numerical and analytic studies of the confinement induced resonance, *Phys. Rev. Lett.* **91**, 163201 (2003).
  28. E. Haller, M. J. Mark, R. Hart, J. G. Danzl, L. Reichsöllner, V. Melezhik, P. Schmelcher, and H.-C. Nägerl, Confinement-induced resonances in low-dimensional quantum systems, *Phys. Rev. Lett.* **104**, 153203 (2010).
  29. S. Sala, P.-I. Schneider, and A. Saenz, Inelastic confinement-induced resonances in low-dimensional quantum systems, *Phys. Rev. Lett.* **109**, 073201 (2012).
  30. S. Sala, G. Zürn, T. Lompe, A. N. Wenz, S. Murmann, F. Serwane, S. Jochim, and A. Saenz, Coherent molecule formation in anharmonic potentials near confinement-induced resonances, *Phys. Rev. Lett.* **110**, 203202 (2013).
  31. D. S. Petrov, C. Salomon, and G. V. Shlyapnikov, Weakly bound dimers of fermionic atoms, *Phys. Rev. Lett.* **93**, 090404 (2004).
  32. G. V. Skorniakov and K. A. Ter-Martirosian, Three body problem for short range forces. I. Scattering of low energy neutrons by deuterons, *Sov. Phys. JETP.* **4**, 648 (1957).
  33. J. Levinsen and V. Gurarie, Properties of strongly paired fermionic condensates, *Phys. Rev. A.* **73**, 053607 (2006).
  34. R. Combescot, S. Giraud, and X. Leyronas, Normal state of highly polarized Fermi gases: The bound state, *Laser Physics.* **20**, 678–682 (2010).
  35. O. I. Kartavtsev, A. V. Malykh, and S. A. Sofianos, Bound states and scattering lengths of three two-component particles with zero-range interactions under one-dimensional confinement, *ZhETF.* **135**, 419 (2009).
  36. G. Orso, E. Burovski, and T. Jolicoeur, Luttinger liquid of trimers in Fermi gases with unequal masses, *Phys. Rev. Lett.* **104**, 065301 (2010).
  37. L. Pricoupenko and P. Pedri, Universal (1+2)-body bound states in planar atomic waveguides, *Phys. Rev. A.* **82**, 033625 (2010).
  38. O. I. Kartavtsev and A. V. Malykh, Low-energy three-body dynamics in binary quantum gases, *J. Phys. B: At. Mol. Opt. Phys.* **40**, 1429–1441 (2007).
  39. C. J. M. Mathy, M. M. Parish, and D. A. Huse, Trimers, molecules and polarons in imbalanced atomic Fermi gases, *Phys. Rev. Lett.* **106**, 166404 (2011).
  40. N. P. Mehta, Born-Oppenheimer study of two-component few-particle systems under one-dimensional confinement, *Phys. Rev. A.* **89**, 052706 (May, 2014).
  41. J. Levinsen and M. M. Parish, Bound states in a quasi-two-dimensional Fermi gas, *Phys. Rev. Lett.* **110**, 055304 (2013).
  42. D. Blume, Universal four-body states in heavy-light mixtures with a positive scattering length, *Phys. Rev. Lett.* **109**, 230404 (2012).
  43. O. I. Kartavtsev and A. V. Malykh, Recent advances in description of few

- two-component fermions, *Yad. Fiz.* **77**, 458 (2014).
44. E. Wille, F. M. Spiegelhalder, G. Kerner, D. Naik, A. Trenkwalder, G. Hendl, F. Schreck, R. Grimm, T. G. Tiecke, J. T. M. Walraven, S. J. J. M. F. Kokkelmans, E. Tiesinga, and P. S. Julienne, Exploring an ultracold Fermi-Fermi mixture: Interspecies Feshbach resonances and scattering properties of  $^6\text{Li}$  and  $^{40}\text{K}$ , *Phys. Rev. Lett.* **100**, 053201 (2008).
  45. L. Costa, J. Brachmann, A.-C. Voigt, C. Hahn, M. Taglieber, T. W. Hänsch, and K. Dieckmann, *s*-wave interaction in a two-species Fermi-Fermi mixture at a narrow Feshbach resonance, *Phys. Rev. Lett.* **105**, 123201 (2010).
  46. C.-H. Wu, I. Santiago, J. W. Park, P. Ahmadi, and M. W. Zwierlein, Strongly interacting isotopic Bose-Fermi mixture immersed in a Fermi sea, *Phys. Rev. A* **84**, 011601 (2011).
  47. V. N. Efimov, Energy levels of three resonantly interacting particles, *Nucl. Phys. A* **210**, 157 (1973).
  48. T. Kraemer, M. Mark, P. Waldburger, J. G. Danzl, C. Chin, B. Engeser, A. D. Lange, K. Pilch, A. Jaakkola, H.-C. Nägerl, and R. Grimm, Evidence for Efimov quantum states in an ultracold gas of caesium atoms, *Nature* **440**, 315 (2006).
  49. T. B. Ottenstein, T. Lompe, M. Kohnen, A. N. Wenz, and S. Jochim, Collisional stability of a three-component degenerate Fermi gas, *Phys. Rev. Lett.* **101**, 203202 (2008).
  50. Y. Castin, C. Mora, and L. Pricoupenko, Four-body Efimov effect for three fermions and a lighter particle, *Phys. Rev. Lett.* **105**, 223201 (2010).
  51. Y. Nishida and S. Tan, Liberating Efimov physics from three dimensions, *Few-Body Systems* **51**, 191 (2011).
  52. J. Levinsen, P. Massignan, and M. M. Parish, Efimov trimers under strong confinement, *Phys. Rev. X* **4**, 031020 (2014).
  53. V. Ngampruetikorn, M. M. Parish, and J. Levinsen, Three-body problem in a two-dimensional Fermi gas, *EPL* **102**, 13001 (2013).
  54. J. Levinsen, T. G. Tiecke, J. T. M. Walraven, and D. S. Petrov, Atom-dimer scattering and long-lived trimers in fermionic mixtures, *Phys. Rev. Lett.* **103**, 153202 (2009).
  55. G. Bertaina and S. Giorgini, BCS-BEC crossover in a two-dimensional Fermi gas, *Phys. Rev. Lett.* **106**, 110403 (2011).
  56. D. S. Petrov, M. A. Baranov, and G. V. Shlyapnikov, Superfluid transition in quasi-two-dimensional Fermi gases, *Phys. Rev. A* **67**, 031601 (2003).
  57. F. F. Bellotti, T. Frederico, M. T. Yamashita, D. V. Fedorov, A. S. Jensen, and N. T. Zinner, Mass-imbalanced three-body systems in two dimensions, *Journal of Physics B: Atomic, Molecular and Optical Physics* **46**, 055301 (2013).
  58. M. Jag, M. Zaccanti, M. Cetina, R. S. Lous, F. Schreck, R. Grimm, D. S. Petrov, and J. Levinsen, Observation of a strong atom-dimer attraction in a mass-imbalanced Fermi-Fermi mixture, *Phys. Rev. Lett.* **112**, 075302 (2014).
  59. S. Flügge and H. Marschall, *Rechenmethoden der Quantentheorie*. Springer-Verlag, Berlin (1952).

60. Y. F. Smirnov, Talmi transformation for particles with different masses (ii), *Nucl. Phys.* **39**, 346–352 (1962).
61. J. Levinsen, N. R. Cooper, and V. Gurarie, Stability of fermionic gases close to a  $p$ -wave Feshbach resonance, *Phys. Rev. A.* **78**, 063616 (2008).
62. Y. Nishida, S. Moroz, and D. T. Son, Super Efimov effect of resonantly interacting fermions in two dimensions, *Phys. Rev. Lett.* **110**, 235301 (2013).
63. A. J. Leggett. Diatomic molecules and Cooper pairs. In eds. A. Pekalski and J. Przystawa, *Modern Trends in the Theory of Condensed Matter*, p. 14. Springer-Verlag, Berlin (1980).
64. D. M. Eagles, Possible pairing without superconductivity at low carrier concentrations in bulk and thin-film superconducting semiconductors, *Phys. Rev.* **186**, 456 (1969).
65. C. A. Regal, M. Greiner, and D. S. Jin, Observation of resonance condensation of fermionic atom pairs, *Phys. Rev. Lett.* **92**, 040403 (2004).
66. M. W. Zwierlein, C. A. Stan, C. H. Schunck, S. M. F. Raupach, A. J. Kerman, and W. Ketterle, Condensation of pairs of fermionic atoms near a Feshbach resonance, *Phys. Rev. Lett.* **92**, 120403 (2004).
67. J.-P. Martikainen and P. Törmä, Quasi-two-dimensional superfluid fermionic gases, *Phys. Rev. Lett.* **95**, 170407 (2005).
68. A. M. Fischer and M. M. Parish, BCS-BEC crossover in a quasi-two-dimensional Fermi gas, *Phys. Rev. A.* **88**, 023612 (2013).
69. R. Chasman and S. Wahlborn, Transformation scheme for harmonic-oscillator wave functions, *Nuclear Physics A.* **90**, 401 (1967).
70. J. R. Engelbrecht and M. Randeria, New collective mode and corrections to Fermi-liquid theory in two dimensions, *Phys. Rev. Lett.* **65**, 1032 (1990).
71. J. R. Engelbrecht, M. Randeria, and L. Zhang, Landau  $f$  function for the dilute Fermi gas in two dimensions, *Phys. Rev. B.* **45**, 10135 (1992).
72. J. R. Engelbrecht and M. Randeria, Low-density repulsive Fermi gas in two dimensions: Bound-pair excitations and Fermi-liquid behavior, *Phys. Rev. B.* **45**, 12419 (1992).
73. P. Bloom, Two-dimensional Fermi gas, *Phys. Rev. B.* **12**, 125 (1975).
74. C. Mora and Y. Castin, Ground state energy of the two-dimensional weakly interacting Bose gas: First correction beyond Bogoliubov theory, *Phys. Rev. Lett.* **102**, 180404 (2009).
75. M. Bauer, M. M. Parish, and T. Enss, Universal equation of state and pseudogap in the two-dimensional Fermi gas, *Phys. Rev. Lett.* **112**, 135302 (2014).
76. A. M. Fischer and M. M. Parish. Quasi-two-dimensional Fermi gases at finite temperature. arXiv:1408.0476 .
77. S. Tan, Large momentum part of a strongly correlated Fermi gas, *Annals of Physics.* **323**, 2971 (2008).
78. F. Werner and Y. Castin, General relations for quantum gases in two and three dimensions: Two-component fermions, *Phys. Rev. A.* **86**, 013626 (2012).
79. J. Hofmann, Current response, structure factor and hydrodynamic quantities of a two- and three-dimensional Fermi gas from the operator-product

- expansion, *Phys. Rev. A* **84**, 043603 (2011).
80. C. Langmack, M. Barth, W. Zwerger, and E. Braaten, Clock shift in a strongly interacting two-dimensional Fermi gas, *Phys. Rev. Lett.* **108**, 060402 (2012).
  81. V. Ngampruetikorn, J. Levinsen, and M. M. Parish, Pair correlations in the two-dimensional Fermi gas, *Phys. Rev. Lett.* **111**, 265301 (2013).
  82. N. Trivedi and M. Randeria, Deviations from Fermi-liquid behavior above  $T_c$  in 2D short coherence length superconductors, *Phys. Rev. Lett.* **75**, 312 (1995).
  83. V. M. Loktev, R. M. Quick, and S. G. Sharapov, Phase fluctuations and pseudogap phenomena, *Physics Reports*. **349**, 1 (2001).
  84. D. S. Fisher and P. C. Hohenberg, Dilute Bose gas in two dimensions, *Phys. Rev. B* **37**, 4936 (1988).
  85. M. Holzmann, G. Baym, J.-P. Blaizot, and F. Laloë, Superfluid transition of homogeneous and trapped two-dimensional Bose gases, *Proc. Natl. Acad. Sci.* **104**, 1476 (2007).
  86. Z. Hadzibabic, P. Krüger, M. Cheneau, B. Battelier, and J. Dalibard, Berezinskii–Kosterlitz–Thouless crossover in a trapped atomic gas, *Nature*. **441**, 1118 (2006).
  87. S. S. Botelho and C. A. R. Sá de Melo, Vortex-antivortex lattice in ultracold fermionic gases, *Phys. Rev. Lett.* **96**, 040404 (2006).
  88. K. Miyake, Fermi liquid theory of dilute submonolayer  $^3\text{He}$  on thin  $^4\text{He}$  II film dimer bound state and Cooper pairs, *Progr. Theor. Phys.* **69**, 1794 (1983).
  89. X.-J. Liu, Virial expansion for a strongly correlated Fermi system and its application to ultracold atomic Fermi gases, *Physics Reports*. **524**, 37 (2013).
  90. X.-J. Liu, H. Hu, and P. D. Drummond, Exact few-body results for strongly correlated quantum gases in two dimensions, *Phys. Rev. B* **82**, 054524 (2010).
  91. X. Leyronas, Virial expansion with Feynman diagrams, *Phys. Rev. A* **84**, 053633 (2011).
  92. Y. He, Q. Chen, and K. Levin, Radio-frequency spectroscopy and the pairing gap in trapped Fermi gases, *Phys. Rev. A* **72**, 011602 (2005).
  93. Q. Chen, C. A. Regal, M. Greiner, D. S. Jin, and K. Levin, Understanding the superfluid phase diagram in trapped Fermi gases, *Phys. Rev. A* **73**, 041601 (2006).
  94. J. P. Gaebler, J. T. Stewart, T. E. Drake, D. S. Jin, A. Perali, P. Pieri, and G. C. Strinati, Observation of pseudogap behaviour in a strongly interacting Fermi gas, *Nature Phys.* **6** (2010).
  95. A. Perali, F. Palestini, P. Pieri, G. C. Strinati, J. T. Stewart, J. P. Gaebler, T. E. Drake, and D. S. Jin, Evolution of the normal state of a strongly interacting Fermi gas from a pseudogap phase to a molecular Bose gas, *Phys. Rev. Lett.* **106**, 060402 (2011).
  96. M. Barth and J. Hofmann, Pairing effects in the nondegenerate limit of the two-dimensional Fermi gas, *Phys. Rev. A* **89**, 013614 (2014).
  97. R. Watanabe, S. Tsuchiya, and Y. Ohashi, Low-dimensional pairing fluc-

- tuations and pseudogapped photoemission spectrum in a trapped two-dimensional Fermi gas, *Phys. Rev. A* **88**, 013637 (2013).
98. M. J. H. Ku, A. T. Sommer, L. W. Cheuk, and M. W. Zwierlein, Revealing the superfluid lambda transition in the universal thermodynamics of a unitary Fermi gas, *Science* **335**, 563 (2012).
  99. P. Fulde and R. A. Ferrell, Superconductivity in a strong spin-exchange field, *Phys. Rev.* **135**, A550–A563 (1964).
  100. A. I. Larkin and Y. N. Ovchinnikov, Inhomogeneous state of superconductors, *Sov. Phys. JETP* **20**, 762–769 (1965).
  101. M. W. Zwierlein, A. Schirotzek, C. H. Schunck, and W. Ketterle, Fermionic superfluidity with imbalanced spin populations, *Science* **311**, 492 (2006).
  102. G. B. Partridge, W. Li, R. I. Kamar, Y. Liao, and R. G. Hulet, Pairing and phase separation in a polarized Fermi gas, *Science* **311**, 503 (2006).
  103. Y. Shin, C. H. Schunck, A. Schirotzek, and W. Ketterle, Phase diagram of a two-component Fermi gas with resonant interactions, *Nature* **451**, 689–693 (2008).
  104. S. Nascimbène, N. Navon, K. J. Jiang, L. Tarruell, M. Teichmann, J. McKeever, F. Chevy, and C. Salomon, Collective oscillations of an imbalanced Fermi gas: Axial compression modes and polaron effective mass, *Phys. Rev. Lett.* **103**, 170402 (2009).
  105. Y.-A. Liao, A. S. C. Rittner, T. Paprotta, W. Li, G. B. Partridge, R. G. Hulet, S. K. Baur, and E. J. Mueller, Spin-imbalance in a one-dimensional Fermi gas, *Nature* **467**, 567–569 (2010).
  106. F. Chevy and C. Mora, Ultra-cold polarized Fermi gases, *Reports on Progress in Physics* **73**, 112401 (2010).
  107. D. E. Sheehy and L. Radzihovsky, BEC-BCS crossover, phase transitions and phase separation in polarized resonantly-paired superfluids, *Annals of Physics* **322**, 1790 (2007).
  108. S. Zöllner, G. M. Bruun, and C. J. Pethick, Polarons and molecules in a two-dimensional Fermi gas, *Phys. Rev. A* **83**, 021603 (2011).
  109. M. M. Parish, Polaron-molecule transitions in a two-dimensional Fermi gas, *Phys. Rev. A* **83**, 051603 (2011).
  110. R. Schmidt, T. Enss, V. Pietilä, and E. Demler, Fermi polarons in two dimensions, *Phys. Rev. A* **85**, 021602 (2012).
  111. V. Ngampruetikorn, J. Levinsen, and M. M. Parish, Repulsive polarons in two-dimensional Fermi gases, *EPL* **98**, 30005 (2012).
  112. N. Prokof'ev and B. Svistunov, Fermi-polaron problem: Diagrammatic Monte Carlo method for divergent sign-alternating series, *Phys. Rev. B* **77**, 020408 (2008).
  113. N. V. Prokof'ev and B. V. Svistunov, Bold diagrammatic Monte Carlo: A generic sign-problem tolerant technique for polaron models and possibly interacting many-body problems, *Phys. Rev. B* **77**, 125101 (2008).
  114. G. M. Bruun and P. Massignan, Decay of polarons and molecules in a strongly polarized Fermi gas, *Phys. Rev. Lett.* **105**, 020403 (2010).
  115. G.-B. Jo, Y.-R. Lee, J.-H. Choi, C. A. Christensen, T. H. Kim, J. H. Thywissen, D. E. Pritchard, and W. Ketterle, Itinerant ferromagnetism in a

- Fermi gas of ultracold atoms, *Science*. **325**, 1521 (2009).
116. D. Pekker, M. Babadi, R. Sensarma, N. Zinner, L. Pollet, M. W. Zwierlein, and E. Demler, Competition between pairing and ferromagnetic instabilities in ultracold Fermi gases near Feshbach resonances, *Phys. Rev. Lett.* **106**, 050402 (2011).
  117. C. Sanner, E. J. Su, W. Huang, A. Keshet, J. Gillen, and W. Ketterle, Correlations and pair formation in a repulsively interacting Fermi gas, *Phys. Rev. Lett.* **108**, 240404 (2012).
  118. P. Massignan, M. Zaccanti, and G. M. Bruun, Polarons, dressed molecules and itinerant ferromagnetism in ultracold Fermi gases, *Reports on Progress in Physics*. **77**, 034401 (2014).
  119. F. Chevy, Universal phase diagram of a strongly interacting Fermi gas with unbalanced spin populations, *Phys. Rev. A*. **74**, 063628 (2006).
  120. M. M. Parish and J. Levinsen, Highly polarized Fermi gases in two dimensions, *Phys. Rev. A*. **87**, 033616 (2013).
  121. X. Cui and H. Zhai, Stability of a fully magnetized ferromagnetic state in repulsively interacting ultracold Fermi gases, *Phys. Rev. A*. **81**, 041602 (2010).
  122. P. Massignan and G. M. Bruun, Repulsive polarons and itinerant ferromagnetism in strongly polarized Fermi gases, *Eur. Phys. J. D*. **65**, 83–89 (2011).
  123. R. Combescot and S. Giraud, Normal state of highly polarized Fermi gases: Full many-body treatment, *Phys. Rev. Lett.* **101**, 050404 (2008).
  124. C. Kohstall, M. Zaccanti, M. Jag, A. Trenkwalder, P. Massignan, G. M. Bruun, F. Schreck, and R. Grimm, Metastability and coherence of repulsive polarons in a strongly interacting Fermi mixture, *Nature*. **485**, 615 (2012).
  125. R. Combescot, S. Giraud, and X. Leyronas, Analytical theory of the dressed bound state in highly polarized Fermi gases, *Europhys. Lett.* **88**, 60007 (2009).
  126. M. Punk, P. T. Dumitrescu, and W. Zwerger, Polaron-to-molecule transition in a strongly imbalanced Fermi gas, *Phys. Rev. A*. **80**, 053605 (2009).
  127. C. Mora and F. Chevy, Ground state of a tightly bound composite dimer immersed in a Fermi sea, *Phys. Rev. A*. **80**, 033607 (2009).
  128. G. J. Conduit, Itinerant ferromagnetism in a two-dimensional atomic gas, *Phys. Rev. A*. **82**, 043604 (2010).
  129. D. S. Petrov, Three-body problem in Fermi gases with short-range interparticle interaction, *Phys. Rev. A*. **67**, 010703 (2003).
  130. V. Ngampruetikorn, Ph.D. thesis, in preparation.
  131. V. Pietilä, D. Pekker, Y. Nishida, and E. Demler, Pairing instabilities in quasi-two-dimensional Fermi gases, *Phys. Rev. A*. **85**, 023621 (2012).
  132. J. Levinsen and S. K. Baur, High-polarization limit of the quasi-two-dimensional Fermi gas, *Phys. Rev. A*. **86**, 041602 (2012).
  133. A. Schirotzek, C.-H. Wu, A. Sommer, and M. W. Zwierlein, Observation of Fermi polarons in a tunable Fermi liquid of ultracold atoms, *Phys. Rev. Lett.* **102**:230402 (2009).
  134. J. B. McGuire, Interacting fermions in one dimension. II. Attractive poten-

- tial, *J. Math. Phys.* **7**, 123 (1966).
135. L. He and P. Zhuang, Phase diagram of a cold polarized fermi gas in two dimensions, *Phys. Rev. A.* **78**, 033613 (2008).
  136. G. J. Conduit, P. H. Conlon, and B. D. Simons, Superfluidity at the BEC-BCS crossover in two-dimensional Fermi gases with population and mass imbalance, *Phys. Rev. A.* **77**, 053617 (2008).
  137. J. Tempere, S. N. Klimin, and J. T. Devreese, Effect of population imbalance on the Berezinskii-Kosterlitz-Thouless phase transition in a superfluid Fermi gas, *Phys. Rev. A.* **79**, 053637 (2009).
  138. S. Yin, J.-P. Martikainen, and P. Törmä, Fulde-Ferrell states and Berezinskii-Kosterlitz-Thouless phase transition in two-dimensional imbalanced Fermi gases, *Phys. Rev. B.* **89**, 014507 (2014).
  139. J. Vlietinck, J. Ryckebusch, and K. Van Houcke, Diagrammatic Monte Carlo study of the Fermi polaron in two dimensions, *Phys. Rev. B.* **89**, 085119 (2014).
  140. P. Kroiss and L. Pollet, Diagrammatic Monte Carlo study of quasi-two-dimensional Fermi polarons, *ArXiv e-prints* (2014).
  141. M. Köhl, talk at the 2012 APS March meeting.
  142. C. Lobo, A. Recati, S. Giorgini, and S. Stringari, Normal state of a polarized Fermi gas at unitarity, *Phys. Rev. Lett.* **97**:200403 (2006).
  143. M. M. Parish, F. M. Marchetti, and P. B. Littlewood, Supersolidity in electron-hole bilayers with a large density imbalance, *Europhys. Lett.* **95**, 27007 (2011).
  144. S. Gopalakrishnan, A. Lamacraft, and P. M. Goldbart, Universal phase structure of dilute Bose gases with Rashba spin-orbit coupling, *Phys. Rev. A.* **84**, 061604 (2011).
  145. L. P. Pitaevskii and A. Rosch, Breathing modes and hidden symmetry of trapped atoms in two dimensions, *Phys. Rev. A.* **55**, R853 (1997).
  146. M. Olshanii, H. Perrin, and V. Lorent, Example of a quantum anomaly in the physics of ultracold gases, *Phys. Rev. Lett.* **105**, 095302 (2010).
  147. M. Koschorreck, D. Pertot, E. Vogt, and M. Köhl, Universal spin dynamics in two-dimensional Fermi gases, *Nature Physics.* **9**, 405 (2013).
  148. S. K. Baur, E. Vogt, M. Köhl, and G. M. Bruun, Collective modes of a two-dimensional spin-1/2 Fermi gas in a harmonic trap, *Phys. Rev. A.* **87**, 043612 (2013).
  149. S. Chiacchiera, D. Davesne, T. Enss, and M. Urban, Damping of the quadrupole mode in a two-dimensional Fermi gas, *Phys. Rev. A.* **88**, 053616 (2013).
  150. F. Werner and Y. Castin, Unitary gas in an isotropic harmonic trap: Symmetry properties and applications, *Phys. Rev. A.* **74**, 053604 (2006).
  151. Y. Nishida and D. T. Son, Nonrelativistic conformal field theories, *Phys. Rev. D.* **76**, 086004 (2007).
  152. E. Taylor and M. Randeria, Apparent low-energy scale invariance in two-dimensional Fermi gases, *Phys. Rev. Lett.* **109**, 135301 (2012).
  153. J. Hofmann, Quantum anomaly, universal relations, and breathing mode of a two-dimensional Fermi gas, *Phys. Rev. Lett.* **108**, 185303 (2012).

154. C. Gao and Z. Yu, Breathing mode of two-dimensional atomic Fermi gases in harmonic traps, *Phys. Rev. A.* **86**, 043609 (2012).
155. S. Moroz, Scale-invariant Fermi gas in a time-dependent harmonic potential, *Phys. Rev. A.* **86**, 011601 (Jul, 2012).
156. C. Chafin and T. Schäfer, Scale breaking and fluid dynamics in a dilute two-dimensional Fermi gas, *Phys. Rev. A.* **88**, 043636 (2013).
157. D. T. Son, Vanishing bulk viscosities and conformal invariance of the unitary Fermi gas, *Phys. Rev. Lett.* **98**, 020604 (2007).
158. L. Wu and Y. Zhang, Applicability of the Boltzmann equation for a two-dimensional Fermi gas, *Phys. Rev. A.* **85**, 045601 (2012).
159. G. M. Bruun, Shear viscosity and spin-diffusion coefficient of a two-dimensional Fermi gas, *Phys. Rev. A.* **85**, 013636 (2012).
160. T. Schäfer, Shear viscosity and damping of collective modes in a two-dimensional Fermi gas, *Phys. Rev. A.* **85**, 033623 (2012).
161. T. Enss, C. Küppersbusch, and L. Fritz, Shear viscosity and spin diffusion in a two-dimensional Fermi gas, *Phys. Rev. A.* **86**, 013617 (2012).
162. A. Sommer, M. Ku, G. Roati, and M. W. Zwierlein, Universal spin transport in a strongly interacting Fermi gas, *Nature.* **472**, 201 (2011).
163. G. Policastro, D. T. Son, and A. O. Starinets, Shear viscosity of strongly coupled N=4 supersymmetric Yang-Mills plasma, *Phys. Rev. Lett.* **87**, 081601 (2001).
164. T. Enss, Transverse spin diffusion in strongly interacting Fermi gases, *Phys. Rev. A.* **88**, 033630 (2013).